THE U6 SNRNA M^6A METHYLTRANSFERASE METTL16 REGULATES MAT2A INTRON RETENTION THROUGH CO-TRANSCRIPTIONAL SPLICING

APPROVED BY SUPERVISORY COMMITTEE

Nicholas Conrad, Ph.D., Supervising Professor

David Corey, Ph.D.

Joshua Mendell, Ph.D.

Benjamin Tu, Ph.D.

DEDICATION

To the members of the Conrad Lab during my duration—Nick, Olga, Stefan, Emi, sort of Ryan, Sarah, Ally, Julio, Sung-Kyun, Aparna, and Anna—thank you for all your support and help. Nick, our conversations really helped me grow as a scientist, and your relentless optimism about my project even when I didn't have it was, overall, very helpful. You also turned out to be right, so I can't really say anything. Olga, you're the best. You've always been so supportive and just generally a really positive influence. Stefan, thanks for putting up with me sitting three feet away from you for a few years. You were really helpful as a mentor even though I, allegedly, killed your evil fish. Emi, when you left, so did the persistent threat that I could be a victim of a prank at any time. It was fun working with you. To everyone else, it has been such a pleasure! Good luck on all your future endeavors!

To my committee, thank you for all the feedback and advice. Dr. Corey, as well as my great experience as a SURF student in his lab, was a major reason why I came to UTSW. I really appreciated his continued support throughout my graduate career. Dr. Mendell was always very helpful and willing to direct me to members in his lab to learn new RNA techniques that I could

use. Dr. Tu helped guide me during my unexpected journey in the field of metabolism, and I couldn't have completed my project without the help of his lab.

Mom, dad, and Caroline—I appreciate the love and support even though you have no idea what I do.

To all my Dallas friends, science and non-science, thank you so much for all the outings, laughs, board games, and food throughout the past five years. I don't know how I would have done any of it without you.

Austin, you were one of my best discoveries in grad school. You know the words "RNA," "methylation," and "hairpin," are very important to me, though perhaps not exactly why. You've let me rant about technical problems to you and have tried to understand them. You got a dog with me during my quals, even though that was probably, objectively, a bad idea. You cooked for me the week that I wrote the bulk of this dissertation. Thank you.

THE U6 SNRNA M^6A METHYLTRANSFERASE METTL16 REGULATES MAT2A INTRON RETENTION THROUGH CO-TRANSCRIPTIONAL SPLICING

by

KATHRYN ELIZABETH PENDLETON

DISSERTATION

Presented to the Faculty of the Graduate School of Biomedical Sciences

The University of Texas Southwestern Medical Center at Dallas

In Partial Fulfillment of the Requirements

For the Degree of

DOCTOR OF PHILOSOPHY

The University of Texas Southwestern Medical Center at Dallas

Dallas, Texas

August, 2017

THE U6 SNRNA M^6A METHYLTRANSFERASE METTL16 REGULATES MAT2A INTRON RETENTION THROUGH CO-TRANSCRIPTIONAL SPLICING

Publication No. 1

Kathryn Elizabeth Pendleton, Doctor of Philosophy of Biological Chemistry

The University of Texas Southwestern Medical Center at Dallas, 2017

Supervising Professor: Nicholas Conrad, Ph.D.

Maintenance of proper levels of the methyl donor S-adenosylmethionine (SAM) is critical for a wide variety of biological processes. We demonstrate that the N^6-adenosine methyltransferase METTL16 regulates expression of human MAT2A, which encodes the SAM synthetase expressed in most cells. Upon SAM depletion by methionine starvation, cells induce MAT2A expression by enhanced splicing of a retained intron. Unlike previously studied intron retention events, we show that splicing induction of the MAT2A retained intron is regulated at the level of co-transcriptional splicing. This induction requires METTL16 and its methylation substrate, a vertebrate conserved hairpin (hp1) in the MAT2A 3´ UTR. Increasing METTL16

occupancy on the MAT2A 3´ UTR is sufficient to induce efficient splicing. We propose that under SAM-limiting conditions, METTL16 occupancy on hp1 increases due to inefficient enzymatic turnover, which promotes MAT2A splicing. We further show that METTL16 is the long-unknown methyltransferase for the U6 spliceosomal snRNA. These observations suggest that the conserved U6 snRNA methyltransferase evolved an additional function in vertebrates to regulate SAM homeostasis.

TABLE OF CONTENTS

PRIOR PUBLICATIONS

Pendleton, K.E.; Chen, B.; Liu, K.; Hunter, O.V.; Xie, Y.; Tu, B.P.; Conrad, N.K. The U6 snRNA m^6A Methyltransferase METTL16 Regulates SAM Synthetase Intron Retention. *Cell*. **2017**, *169* (5), 824-835.

LIST OF FIGURES

LIST OF TABLES

LIST OF APPENDICES

LIST OF DEFINITIONS

3/5′ss – 3′ or 5′ splice site

4SU – 4-thiouridine

ActD – actinomycin D

CLIP – UV cross-linking and immunoprecipitation

CMV – cytomegalovirus

CRISPR – clustered regularly interspaced short palindromic repeats

CTD – RNA Polymerase II C-terminal domain

E/ISE – exonic/intron splicing element

E/ISS – exonic/intron splicing silencer

HCC – hepatocellular carcinoma

hnRNPs – heterogeneous ribonucleoproteins

hp – hairpin

IP – immunoprecipitation

K_m – Michaelis-Menten Constant

LC-MS/MS – liquid chromatography tandem mass spectrometry

LSm – Sm-like

m^6A – N^6-methyladenosine

MAT – methionine adenosyltransferase

Met – L-methionine

miRNA – microRNA

mRNA – messenger RNA

MTAP – S-methyl-5'-thioadenosine phosphorylase

MTD – methyltransferase domain

NMD – nonsense mediated decay

Nt – nucleotide

PolII – RNA Polymerase II

Poly(A) – polyadenylation

RI – retained intron

RIP – RNA immunoprecipitation

RNA – ribonucleic acid

SAH – S-adenosylhomocysteine

SAM – S-adenosylmethioinine

siRNA – small interfering RNA

SMASh – small molecule-associated shutoff

snRNA – small nuclear RNA

snRNP – small nuclear ribonucleoprotein

SR proteins – serine/arginine rich protein

TIC – total ion count

TLC – thin layer chromatography

WT – wild-type

UTR – untranslated region

VCR – vertebrate conserved region

CHAPTER ONE
Introduction

S-adenosylmethionine (SAM) is one of the most commonly used enzymatic substrates in the cell (Cantoni, 1975). SAM serves as a methyl donor for the methylation of nucleic acids, proteins, and lipids; these methylation modifications serve vital regulatory functions. Deregulation of SAM levels has been linked oncogenic epigenetic changes, differentiation, and autophagy (Lu and Mato, 2005; Shiraki et al., 2014; Shyh-Chang et al., 2013; Sutter et al., 2013). These examples emphasize the importance of understanding the regulation of intracellular SAM levels.

In bacteria, SAM-binding riboswitches on the SAM synthetase mRNA regulate the expression of the SAM synthetase in response to SAM levels (Wang and Breaker, 2008). While mammalian SAM synthetase genes do not contain riboswitches, there has been great interest in understanding mechanisms that regulate these genes.

Methionine adenosyltransferase 2A (MAT2A) is the predominant SAM synthetase in vertebrates, with expression in every organ but the liver (Horikawa et al., 1990). It converts methionine (Met) and ATP into SAM. Deregulation of MAT2A has been linked to hepatocellular carcinoma (HCC), and MAT2A expression is a potential vulnerability for MTAP deficient cancers (Lu and Mato, 2005; Mavrakis et al., 2016). Previous work indicates that the MAT2A mRNA is highly regulated. Upon Met depletion, MAT2A mRNA accumulates in cells at high levels, though the response is not directly caused by the reduction in Met (Martinez-Chantar et al., 2003b). Rather, the cells upregulate MAT2A to respond to the reduction of SAM. In addition, the MAT2A 3′ UTR contains highly vertebrate-conserved hairpin (hp) structures with a

common hp loop motif (Parker et al., 2011). Though they do not appear to act as a riboswitch, their conservation implies that they possess a regulatory function. Finally, MAT2A expresses a significant amount of a retained intron isoform that is subject to nuclear degradation (Bresson et al., 2015). While not much is known about intron retention, recent studies have suggested that it might play a regulatory function in the expression of thousands of mRNAs (Boutz et al., 2015; Braunschweig et al., 2014; Yap et al., 2012). Together, these observations hint towards a potential role of the MAT2A mRNA in the regulation of SAM homeostasis.

The purpose of my project was to identify regulatory elements that controlled MAT2A intron retention in response to SAM levels and elucidate the function, if any, of the MAT2A retained intron isoform. These studies detail a feedback loop of SAM concentration on MAT2A expression through the methyltransferase METTL16. As suggested by previous m^6A-seq data (Dominissini et al., 2012; Linder et al., 2015; Schwartz et al., 2014), we confirmed *in vivo* and *in vitro* that MAT2A is m^6A modified at the conserved hp motifs. This motif, UACm^6AGAGAA, is distinct from the previously identified METTL3 consensus sequence, RRm^6ACH (where R=purine and H=A, C, or U)(Dominissini et al., 2012; Ke et al., 2015; Meyer et al., 2012; Yue et al., 2015). We discovered that the highly conserved methyltransferase METTL16 is the m^6A methyltransferase for the MAT2A hps and the U6 snRNA.

We further attempted to define the mechanism that METTL16 uses to regulate MAT2A expression. We used a variety of RNA labeling and transcriptional inhibition experiments to confirm that the retained intron isoform of MAT2A does not splice under low SAM conditions. Rather, protein-RNA tethering assays and RNA labeling experiments demonstrated that the retained intron is more efficiently co-transcriptionally spliced upon prolonged METTL16

association with hp1. We used transcriptional inhibition assays to show that the other hps in the MAT2A 3′ UTR act as cytoplasmic stability factors; MAT2A mRNA becomes more stable when they are not methylated. Their effect on translation is yet unknown.

In order to identify other potential mRNA targets of METTL16, we performed an m^6A-seq comparing fragmented RNA from METTL16 knockdown cells to control cells to identify additional mRNAs that are methylated by METTL16. Somewhat surprisingly, we did not find an enrichment of the UACAGAGAA motif in the downregulated m^6A sites. However, we did find an enrichment of METTL16-dependent sites near shorter than average, GC-rich introns or intron-exon junctions proximal to the 3′ end of the RNAs. Whether these m^6A sites are direct METTL16 targets or sensitive to the decrease in SAM that occurs during METTL16 knockdown remains unknown.

Overall, we have discovered that METTL16 acts as a SAM sensor in the cell by inducing the co-transcriptional splicing of the MAT2A retained intron, and thereby upregulating MAT2A protein levels, upon conditions of low SAM. This work is informative not only in understanding SAM homeostasis, but also in expanding knowledge of the writers and function of m^6A methylation.

CHAPTER TWO
Review of the Literature

Vertebrate SAM Homeostasis and MAT2A

SAM synthesis exists in a metabolic cycle (Figure 1). Generally, SAM is synthesized from Met and ATP using a methionine adenosyltransferase. SAM is most commonly used by enzymes as a methyl donor, resulting in a methylated substrate and S-adenosylhomocysteine (SAH). Additional roles of SAM have also been reported, such as a source of methylene groups, amino groups, ribosyl groups, aminoalkyl groups, and 5′deoxyadenosyl radicals (Fontecave et al., 2004). SAH can then be recycled back into SAM. The SAH hydrolase can convert SAH into homocysteine (Palmer and Abeles, 1979). Homocysteine can then enter into the transsulfuration

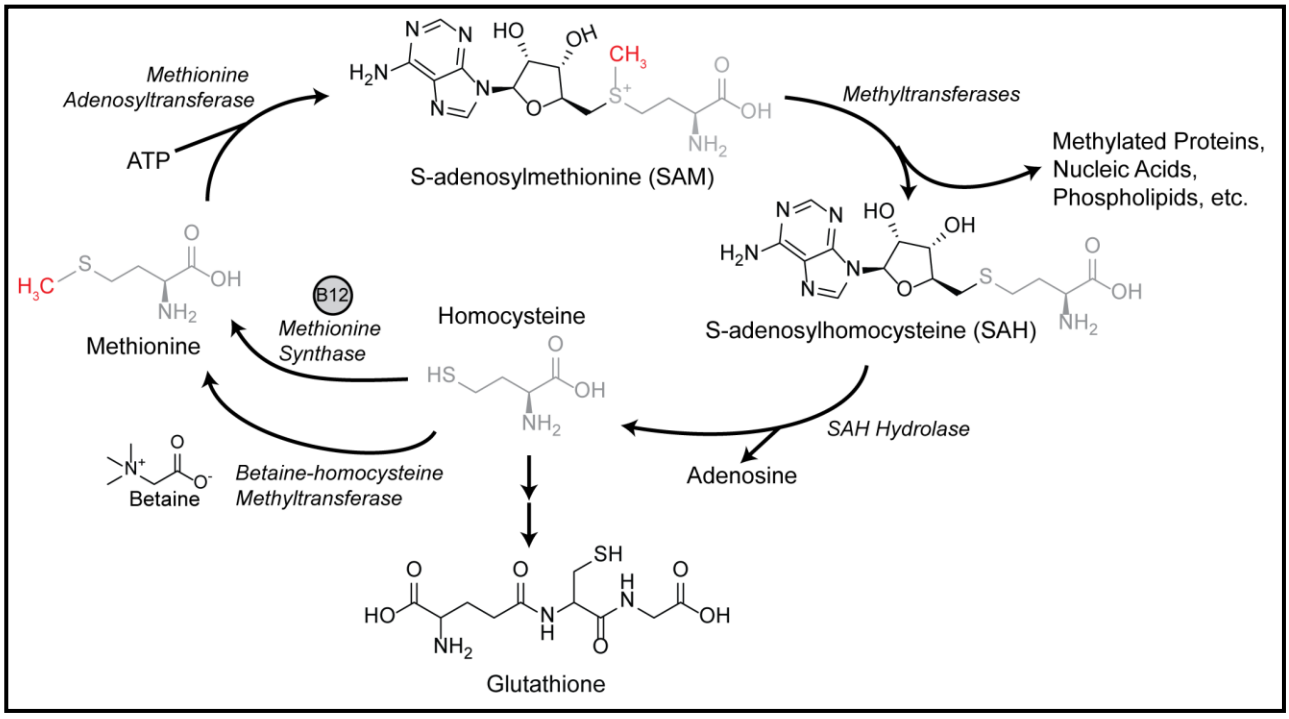

Figure 1. The SAM Cycle

This diagram shows a summary of the major enzymes and substrates that produce and recycle SAM. Adapted from (Fontecave et al., 2004).

pathway to eventually make glutathione (Brosnan and Brosnan, 2006), or produce methionine through either the methionine synthase and vitamin B12 or the betaine-homocysteine methyltransferase (Ludwig and Matthews, 1997), and thus produce more SAM. Though this cycle is the main source of SAM, additional pathways also contribute to maintaining cellular SAM levels; both threonine and serine provide substrates for SAM synthesis (Maddocks et al., 2016; Shyh-Chang et al., 2013), while histone and phospholipid methylation can act as SAM sinks within the cell (Ye et al., 2017). This complexity emphasizes that the cell must tightly regulate its SAM homeostasis.

Though many different enzymes can feed into and contribute to the SAM pathway, there is much interest in defining the regulation of the vertebrate SAM synthetases, the methionine adenosyltransferase (MAT) enzymes. There are three major genes involved in this process. MAT1A is a liver-specific SAM synthetase enzyme, and exists in both a dimer (MATIII) and a tetramer (MATI). MAT2A is the broadly expressed, though lowly expressed in the liver, SAM synthetase that can act alone or interact with MAT2B to form a hetero-oligomer (MATII) for increased activity (Finkelstein, 1990). These complexes have vastly different affinities for methionine. MATI has a K_m of ~100μM, MATII has a K_m of ~3.3μM (Kotb and Kredich, 1985), and MATIII has a K_m of ~600μM (Mato et al., 1997).

The tight regulation of the liver's SAM synthetase expression and activity has made it particularly interesting for studying SAM metabolism. The fetal liver predominantly expresses MAT2A, but during development, switches to MAT1A (Garcia-Trevijano et al., 2000). This switch corresponds with increased SAM levels, and the developed liver produces the most SAM in the body (Mato et al., 2013). This difference in SAM production is largely explained by the

different MAT enzymes and their regulation. High levels of SAM inhibit both MATI and MATII, but activate the liver-predominant MATIII (Finkelstein, 1990). If liver cells become de-differentiated, such as in culture or in HCC, MAT2A becomes the predominant SAM synthetase (Huang et al., 1998; Liu et al., 2007; Martinez-Chantar et al., 2003a; Paneda et al., 2002), and cellular levels of SAM decrease. The decreased SAM levels seem to assist in cell proliferation. In addition, studies utilizing MAT1A knockouts suggest that this switch from MAT1A to MAT2A helps to activate a variety of abnormal cellular pathways that contribute to HCC (Mato et al., 2013).

While MAT2A expression is linked to HCC, more recent studies have suggested that it could also be a potential target of interest in other cancers. ShRNA screens in MTAP-deleted cancers showed that the loss of MAT2A was particularly lethal to these cancers (Marjon et al., 2016; Mavrakis et al., 2016). In addition, many cancers show a dramatic increase in Met uptake (Agrawal et al., 2012; Glaudemans et al., 2013). For these reasons, much interest exists in understanding MAT2A's regulation within the cell. Previous work has shown that decreased Met concentrations cause an increase in the MAT2A protein and RNA, as well as an increase in the mRNA half-life (Gomes Trolin et al., 1998; Martinez-Chantar et al., 2003b). The mechanism that mediated these effects was unknown. Additional studies suggested that AU-rich element binding proteins AUF1 and HuR also regulate the stability of the MAT2A mRNA (Vazquez-Chantada et al., 2010). Another report demonstrated that an acetylation post-translational modification on the MAT2A lysine 81 promotes its proteasomal degradation and becomes less prevalent in HCC (Yang et al., 2015). Finally, one group noted that the MAT2A mRNA has highly vertebrate-conserved hairpin structures in its 3′ UTR that are likely regulatory, though

they did not identify their function (Parker et al., 2011). Despite this work, MAT2A's response to changes in SAM remains poorly understood.

M^{6}A Modification

Recent studies have demonstrated the prominence and importance of the m^{6}A modification of RNA. M^{6}A is present in virtually all organisms and plays essential roles in yeast, plants, fruit flies, and mammals (Clancy et al., 2002; Dominissini et al., 2013; Hongay and Orr-Weaver, 2011; Schwartz et al., 2013). This modification is the most abundant mRNA modification present in cells (Desrosiers et al., 1974; Wei et al., 1975), and transcriptomic approaches have demonstrated that there are roughly three to five m^{6}A modifications per mRNA (Dominissini et al., 2012; Linder et al., 2015; Meyer et al., 2012; Yue et al., 2015). The majority of m^{6}A modifications are located in the 3′ UTR of transcripts (Dominissini et al., 2012; Ke et al., 2015; Meyer et al., 2012), though a substantial portion of mRNAs also have m^{6}A at the 5′ end of transcripts (Keith et al., 1978; Mauer et al., 2017), the coding sequence, and introns (Dominissini et al., 2012; Haussmann et al., 2016).

In addition, many m^{6}A sites are conserved between species, suggesting a functional importance for this modification (Meyer et al., 2012; Schwartz et al., 2014). Indeed, m^{6}A modifications have been linked to regulating transcript stability, splicing, and translation (Carroll et al., 1990; Dominissini et al., 2012; Haussmann et al., 2016). M^{6}A promotes alteration of RNA structure (Engel and von Hippel, 1978; Liu et al., 2015; Liu et al., 2017) and allows recognition with m^{6}A-specific RNA binding proteins. These m^{6}A "readers" and their functions will be discussed in more detail below. Genes with the highest expression and fastest transcription tend to have the least amount of methylation (Schwartz et al., 2014; Slobodin et al., 2017), indicating

that the primary role of m^{6}A is to provide a method to regulate levels of RNA transcripts. The m^{6}A writers, erasers, and readers all play essential roles in the mechanisms of this regulation (Figure 2).

M^{6}A Writers

A complex of the proteins METTL3, METTL14, and WTAP is the main source of the m^{6}A modification in mammalian cells and target an RRACH motif. While both METTL3 and METTL14 are structurally similar to class I methyltransferases, METTL3 is the catalytically active subunit that utilizes SAM to methylate adenosines, while METTL14 acts as a support structure for METTL3 and recognizes RNA substrates (Wang et al., 2016a; Wang et al., 2016b). Originally identified as a splicing protein, WTAP's precise role in this complex remains uncertain; however, some data suggests that it is necessary for the proper localization of the complex to nuclear speckles (Ping et al., 2014).

Disparate data exists on how much a knockout of METTL3 affects m^{6}A mRNA levels. Though both studies (Batista et al., 2014; Geula et al., 2015) were performed in mESCs and saw

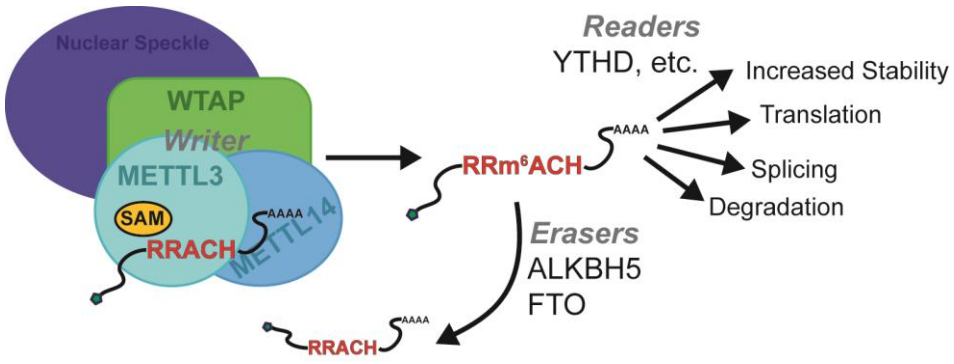

Figure 2. The m^{6}A modification is regulated and confers function to RNAs

The RRACH motif can be methylated by a complex of METTL3, METTL14, and WTAP located in nuclear speckles. This m^{6}A modification can be demethylated by m^{6}A erasers or recognized by m^{6}A readers to promote different RNA functions.

a similar lack of differentiation, one group reported a 60% decrease in the m^6A on mRNA (Batista et al., 2014), and the other near total depletion of m^6A from mRNAs (Geula et al., 2015). Differences in cell treatment and RNA preparation could potentially account for this disparity, though it is unclear which group has more accurate data. Neither group looked at the effect of knockout on total RNA m^6A levels. Knockdowns of METTL3 and METTL14 consistently result in a 20-40% decrease in mRNA m^6A (Liu et al., 2014). In addition, METTL3 and METTL14 must be together *in vitro* to have significant activity (Liu et al., 2014; Wang et al., 2016a). This data demonstrates the essentiality of the heterodimer for catalysis. It does not show that they are the only m^6A methyltransferases.

Knockdowns of METTL3, METTL14, and WTAP have many effects on gene expression, alternative splicing, and transcript stability. These changes seem largely a result of the decrease in m^6A. METTL3 also plays a role in regulation of microRNA (miRNA) function. METTL3 methylates pri-miRNAs and allows for their recognition by the processing factor DGCR8. While m^6A did not seem necessary for DGCR8 binding, structural changes mediated by m^6A likely play a role (Alarcon et al., 2015). In addition, evidence also suggests that METTL3 has non-catalytic functions in RNA regulation. METTL3 is localized in both the cytoplasm and the nucleus. In the cytoplasm, METTL3 can recognize m^6A sites in a non-catalytic manner and interact with translation initiation machinery to promote translation (Lin et al., 2016).

Despite the broad mRNA targets of METTL3 and METTL14, m^6A modifications occur in locations other than their consensus sequence (Shimba et al., 1995), suggesting the existence of additional m^6A methyltransferases. While the RRACH motif is enriched in many of the original m^6A-seq peaks, this motif is not incredibly difficult to find in a 100-200nt span as it occurs

roughly once every 200nt. More precise methods that allow identification with single nucleotide precision are now available (Linder et al., 2015), but the accuracy of the site is still scored partially based upon whether it exists in an RRACH, and part of the site recognition is reliant on a mutation of the C following the m^6A. Though this method can also determine m^6A sites by identifying truncations at the +1 position relative to the m^6A, roughly a third less sites are called with the truncation method compared to the mutation method. While it is clear that METTL3 and METTL14 account for the majority of the m^6A sites in mRNAs, more exploration is needed to identify motifs for other m^6A sites.

M^6A Erasers

M^6A methylation is a reversible process, and FTO and ALKBH5 have been identified as two m^6A demethylases (Jia et al., 2011; Zheng et al., 2013). Both of these enzymes are alpha-ketoglutarate-dependent dioxygenases and remove m^6A in an oxidative manner. Overexpression of either decreases global m^6A levels, while knockdown or knockout causes mild increases in m^6A (Jia et al., 2011; Zheng et al., 2013). The mechanism that directs the m^6A demethylases to specific m^6A sites is not well understood, though evidence indicates that they have different targets.

FTO, or the fat mass and obesity-associated protein, variations had long been thought to contribute to obesity in humans (Dina et al., 2007; Do et al., 2008; Frayling et al., 2007), though its m^6A demethylation activity was only recently discovered. An initial report suggested that FTO regulated m^6A sites at exon-intron and exon-exon junctions to modify alternative splice sites in genes associated with adipogenesis (Zhao et al., 2017). A more recent paper suggested that FTO has a binding preference to m^6A_m, an adenosine methylated at the N^6 and 2′O-methyl

positions and often near the 5′ cap of transcripts that gives them resistance to decapping by DCP2. M^6A_m is strongly associated with promoting stability of transcripts, and its demethylation by FTO results in a broad range of transcripts becoming less stable (Mauer et al., 2017). Whether m^6A_m also affects the previously reported splicing phenotype associated with FTO remains unclear.

ALKBH5 seems to have general effects on mRNA export, stability, and has more examples of specific mRNA regulation. Knockout of ALKBH5 leads to an increase of mRNA in the cytoplasm and decrease in global mRNA stability (Zheng et al., 2013). Consistent with this observation, ALKBH5 demethylation of an m^6A site on the 3′ UTR of NANOG promoted the stability of the RNA (Zhang et al., 2016). ALKBH5 was also shown to have elevated expression in glioblastoma stem-like cells compared to the paired match tumor, and this increase promoted the demethylation of the FOXM1 nascent mRNA, which encodes for a transcription factor necessary for cell cycle regulation and improves its expression (Zhang et al., 2017).

While clearly m^6A demethylases assist in the regulation of m^6A sites on RNAs, much remains to be discovered about the function and regulation of these enzymes. Further studies that probe whether they have sequence preference, interacting factors, or post-translational modifications that drive demethylation of certain targets deserve attention. These data could help determine if FTO and ALKBH5 truly have different activities, or if there might be additional m^6A demethylases.

M^6A Readers

In addition to m^6A writers and erasers, there are a variety of proteins that act as m^6A readers. These proteins recognize m^6A modifications on transcripts and drive different forms of

regulation. YTHDF1, YTHDF2, YTHDF3, and YTHDC1, though different in function, all have the same YTH domain that binds to m^6A. Proteins without a YTH domain, such as RBM15, hnRNPC, hnRNPA2B1, and hnRNPG, have also been found to bind to m^6A sites. It is less clear why these proteins have a preference for m^6A over A, though some evidence suggests that structural changes induced by m^6A assist in the interaction (Liu et al., 2015). While both the m^6A writers and erasers can affect RNA properties through m^6A, m^6A readers and their varied roles seem to be primarily responsible for differentially regulating transcripts based on the modification.

Though YTH components are similar in their interacting domains with m^6A, they have diverse functions. YTHDC1 is the nuclear YTH domain protein, and it has reported localization at YT bodies and interacts with nuclear speckles (Nayler et al., 2000). YTHDC1 seems to play a role in promoting exon inclusion for mRNAs (Xiao et al., 2016), though it is also necessary for the heavily methylated lncRNA XIST to promote X chromosome silencing (Patil et al., 2016). YTHDF1-3 are all cytoplasmic, and while some papers suggested that they have redundant function (Tirumuru et al., 2016), most demonstrate differences. YTHDF1 can interact with the translation factors and has been linked to promoting increased translational efficiency (Li et al., 2017; Wang et al., 2014; Wang et al., 2015b). YTHDF2 interaction is strongly correlated with promoting RNA decay, though two different mechanisms have been proposed. One report proposes that YTHDF2 moves the mRNAs from translation sites to decay sites, while another details its interaction and recruitment of the CCR4-NOT deadenylase complex to promote decay (Du et al., 2016; Wang et al., 2014). YTHDF3 has been linked to both translation and decay of

m^{6}A-modified transcripts (Li et al., 2017; Shi et al., 2017), and further investigation is warranted to understand the way it can differentiate between these effects.

The non-YTH domain m^{6}A-interacting proteins that have been discovered all affect nuclear functions of m^{6}A-modified RNA. HnRNPA2B1, hnRNPG, hnRNPC all regulate splicing near m^{6}A sites (Alarcon et al., 2015; Liu et al., 2015). RBM15's exact function is unknown. It was proposed to recruit the m^{6}A machinery to promote methylation, though has fairly broad RNA association, suggesting that it could also have additional functions (Patil et al., 2016). Given that none of these proteins have an obvious m^{6}A-interaction domain, future investigations are necessary to determine if RNA-protein interaction sequencing data from other nuclear RNA binding proteins overlaps with predicted m^{6}A sites, and if those proteins play different roles.

Though general effects are known, much remains to be understood about the mechanism that m^{6}A readers use to interact with each other and compete for binding to m^{6}A. With a large variety of potential regulation, additional signals must be necessary to promote regulation by one m^{6}A reader over another. In addition, it will be interesting to determine if any of these proteins act synergistically considering that most modified mRNAs have multiple m^{6}A sites. Regardless, it is clear that the m^{6}A-modified RNA have additional regulation through the m^{6}A readers.

METTL16

While METTL3 is the only active RNA m^{6}A methyltransferase identified in humans, its consensus sequence does not account for all the m^{6}A modifications identified. U6, U2, and the ribosomal RNAs (Bringmann and Luhrmann, 1987; Shimba et al., 1995) are suspected to be modified by unknown m^{6}A methyltransferases. Additional RNA m^{6}A methyltransferases have been identified in other organisms. *Escherichia coli* has two known rRNA m^{6}A

methyltransferases, *rlmJ* and *rlmF* (Deng et al., 2015; Sergiev et al., 2008). While *rlmJ* has no obvious human homolog, the human homolog of *rlmF* is the protein METTL16.

METTL16 is highly conserved in most organisms, and while it's largely uncharacterized, mutation or loss of METTL16 homologs is associated with a variety of negative phenotypes. First, in *E. coli*, deletion or overexpression of *rlmF* results in slowed growth and decreased cell fitness (Deng et al., 2015). Second, *S. pombe* requires its METTL16 homolog for efficient DNA replication initiation (Pan et al., 2012). Third, the *C. elegans* homolog is nuclear and mutations of this protein result in cell cycle arrest during M-phase (Dorsett et al., 2009). Fourth, an *A. thaliana* homolog mutant disrupts the circadian clock. Fifth, in humans, gene essentiality screens suggest that METTL16 is an essential gene, and a recent report shows a non-catalytic interaction with the MALAT1 triple helix (Brown et al., 2016; Wang et al., 2015a).

Methyltransferases are divided into either α, β, or γ groups based upon the order of their SAM binding, target binding, and catalytic motifs (Figure 3). Different order in the methyltransferase motifs has been previously linked to greater differences in methyltransferase recognition sequence. Despite both being m^6A methyltransferases, METTL16 and METTL3 are categorized into different methyltransferase groups. METTL3 has a β methyltransferase structure, while METTL16 has a γ methyltransferase structure (Bujnicki et al., 2002; Malone et al., 1995). Accordingly, *rlmF*

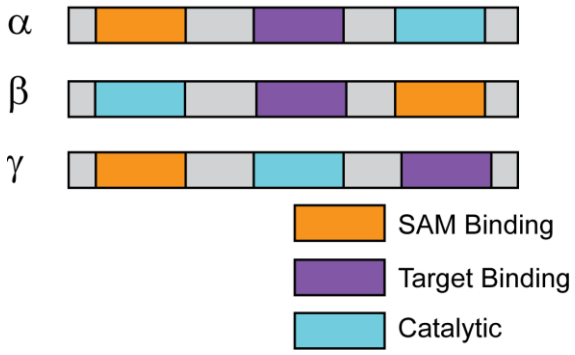

Figure 3. Different Methyltransferase Groups

Methyltransferases are classified into three different groups (α, β, γ) depending on the order of different functional elements.

methylates the sequence ACACm^{6}AG, different from METTL3 RRACH motif (Sergiev et al., 2008).

In my work, I have documented that METTL16 is a functional m^{6}A methyltransferase in human cells that methylates both the U6 snRNA and the MAT2A hairpins. This work suggests that there are likely additional m^{6}A methyltransferases that modify human RNA, and that they might be utilized for different regulatory functions besides the METTL3-mediated m^{6}A sites.

Splicing

Before an mRNA can be exported into the cytoplasm for translation, it must be capped, spliced, and polyadenylated. Splicing out introns is not only an essential processing step for a mature mRNA, but also a source of mRNA variability and regulation. Alternatively spliced mRNAs, or differentially spliced isoforms of the same gene, can lead to additional functions. Proper splicing is essential for cell function, many proteins contribute to splicing regulation, and mis-spliced transcripts have been associated with malfunction of the cell and certain disease states (Daguenet et al., 2015; Lopez-Bigas et al., 2005; Singh and Cooper, 2012). For these purposes, much interest exists in understanding the various processes and mechanisms that regulate pre-mRNA splicing.

The Spliceosome

The major component that mediates splicing in the cell is a RNA-protein complex called the spliceosome. The spliceosome catalyzes splicing of an intron in two steps and consumes ATP in the process (Lerner et al., 1980; Will and Luhrmann, 2011). The majority of introns are spliced by the major spliceosome, which recognizes introns with GU at their 5′ splice site (5′ss) and AG at their 3′ splice site (3′ss) (Wang and Burge, 2008). The minor spliceosome recognizes

a rarer group of introns that often have AU at their 5′ss and AC at their 3′ss (Tarn and Steitz, 1996). Both of these utilize similar protein and RNA components.

Small nuclear RNAs (snRNAs) are the major RNA component of the spliceosome and are necessary for properly orienting the intron and driving the catalytic activity of splicing. SnRNAs are nucleoplasmic, highly abundant, and non-coding. There are two different classes of snRNA, the Sm and Sm-like (LSm), that are divided by their processing and interacting proteins. The Sm class of snRNAs interacts with the Sm proteins and consists of U1, U2, U4, $U4_{ATAC}$, U5, U7, U11, and U12. These snRNAs have 5′ trimethylguanosine caps, a 3′ stem loop, and are transcribed by RNA Polymerase II (PolII) (Hernandez and Weiner, 1986; Will and Luhrmann, 2011). In order to mature, the Sm class snRNAs are exported to the cytoplasm through the PHAX export pathway, assembled into protein complexes with Sm proteins, and imported back into the nucleus for further modification in Cajal bodies (Eggert et al., 2006; Matera and Shpargel, 2006; Ohno et al., 2000). Except for U7, which performs histone pre-mRNA 3′ end processing, the Sm snRNAs form the core of the spliceosome and catalyze the removal of introns from pre-mRNA (Valadkhan, 2005).

The LSm class consists of the snRNAs U6 and $U6_{ATAC}$, as well as the LSm proteins. U6 and $U6_{ATAC}$ are transcribed by RNA Polymerase III, have monomethylphosphate caps, a 3′ stem loop, and end with a poly(U) stretch (Schramm and Hernandez, 2002; Will and Luhrmann, 2011). Unlike their Sm counterparts, the LSm snRNAs are only modified in the nucleus and never leave, though they also go to Cajal bodies for recycling and restructuring (Stanek and Neugebauer, 2004; Stanek et al., 2003).

Splicing in complex organisms often requires more than just the spliceosome; however, different components are variable for different introns. In order to understand the general mechanism of just the spliceosome, simpler organisms like yeast or reconstitution of the spliceosome *in vitro* have been used. These systems suggest that splicing catalysis often occurs as follows (Figure 4). First, the U1 small nuclear ribonucleoprotein (snRNP) identifies the 5′ss and basepairs to the mRNA with the help of RNA binding proteins and the PolII C-terminal domain (CTD) (Cho et al., 2011; Morris and Greenleaf, 2000; Staknis and Reed, 1994). Second, the U2 snRNP and its interacting factors recognize and bind to the 3′ss. Third, additional proteins identify the branchpoint adenosine, or the adenosine that will eventually act as a nucleophile to sever the connection between the end of the exon and beginning of the intron. During this time, U1 and U2 also rearrange to form an intron-spanning complex and bring the different splicing components closer together for long introns (De Conti et al., 2013; Fox-Walsh et al., 2005; Sterner et al., 1996). Fourth, the interacting

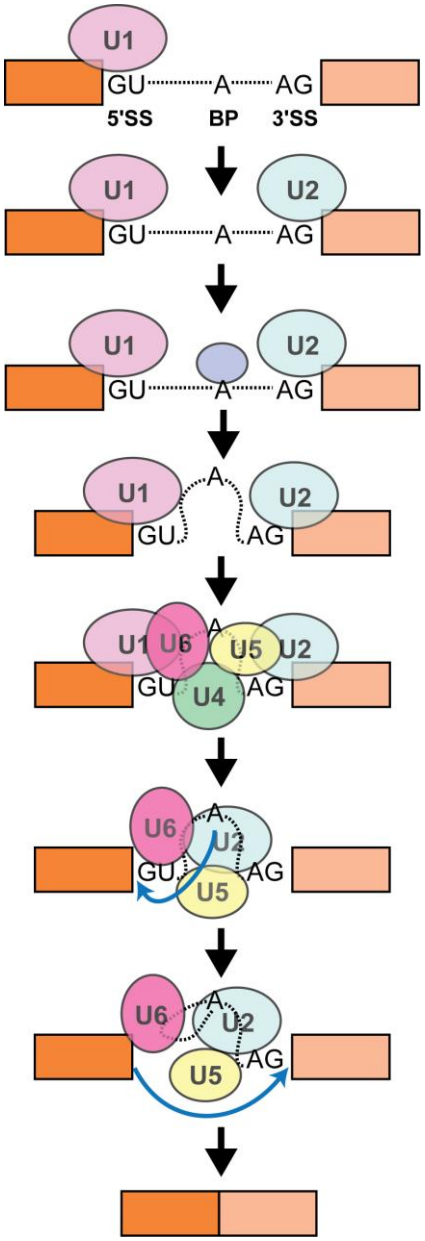

Figure 4. Vertebrate Intronic Splicing

This diagram displays the different steps and snRNPs involved in vertebrate intronic splicing. Adapted from (Lee and Rio, 2015).

U4-U6 snRNPs and the U5 snRNP are recruited to the intron. Fifth, these snRNPs then rearrange to become active, resulting in U2 interacting with U6, and U1 and U4 leaving. The U2 and U6 interaction with the 5′ss allows for it to interact with the branchpoint adenosine (Raghunathan and Guthrie, 1998). Sixth, the branchpoint adenosine 3′hydroxyl group then attacks the 5′ss, freeing it from exon 1, and forming an intron-exon 2 lariat structure. The U5 snRNP helps to keep the two exons together at this point. Seventh, the intron-exon 2 lariat and the bound snRNPs re-arrange again, splicing together the exons and splicing out the intron in the process. Eighth, the remaining snRNPs leave the intron.

While the general process of splicing is relatively well understood, many subtle points are not. For example, how these spliceosomal elements are coordinated to their intronic positions at the proper time in splicing catalysis is still largely unknown. Furthermore, many of the snRNAs are heavily modified at conserved positions, but the purpose of these modifications for their activity is largely undetermined.

Regulatory Splicing Elements

Though the spliceosome plays an important general role in splicing, a variety of additional splicing elements contribute to intron recognition and efficient splicing. Certain RNA sequences, regulatory proteins, chromatin structures, and PolII processivity have all been found to modulate splicing and even determine alternative splicing.

RNA sequences are essential for splice site recognition by the spliceosome, but additional RNA elements also assist with splicing. Short sequences within a 300nt span of the splice sites can act as exonic/intronic splicing enhancers (E/ISEs) and silencers (E/ISSs). The enhancers help promote recognition of splice sites, while silencers repress them (Wang and Burge, 2008).

Constitutively spliced introns typically have ESEs, while alternatively spliced exons more commonly have ISEs (Barash et al., 2010). The GC content of exons and their flanking introns also plays a role in regulating splicing. Exons often have higher GC content than introns, and this can help cellular components distinguish between exon-intron boundaries. GC-rich introns are more likely to have inefficient splicing (Amit et al., 2012; Braunschweig et al., 2014; Tillo and Hughes, 2009).

A variety of RNA binding proteins contribute to splicing regulation, though the most prominent are the serine-arginine rich proteins (SR proteins) and the heterogeneous ribonucleoproteins (hnRNPs). These proteins both associate with short RNA motifs to influence splicing, and their expression can drive different isoforms of mRNAs (Long and Caceres, 2009; Martinez-Contreras et al., 2007). SR proteins most commonly interact with either ESE or ISSs, while hnRNPs mostly act as silencers (Anko, 2014; Martinez-Contreras et al., 2007; Zhou and Fu, 2013). Tissue-specific *trans*-acting factors, such as RBFOX, PTBP2, and TIA, drive RNA isoforms only in certain cell types (Irimia and Blencowe, 2012).

Because the vast majority of splicing occurs co-transcriptionally (Ameur et al., 2011; Gornemann et al., 2005; Khodor et al., 2011; Lacadie and Rosbash, 2005), chromatin and PolII processivity can influence splicing regulation. Nucleosomes are more occupied at exons than at introns, and histones have enriched H3K36me3 modification around exons (Andersson et al., 2009; Huff et al., 2010; Spies et al., 2009). These features not only can recruit certain proteins that affect splicing (Sims et al., 2007), but also affect PolII elongation. In addition to chromatin, proteins that bind directly with PolII can affect its elongation. Varied PolII elongation time on a gene can promote RNA interactions with different splicing factors, and therefore alter the

isoform of the mRNA produced (Batsche et al., 2006; Dermody et al., 2008; Neish et al., 1998; Rosonina et al., 2005).

The cell has a variety of mechanisms to regulate the splicing of an mRNA. While isoform expression is easily determined with RNA sequencing, it is often difficult to determine what controls alternative isoforms given the variety of mechanisms. Understanding of these elements and ways to identify their influence on splicing is essential to defining how RNAs can be differentially regulated.

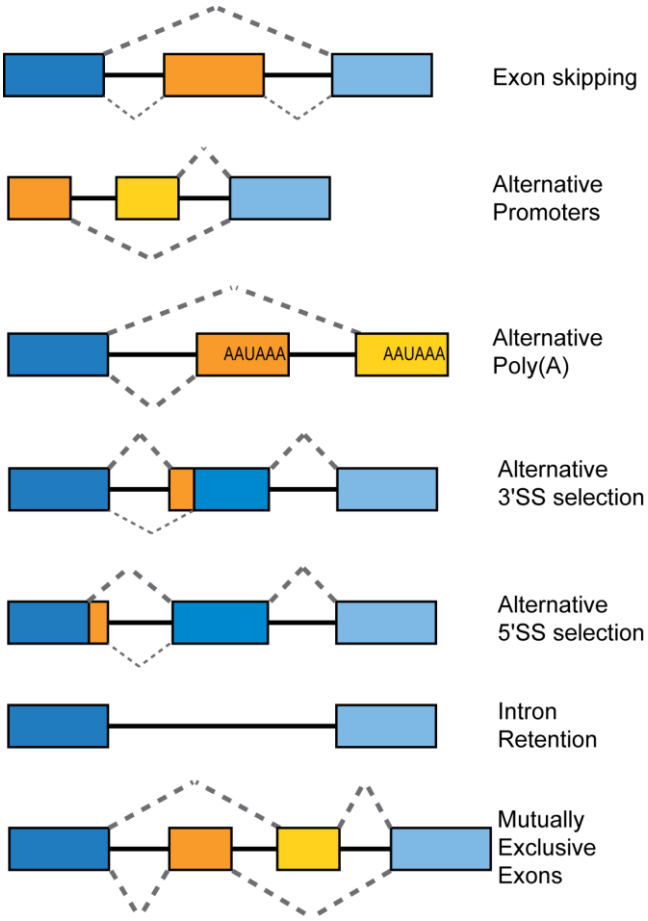

Figure 5. Forms of Alternative Splicing

The main forms of alternative splicing: exon skipping (and potential alternative promoters and alternative poly(A)), alternative splice sites, intron retention, and mutually exclusive exons. Adapted from (Keren et al., 2010).

Alternative Splicing

Over 95% of human genes with multiple exons undergo alternative splicing (Pan et al., 2008; Wang et al., 2008). Alternative splicing occurs more frequently as organisms become more complex and provides a greater variety of functions from a single gene (Keren et al., 2010). While different elements that modulate splicing have previously been discussed, alternative splicing falls into several categories (Figure 5).

The most common form of alternative splicing in higher eukaryotes is exon-

skipping. In this method, an exon is spliced out with its adjacent introns. These exons tend to be shorter, surrounded by longer introns, and have highly conserved regulatory splicing elements (Keren et al., 2010). While exon-skipping is most often associated with internal exons, it can result in alternative promoters or alternative poly(A) sites. Alternative promoters start transcription at different points to utilize different start codons within a gene. Alternative poly(A) ends transcription at different exons or different points in an exon and uses different poly(A) signals for each isoform (Keren et al., 2010).

The next most frequent form of alternative splicing is alternative 5′ss or 3′ss selection. In this method, there are multiple splice sites at the end of an exon, and which one used can vary. These alternative splice sites have also been suggested to be an early evolutionary stage for a skipped exon. The alternative signals often have weaker splice sites and more conserved flanking introns (Keren et al., 2010).

Intron retention occurs when a mature mRNA still contains one or more unspliced introns. While intron retention plays a regulatory role in plants (Braunschweig et al., 2014) and is common in lower metazoans, fungi, and protozoa, it was long thought to be relatively uncommon and non-regulatory in higher eukaryotes (Sibley et al., 2016). More recent studies suggest otherwise and will be described in more detail below.

Mutually exclusive exons are the least common forms of alternative splicing. In mutually exclusive exons, only one exon in a sequence of at least two exons can be included in the final spliced product.

Though improved depth of sequencing allows greater detection of alternative splicing events, it remains difficult to discern their function and causes. Often, the purpose of

alternatively spliced isoforms is only understood when they are linked to disease (Kornblihtt et al., 2013). However, given the complexity of alternative splicing, and that many signals that drive alternative splicing affect many genes simultaneously, it is difficult to discern the purpose of all alternative splicing events.

Intron Retention

Recent work demonstrates that intron retention is more common than previously thought. One study suggested that roughly one out of seven genes expresses a retained intron isoform (Galante et al., 2004), though a more expansive study that looked at a variety of cell types suggested that intron retention occurred in up to three out of four multiexonic transcripts (Braunschweig et al., 2014). Furthermore, roughly 50% of introns had the potential to be retained in 10% of their respective transcripts, and up to 9% of these introns were retained in 50% of their transcripts (Braunschweig et al., 2014). In addition, the frequency of intron retention is dependent on cell type; intron retention is more common in neural and immune cells, and less common in embryonic stem cells and muscle cells (Braunschweig et al., 2014). Overall, these data strongly suggest that intron retention is not just a splicing error, but a common, regulatory process.

Certain characteristics tend to promote intron retention. While no specific sequence has been identified connecting retained introns, these introns are often highly evolutionarily conserved (Boutz et al., 2015). In addition, the introns generally had weaker 5′ and 3′ splice sites, were shorter, more GC rich, and had a slight bias towards 3′ ends of transcripts (Boutz et al., 2015; Braunschweig et al., 2014; Sakabe and de Souza, 2007; Wong et al., 2013). Certain chromatin components, like H3K27ac and CHD2 association, were more enriched in retained

introns compared to those that were efficiently spliced (Braunschweig et al., 2014). Gene ontology analysis demonstrated that intron retention occurs in genes from a broad spectrum of biological processes, though it might occur more frequently in transcripts that are less important for the physiology of the cell as a way to reduce their levels (Boutz et al., 2015; Braunschweig et al., 2014).

While intron retention is common, studies on retained intron transcripts suggest that they can undergo multiple potential fates. Clk1, an SR protein kinase, expresses a retained intron isoform that stays in the nucleus, though upon treatment with CB19, a Clk1 inhibitor, the retained intron is spliced out to produce more mRNA (Boutz et al., 2015; Ninomiya et al., 2011). This example proposes a model in which the retained intron transcripts act as reservoirs for mRNA upon an inducing signal. In another example, retained intron transcripts in granulocytes were suggested to be exported to the cytoplasm and subject to nonsense mediated decay (NMD) (Wong et al., 2013). Finally, several studies have suggested that the retained intron transcripts remain nuclear and are degraded by the exosome machinery (Bergeron et al., 2015; Boutz et al., 2015; Bresson et al., 2015; Yap et al., 2012). Though it is unclear if degraded retained intron transcripts could be spliced upon some yet undiscovered stimulatory cue, the model of retained intron transcripts' degradation as a form of gene expression is consistent with the observation that many of the genes with retained introns are not necessary for the physiology of the cell (Braunschweig et al., 2014). Realistically, all of these models might be utilized, though what determines the fate of the retained intron transcripts is still poorly understood.

Our studies have characterized an additional regulated intron retention event in the gene MAT2A. Under conditions of high SAM, MAT2A expresses both a retained intron and a fully

spliced isoform. Under conditions of low SAM, MAT2A switches to just the expression of the fully spliced mRNA. The m^6A methyltransferase METTL16 helps to drive splicing upon low SAM levels through prolonged association with its m^6A consensus site near the retained intron. METTL16 also serves at the m^6A methyltransferase for the U6 snRNA. This discovery explains the mechanism used by MAT2A to change its gene expression in response to cellular SAM levels and identifies another m^6A methyltransferase.

CHAPTER THREE
Methodology

GENERAL PROCEDURES

Cell culture

HEK293 and HEK293T cells were grown at 37°C in DMEM (Sigma) supplemented with 10% FBS (Sigma), penicillin-streptomycin, and 2mM L-glutamate. 293A-TOA cells were cultured in the same conditions, but Tet-Free FBS (Atlanta Biologicals) was used instead. Methionine-free DMEM (Thermo Fisher 21013024) was additionally supplemented with 1mM sodium pyruvate and 0.4mM L-cysteine (Sigma). Due to SAM sensitivity of MAT2A splicing, care was taken to use fresh media so Met levels would not be depleted. When necessary, we supplemented Met and/or changed media, as specified for each assay.

Yeast strains

Haploid yeast strain agar stabs (ΔDuf890/SPAC27D7.08c and wild-type/ED666) were purchased from Bioneer. The ΔDuf890 strain was grown in YES media supplemented with 100µg/mL G418 at 30°C. Wild-type was grown in YES media without G418 at 30°C.

Transfection

Cells were transfected using TransIT-293 (Mirus) according to the manufacturer's protocol. For a typical 12-well transfection, 2µL of TransIT-293 was mixed with 40µL Opti-MEM (Thermo Fisher) and incubated for 5 minutes at room temperature. This mixture was then added to 800ng of DNA and incubated for 15 minutes before adding to cells. For the reporter assays, we generally used 30ng of β-globin reporter plasmid balanced with 770ng pcDNA3. METTL16

expression plasmids were added as indicated. In the MS2 reporter assays, 15ng of the β-globin reporter was used with 200ng of the MS2-METTL16 plasmid and 585ng of pcDNA3.

siRNA knockdown experiments

293A-TOA cells were transfected with 30nM siRNA for METTL16 knockdowns (15nM of siMETTL16-1 and 15nM of siMETTL16-2) and 20nM siRNA for MAT2A knockdowns (Thermo Fisher) using RNAiMax transfection reagent (Thermo Fisher) according to the manufacturer's instructions. Twenty-four hours following transfection, ~100% confluent cells were diluted to new plates to allow the cells to divide for an additional 72 hours (total 96 hour knockdown).

For puromycin-resistant rescue, we transfected HEK293T cells with siMETTL16-2 at 20nM. After 24 hours of knockdown, ~100% confluent cells were diluted to new 6-well plates to allow the cells to divide for an additional 72 hours. The next day, we transfected 1µg of siRNA Resistant FLAG-METTL16 plasmid (or pcDNA3-Flag control) with 1µg of pX459 of puromycin-resistance plasmid into the cells. 12 hours later, 3µg/mL of puromycin was added to the media. At 48 hours after plasmid transfection (96 hours of knockdown), we changed to +/- L-methionine media for 4 hours.

Cycloleucine

Cycloleucine (Sigma) was resuspended in H_2O at 300mM and added to cell media at a final concentration of 30mM.

CB19

CB19 was resuspended in DMSO at a concentration of 10mM and added to a final concentration of 10µM to cells.

Methionine depletion

For methionine depletion, cells were washed two times with Dulbecco's Phosphate Buffer Saline (PBS) with calcium chloride and magnesium chloride (Sigma). Media was then replaced with supplemented Met-free media. 100µM of L-methionine (Sigma) was supplemented as appropriate. Depletion typically occurred from 4-6 hours (specified in experiments).

SAM replacement by digitonin permeabilization

293A-TOA cells were grown to ~95% confluency in a 12-well plate. Cells were washed twice with PBS with calcium chloride and magnesium chloride. Media was then replaced with Met-free media supplemented with Met as indicated. After 4 hrs, cells were washed once with PBS with calcium chloride and magnesium chloride and 800µL of digitonin permeabilization solution (50mM HEPES pH7.0, 100mM KCl, 85mM sucrose, 3mM $MgCl_2$, 0.2% BSA, 1mM ATP, 0.1mM DTT, 10µg/mL digitonin)(Orzalli et al., 2015) was added to cells and supplemented with 100µM L-methionine or S-adenosylmethionine as appropriate. After 10 minutes, permeabilization solution was aspirated from cells, and Met-free media was reapplied to cells, supplemented to 100µM L-methionine or S-adenosylmethionine as appropriate. Cells were kept in this media for another 2 hours then harvested with Trizol.

Northern blotting

Northern blots were performed using standard techniques with RNA probes. The RNA probes were generated from PCR products with a T7 RNA polymerase promoter; primers are listed in Oligonucleotide Table below. Alternatively, probes were made from a digested plasmid. For some northern blots, 35–100 µg of total RNA were selected on Sera-Mag Oligo (dT)-Coated

Magnetic particles (GE Healthcare Lifesciences) to enrich for polyadenylated RNAs prior to gel electrophoresis.

Cell fractionation

For a 6-well plate, cells were trypsinized, pelleted for 3 min at 700 x g at 4°C, washed with cold PBS, and pelleted again. PBS was removed, and then pellets were resuspended in 100µL ice cold Buffer I (10mM Tris-HCl pH 8.0, 0.32M Sucrose, 3mM $CaCl_2$, 2mM magnesium acetate, 0.1mM EDTA, 0.5% Triton X-100, 4U RNasIn Plus (Promega), 1mM DTT) and incubated on ice for 5 min. Cells were then pelleted by centrifugation at 500xg at 4°C for 5 min. The supernatant was added to 1mL TriReagent (Molecular Research Center) for cytoplasmic fraction. The pellet was resuspended in Buffer I-150 (150mM NaCl, 10mM Tris-HCl pH 8.0, 0.32M Sucrose, 3mM $CaCl_2$, 2mM magnesium acetate, 0.1mM EDTA, 0.5% Triton X-100, 4U RNasIn Plus, 1mM DTT) and pelleted by centrifugation at 500xg at 4°C for 5 min. The supernatant was discarded. The pellet was resuspended in Buffer I and 1mL of TriReagent for the nuclear fraction.

Quantitative RT-PCR

RNA was harvested using TriReagent according to the manufacturer's protocol. Following extraction, RNA was treated with RQ1 DNase (Promega). Random hexamers were used to prime cDNA synthesis with MuLV reverse transcriptase (New England Biolabs). Real-time reactions used iTaq Universal SYBR Green Supermix (Biorad). Primers are listed in Oligonucleotide Table; if primer efficiencies are not listed they were assumed to be 100%.

Nuclear run-on assay

Nuclear run-ons were performed essentially as previously described (Stubbs and Conrad, 2015). For a more detailed protocol, please see Appendix A. Two 15cm plates of HEK293 cells at ~90% confluency were used per sample. Cells were incubated in media +/- L-methionine for 2 or 6 hours. Cells were trypsinized, quenched with ice-cold media, and pelleted at 700xg for 3 min at 4°C. Pellets were then rinsed with ice-cold PBS and collected by centrifugation. Cells were resuspended in 1mL HLB buffer (10mM Tris-HCl pH 7.5, 10mM NaCl, 2.5mM $MgCl_2$, 0.5% Igepal CA-630, 1mM DTT) and incubated on ice for 5 min. The solution was underlaid with 1mL HLB-Sucrose (10mM Tris-HCl pH 7.5, 10mM NaCl, 2.5mM $MgCl_2$, 0.5% Igepal CA-630, 1mM DTT, 10% Sucrose). The sample was centrifuged at 600xg for 5 min at 4°C. The supernatant was discarded. Nuclei were isolated and resuspended in an equal volume of transcription reaction buffer (10mM Tris pH 8.0, 90mM KCl, 5mM $MgCl_2$, 25% glycerol, 2.5mM DTT), and an NTP mix containing 4-thio-UTP or rUTP (10mM rATP, rGTP, rCTP, 40µM 4-thio-UTP/rUTP) was added. Transcription proceeded at 30°C for 5 min and the reaction was quenched with 1mL TriReagent. RNA was extracted, then biotinylated at room temperature in a solution of 10mM Tris-HCl pH 7.5, 1mM EDTA, 0.1% SDS, 0.2mg/mL Biotin-HPDP in dimethylformamide. Biotinylated RNA was extracted with chloroform three times, and then ethanol precipitated. Streptavidin selection was performed using 20µL of Dynal MyOne Steptavidin T1 bead slurry (Thermo Fisher) per sample. Beads were washed with MPG 1:10-I (100mM NaCl, 1mM EDTA, 10mM Tris-HCl pH7.5, 0.1% Igepal) and then blocked in the same buffer at 1mL/sample with 0.1µg/µL poly(A), 0.1µg/µL ssDNA, 0.1µg/µL cRNA, 0.1% SDS. Biotinylated RNA was resuspended in water and heated at 65°C for five minutes, then 950µL of blocked beads were added to each sample. Samples were nutated for one hour at room

temperature, and then washed with MPG 1:10-I, MPG 1:10 (100mM NaCl, 1mM EDTA, 10mM Tris-HCl pH7.5) at 55°C, MPG 1:10-I, three times with MPG-I (1M NaCl, 10mM EDTA, 100mM Tris-HCl pH7.5, 0.1% Igepal), MPG 1:10-I, twice with MPG-I no salt (10mM EDTA, 100mM Tris-HCl pH7.5, 0.1% Igepal), and MPG 1:10-I. Samples were eluted twice with MPG 1:10-I with 5% β-mercaptoethanol for five minutes, then PCA and chloroform extracted. Quantitative RT-PCR was used to evaluate the results.

4SU Quick Pulse

For the methionine depletion quick pulse experiments, media was changed on the cells the day before the experiment. The day off, the cells were washed twice with PBS, and Met-free media or Met-free media supplement with 100µM of methionine was added to the cells for one hour. Following, 100µM of 4SU was added to the cells and allowed to incubate for 5 minutes at 37°C. Cells were harvested with 5mL of TriReagent, the RNA was extracted, and 100µg of RNA was biotinylated and streptavidin selected for each sample as described above in the nuclear run on assay. Resulting RNA was reverse transcribed using SuperScript First-Strand Reverse Transcriptase (Thermo Fisher). Quantitative RT-PCR was used to evaluate the results.

For the CB19 quick pulse experiments, either a final concentration of 10µM of CB19 or an equal volume of DMSO was added to cells for one hour. 4SU was added to a final concentration of 100µM and allowed to incubate for 5 minutes at 37°C. Cells were harvested with 5mL of TriReagent, and RNA was processed as previously described.

For the METTL16 overexpression quick pulse experiment, 12µg of Flag-METTL16, PP185/186AA, F187G, or empty vector control was transfected into 10-cm plates of ~50% confluent cells. Two plates were transfected with Flag-METTL16 so one could serve as a -4SU

control. Media was changed at the end of the day. The next day, 100µM 4SU was added to all but the -4SU control plate and allowed to incubate at 37°C for 10 minutes. 5mL of TriReagent was then added to each of the plates, and RNA was processed as previously described.

4SU Pulse Chase

For 4SU pulse chase, 2µM of 4SU was added to the media for 3 hours. Media was then aspirated, cells washed with PBS, and new media without 4SU was applied. Before taking the time zero, cells were allowed to incubate in the new media for one hour to ensure complete 4SU incorporation. Media was then aspirated, cells washed twice with PBS, and either Met-free media or Met-free media supplemented with 100µM Met was added to the cells. Time points were harvested as indicated with TriReagent. RNA was extracted, equal RNA amounts were biotinylated, and streptavidin selected. Resulting RNA was run on a Northern blot and quantified.

Transcription Inhibition

ActD was added to a final concentration of 5µg/mL, and flavopiridol was added to a final concentration of 1µM. For hp mutant stability experiments, cell fractionation was performed as previously described at time points indicated, but only the soluble fraction was recovered.

RNase H Procedure

For 10µg of RNA, RNA pellet suspended in 10µL of water and 1µM of DNA oligonucleotide was added. The mixture was heated to 65°C for 5 min, then the heat block was allowed to slow cool to 37°C. 1x RNaseH Buffer (20mM Tris-HCl pH 7.5, 100mM KCl, 10mM $MgCl_2$), 10mM DTT, 8U RNaseIn Plus, 0.5U RNaseH (Promega) was added to the RNA mixture. This solution was incubated at 37°C for 1 hour. The reaction was quenched with 180µL

of G-50 Buffer (20mM Tris-HCl pH 6.8, 300mM sodium acetate, 2mM EDTA, and 0.25% SDS), phenol:chloroform:iso-amyl alcohol (25:24:1) (PCA) extracted, and ethanol precipitated. Oligonucleotides used are listed in Oligonucleotide Table.

Formaldehyde RIP

Formaldehyde RIP was performed as described in (Conrad, 2008) with a few changes. One 15-cm plate of ~95% confluent HEK293T cells was used for each sample. For crosslinked samples, PBS was supplemented with 0.1% methanol-free formaldehyde (Electron Microscopy Sciences), and 15mL of this solution was applied to the plates with gentle rocking for 10 min. Non-crosslinked samples underwent the same treatment with PBS lacking formaldehyde. The reaction was quenched with 1.875mL of 2M Glycine (pH 7.0) per plate. Cells were scraped, then centrifuged at 700xg for 3 min at 4°C. Cells were resuspended in 10mL of ice-cold PBS and centrifuged again. Pellets were resuspended in 1mL of ice-cold PBS, transferred to a microcentrifuge tube, centrifuged at 2400xg for 1min, and the PBS was aspirated. Pellets were resuspended in 400µL of RIPA-Plus Buffer (1% Igepal CA-630, 0.5% sodium deoxycholate, 0.1% SDS, 150mM NaCl, 50mM Tris-HCl pH 8.0, 2mM EDTA, 1x PMSF (Sigma), 1x protease inhibitor cocktail V (Fisher Scientific), 0.1µg/mL competitor RNA, 10U RNasIn Plus). DNA was sheared using a QIAShredder (Qiagen). Next, $CaCl_2$ was added to 5mM with 30U of RQ1 DNase and incubated for 15 min at 25°C. For RNA digestion, Micrococcal Nuclease (New England Biolabs) was diluted to 10 gel units/µL in RIPA buffer and 5µL of this freshly diluted 1:200 stock was added to the extract. RNA digestion proceeded at 25°C for precisely 10 min, after which 50µL of 300mM EGTA was added to stop the reaction. After clarification of the lysate by two successive centrifugation steps at 16000 x g for 10 min, the METTL16-RNA

complexes were immunoprecipitated overnight with anti-METTL16 or mouse IgG1 antibody. Twenty-five µL of washed Protein A Dynabeads (Invitrogen) were added to each sample for one hour the following day. Beads were washed once with ice-cold RIPA, then twice by adding RIPA-U (1% Igepal CA-630, 0.5% sodium deoxycholate, 0.1% SDS, 150mM NaCl, 50mM Tris-HCl pH 8.0, 2mM EDTA, 1M Urea) to the beads and nutating them for 10 min at room temperature, and once more with ice-cold RIPA. The beads were resuspended in 130µL of reverse buffer (10mM Tris-HCl pH 6.8, 5mM EDTA, 10mM DTT, 1% SDS) and heated for 45 min at 70°C. Proteins were digested by adding 150µL of a 2x proteinase K solution (0.2mg/mL Proteinase K, 40mM Tris-HCl pH 7.5, 5mM EDTA, 0.2mg/mL competitor RNA) followed by 30 min incubation at 37°C. Following digestion, the samples underwent PCA extraction and ethanol precipitation. The resulting RNA was used for quantitative RT-PCR.

Native RIP

Native RIP was performed based on the cell mixing experiments in (Conrad, 2008). One 15-cm plate of ~95% confluent HEK293T cells was used for each sample. Media was changed on the cells to +/- methionine for 6 hours prior to harvest. Cells were harvested by trypsin, quenched with media, and washed with PBS. Pellets were then resuspended in 400µL RSB100-T (10mM Tris-HCl pH 7.5, 100mM NaCl, 2.5mM $MgCl_2$, 0.5% Triton X-100) supplemented with protease inhibitors and RNasIn Plus. Next, $CaCl_2$ was added to 5mM with 45U of RQ1 DNase and incubated for 15 min at 25°C. For RNA digestion, Micrococcal Nuclease was diluted to 10 gel units/µL in RIPA buffer and 10µL of this freshly diluted 1:200 stock was added to the extract. RNA digestion proceeded at 25°C for precisely 10 min, after which 50µL of 300mM EGTA was added to stop the reaction. After clarification of the lysate by centrifugation at 10000

x g for 10 min, the METTL16-RNA complexes were immunoprecipitated for 1 hour with anti-METTL16 or IgG1 antibody. Twenty microliters of washed Protein A Dynabeads were added to each sample for 1 hour. Beads were then washed with ice-cold RSB100-T five times and then eluted with a proteinase K solution (0.1mg/mL Proteinase K, 0.1% SDS, 20mM Tris-HCl pH 7.5, 5mM EDTA, 0.1mg/mL competitor RNA) for 30 min at 37°C. Following digestion, the samples underwent PCA extraction and were ethanol precipitated. The resulting RNA was then used for quantitative RT-PCR.

For anti-Flag native RIP, we transfected one 10-cm plate per sample 24 hours before experiments. Media was changed to Met-free media for 2-3 hours before harvesting. Forty microliters of Anti-Flag M2 affinity gel (Sigma A2220) was used to immunoprecipitate each sample. The remaining procedure was performed as described, with volumes scaled accordingly. For the experiments in Figure 13B, 6μg of Flag-tagged METTL16 (or pcDNA-FLAG) and 6μg pcDNA3 constructs were transfected. For the experiments in Figure 13F, 7.5μg of FLAG-METTL16 (or pcDNA-FLAG) and 2.5μg of either β-MAT-hp1-6 A4G or β-MAT-WT were transfected as indicated. In addition, the experiments in Figure 13F omitted the MNase treatment.

M^{6}A IP and m^{6}A-seq

RNA samples were either total RNA or poly(A)-selected RNA using manufacturer's protocol of Sera-Mag Oligo (dT)-Coated Magnetic particles. In some cases, samples were RNase H treated. After precipitation, the RNA pellet was resuspended in 20μL of water, 130μL of IP Buffer (10mM Tris pH 7.5, 150mM NaCl, 0.1% Igepal), 0.5μL RNasin Plus, and 1μg of anti-m^{6}A or IgG1 antibody. Samples were nutated for 1 hour at 4°C. 15μL of washed Protein A Dynabeads were added to each sample and nutated for an additional hour. Beads were washed

three times with IP buffer. Bound RNA was eluted by adding 200µL of G-50 buffer and 0.1mg/mL Proteinase K (Fisher Scientific) and heated to 37°C for 1 hour. Samples were then PCA extracted and ethanol precipitated.

M^6A-seq was performed as previously described (Dominissini et al., 2013) with the following modifications. On day 3 of knockdown in 293A-TOA cells, we added fresh media supplemented with an additional 200µM of methionine. On day 4 of knockdown, we changed to fresh media supplemented with an additional 200µM for 6 hours. After RNA extraction, 300µg of total RNA from siCtrl or siMETTL16-1,2 treated cells was poly(A)-selected using Sera-Mag Oligo (dT)-Coated Magnetic particles. The RNA was fragmented for 5 min in fragmentation buffer and ethanol precipitated. The RNA pellet was resuspended in 100µL of water, and 5µL was removed as an "input" sample. Immunoprecipitation conditions were used as previously described, except we adjusted the total volume to 500µL. One hundred microliters of washed and pre-blocked Protein A Dynabeads were added and incubated according as previously described. Beads were washed according to (Dominissini et al., 2013). To elute, 250µL of G-50 buffer with 0.1mg/mL of Proteinase K was added to beads and incubated for 1 hour at 37°C. G-50 buffer was then removed to another microcentrifuge tube. Beads were washed once with an additional 250µL of G-50 buffer, and this was added to the previous elution. Samples were then PCA extracted, chloroform extracted, and ethanol precipitated. The resulting RNA constitutes the "pellet" samples. Sequencing libraries and sequencing were performed by the DNA Sequencing Center at Brigham Young University. Sequencing of the 12 samples (3 biological replicates, inputs and pellets, for siCtrl and siM16) was performed on 2 lanes an Illumina - HiSeq High-Output v4 - PE 125 Cycle with paired ends and a read length of 2 x 125 bases.

For evaluation of candidates through quantitative RT-PCR, a similar procedure was performed, though modified as specified. On day 3 of the knockdown, siRNA-treated cells were transfected with 12µg pcDNA3 or Fl-MAT2A. Six hours later, we replaced the media and supplemented with an additional 200µM of methionine. On day 4 of knockdown, we changed to fresh media supplemented with an additional 200µM for 6 hours. We used 150µg per sample and scaled the previously described m^6A IP procedure. Inputs and pellets were then analyzed by quantitative RT-PCR.

M^6A-seq Data Processing

Reads mapping and genomic coverage, gene FPKM calculation

Raw reads were aligned to the human reference genome hg38 using the bwa (v 0.7.9a-r786) aligner with default settings. Only uniquely mapped reads were kept for further analysis. For each pair, the reads were connected from the start of read1 to the end of read2 and the whole region was used for gene coverage in a strand-specific fashion. Input samples were used for calculating gene expression level (FPKM) using StringTie (v1.1.2). All the genes with average FPKM less than 1 in siCtrl sample were removed.

M^6A peak calling and identification of METTL16-dependent peaks

To search for enriched peaks in the m^6A pellet samples, we scanned each remaining gene region (including intron) using sliding windows of 100 nucleotides with 50 nucleotides overlap, and the average coverage of each window was calculated and the data were filtered at four additional steps. First, we kept windows with coverage of ≥20 in at least two of the three replicates of the m^6A pellet (siCtrl). For the remaining windows, for each of the three replicates we independently calculated the window coverage normalized to corresponding mean FPKM for

that gene in the corresponding input samples. We then averaged the normalized values for each independent replicate to generate the average normalized values for the remaining windows for each of the four samples. These average normalized window values were the basis of all subsequent filtering steps. In the second filtering step, we identified all potential m^6A peaks, by including only those windows that had a ratio of m^6A pellet (siCtrl) to input (siCtrl) of ≥2. Third, to select peaks that were lost upon METTL16 knockdown, we then eliminated all windows that had a ratio of m^6A pellet (siCtrl) to m^6A pellet (siM16) ≤3. Fourth, to exclude false positives that resulted low coverage in the siM16 input compared to siCtrl input, we removed windows in which input siCtrl compared to input siMETTL16 was ≥1.5. We merged the remaining windows to identify peak candidates and re-calculated the average normalized values for the merged peaks (Table S1).

Peak annotation

BedTools (v2.26) were used to get intersection of peaks and genome features. When a peak overlaps with multiple features, the feature were selected using this priority:

Coding CDS exon and intron junction > Coding CDS exon > UTR3 > UTR5 > Coding intron > Noncoding exon > Noncoding_intron > Intergenic

Purification of rM16-MTD

Rosetta (DE3) cells (EMD Millipore) were transformed with SUMO-M16-MTD expression plasmid and selected in chloramphenicol and kanamycin. Colonies were inoculated into a 2mL starter culture and grown at 37°C overnight. The next day, the culture was diluted into 200mL fresh LB media with antibiotics and grown to mid-log phase (O.D.≈0.5). IPTG was added to 1mM to induce protein expression and the cultures were grown overnight at 18°C. Bacterial

pellets were harvested by centrifugation at 4000 x g for 10 min and the pellets were resuspended in 1mL lysis buffer (300mM NaCl, 50mM NaH_2PO_4, 0.5% Triton X-100, pH 8.0) supplemented with 0.5mM PMSF. Approximately 2mg lysozyme was added and the mix was incubated on ice for 30 min. Subsequently, benzonase (Sigma) was added to 0.25U/µL and the mix was nutated for 30 min at room temperature. The lysate was cleared by centrifugation at 10000 x g for 30 min at 4°C and then nutated with Ni-NTA agarose beads (Qiagen) for 1 hr at 4°C. The beads were washed with ten column volumes of wash buffer (300mM NaCl, 50mM NaH_2PO_4, 10mM imidazole, 0.5% Triton X-100, pH 8.0) supplemented with 0.5mM PMSF. Proteins were eluted by addition of His elution buffer (300mM NaCl, 50mM NaH_2PO_4, 250mM imidazole, pH 8.0). Glycerol was added to 10% and aliquots of the protein were stored at -80°C.

***In vitro* methylation assays**

Generation of Hela nuclear extracts and methylation assays in nuclear extract were previously reported (Dignam et al., 1983; Shimba et al., 1995). Excluding contributions from nuclear extract, each 25µL methylation reaction contained 10mM HEPES (pH 7.9), 10mM $MgCl_2$, 160mM KCl, 5mM SAM (Sigma), 20µM ATP, 20U RNAsin Plus, ~10nM substrate (see below). The reactions also contained 50% nuclear extract in Buffer D (20mM HEPES [pH 7.9], 20% glycerol, 50mM KCl, 0.2mM EDTA, 0.5mM DTT). After incubation at 30°C for 1 hr, the reactions were stopped by addition of 200µL G-50 buffer supplemented with 0.1 mg/ml Proteinase K and 15µg Glycoblue (Thermo Fisher), and incubated for an additional 30 min at 37°C. RNA was harvested by standard PCA extraction and ethanol precipitation. RNA pellets were resuspended in 3µL of Nuclease P1 mix (30mM sodium acetate [pH 5.2], 0.33U/µL nuclease P1 [Sigma]) and incubated at 37°C for 2 hr. Digested nucleotides were separated

overnight on a cellulose thin layer chromatogroaphy (TLC) plate (Merck) in a solution of isopropanol:HCl:H_2O (70:15:15 by volume) (Liu et al., 2013). The plate was air dried at room temperature and exposed to Phosphorimager for detection and quantification.

Immunodepletion assays were performed as described for the nuclear extract except the extract was subject to immunoprecipitation with either anti-METTL16 or anti-Flag antibodies prior to the assay. To do so, 70µL of nuclear extract plus 0.1% Igepal-CA630 was incubated with 2-3µg of antibody for 1.5 hr at 4°C while nutating. The mix was added to 20µL of washed protein A beads (Pierce) and nutated at 4°C for an additional 1.5 hr. After careful removal from beads, the resulting supernatant was used in place of nuclear extract in a methylation reaction as described above. The beads were washed 3-5 times with Buffer D (lacking DTT) supplemented with 0.1% Igepal and resuspended in 25µL of Buffer D. This resuspended bead mix was used in place of nuclear extract in a methylation reaction as described above.

For assays with recombinant METTL16, a standard 25µL reaction contained final concentrations of 10mM HEPES (pH 7.9), 10mM $MgCl_2$, 150mM KCl, 5mM SAM, 20U RNasIn Plus, ~10nM substrate (see below), excluding contributions from 12.5µL of recombinant protein (1-5µg) in His elution buffer. Methylation of U6 substrates was significantly more salt and magnesium-sensitive than hp1 reactions. For U6 substrates, KCl and $MgCl_2$ were omitted from the reaction. Reactions were incubated at 30°C for 2 hr. The reaction was stopped as described for nuclear extracts except Proteinase K digestion was omitted. Methylation was assessed by TLC of digested nucleotides as described for the nuclear extract assays.

RNA substrates for in vitro methylation assays

Uniformly labeled substrates were generated by incorporation of α-^{32}P-ATP into standard in vitro transcription assays using PCR templates with T7 RNA polymerase promoters. To generate the PCR templates for these substrates we used primers NC2207 and NC1752 for hp1, NC2212 and NC2213 for U6, NC2317 and NC2318 for the METTL3 substrate, NC2742 and NC2743 for GNPTG, NC2744 and NC2745 for GMIP, NC2746 and NC2747 for INPPL1, NC2748 and NC2749 for PTBP1, and NC2750 and NC2751 for PP1R37 (Oligonucleotide Table). To make site-specific radiolabelled substrates, we performed splint ligation (Moore and Query, 2000) using synthesized RNA oligomers (Sigma) and DNA splints (Oligonucleotide Table). Unless otherwise specified, hp1 substrates used NC2535 as the DNA splint. U6 substrates were generated using 3-piece splint ligation. After ligation and DNase treatment, the substrates were gel purified on 6% urea-PAGE and eluted overnight in G-50 buffer. The substrates were then PCA extracted, precipitated and resuspended in water. For nuclear extract experiments, all substrates were heated to 65°C for 5 min and placed on ice immediately prior to their addition to reactions. For recombinant assays, hp1 substrates were heated to 65°C in water and slow cooled in a heat block to ~37°C. U6 RNA substrates were heated to 65°C in 50mM NaCl and slow cooled in a heat block to ~37°C. Of note, hp1 substrates were methylated under a variety of folding conditions, whereas U6 RNA substrates were more dependent on the specific folding conditions.

Ratio of N^6-methyladenosine to adenosine

We treated 50µg of RNA with RQ1 DNase for 1 hour at 37°C. The reaction was quenched with EDTA, then the RNA was PCA extracted and ethanol precipitated. RNA was then resuspended in 103.5µL and digested by adding 7µL of Acidic buffer (0.1M Sodium Acetate,

20mM $ZnCl_2$ at pH 6.8), 5µg RNase A (Thermo Fisher), 3U Nuclease P1 for 4 hours at 37°C. After, 7µL of Basic Buffer (0.3M sodium acetate pH 7.8), 2U calf intestine phosphatase (New England Biolabs), and 0.0005U of Phosphodiesterase I (Sigma) were added. Reaction was incubated overnight at room temperature. Sample was then applied to an Amicon Ultra 10K MWCO column (Millipore) and centrifuged at 16000 x g for an hour. Flow through sent to mass spectrometry.

Nucleosides were detected essentially as described by Laxman et al. with minor modifications (Laxman et al., 2013). The RNA digest was first separated on a Synergi Fusion-RP column (4µm particle size, 80 Å pore size, 150 mm x 2 mm, Phenomenex) using a Shimadzu high performance liquid chromatography machine (HPLC) and simultaneously analyzed by a triple quadrupole mass spectrometer (3200 QTRAP, ABSCIEX). The total run time was 25 min at a flow rate of 0.5 ml/min, with 5mM ammonium acetate (pH 5.5) in water as Solvent A and 5mM ammonium acetate in methanol as Solvent B. The following gradient elution was performed: 0.01 min, 0% B, 4 min, 0% B, 5 min, 0.2% B, 6 min, 1% B, 7 min, 3% B, 8 min, 5% B, 14 min, 25% B, 16 min, 50% B, 18 min, 100% B, 22 min, 100% B, 23 min, 0% B, 25 min, 0% B. N6-methyladensoine and adenosine were detected by multiple reaction monitoring (MRM) using the ion pairs 282/150 and 268/136, respectively. N^6-methyladensoine was quantified using the Analyst® 1.6.1 Software package by calculating the total peak area and normalized by that of adenosine. For each experiment, authentic pure standards were injected and analyzed alongside samples.

SAM Metabolite Extraction

Procedure was adapted from published protocols (Dettmer et al., 2011; Tu et al., 2007). In a 6-well plate, cells were washed 3 times with ice-cold PBS and 600µL of 80% methanol was added to cells. The plate was chilled on liquid N_2 for 30 seconds and moved to ice to scrape the cells. The cell/methanol solution was transferred to Eppendorf tubes and flash frozen in liquid N_2. The tubes were thawed and centrifuged at 16000 x g at 4°C for 10 min. Methanol supernatants were then transferred into new Eppendorf tubes. Cell pellets were washed with PBS, resuspended in RSB100-T and 1x SDS Buffer (2% SDS, 62.5mM Tris-HCl pH 6.8, 10% glycerol, 1% β-mercaptoethanol), and sonicated. Protein concentration was calculated to estimate cell number between samples, and methanol supernatant volumes were adjusted accordingly. A speed vacuum was used to dry pellets. Pellets were then resuspended in Solvent A (0.1% formic acid in water), centrifuged twice, and passed through a 0.2µm PVDF filter to remove insoluble particulates. Samples were analyzed using the same LC-MS/MS system as described above. The total run time was 20 min at a flow rate of 0.5 ml/min, with 0.1% formic acid in water as Solvent A and 0.1% formic acid in methanol as Solvent B. The following gradient was performed: 0.01 min, 0% B, 4 min, 0% B, 11 min, 50 % B, 13 min, 100% B, 15 min, 100% B, 16 min, 0% B, 20 min, 0% B. SAM was detected by multiple reaction monitoring (MRM) using the ion pair 399/250, quantified using the Analyst® 1.6.1 Software package by calculating the total peak area, and normalized by the total ion count (TIC). For each experiment, authentic pure SAM was injected and analyzed alongside samples.

Yeast RNA Preparation

RNA was harvested from yeast in exponential growth phase (O.D.≈0.7) using the protocol described in (Schmitt et al., 1990). Briefly, yeast were harvested by centrifugation and then

resuspended in 400µL of AE buffer (50mM sodium acetate pH 5.3, 10mM EDTA). 20µL of 20% SDS was then added and the sample was vortexed. An equal volume of phenol pre-equilibrated with AE buffer was then added and mixed by vortexing. The samples were incubated at 65°C for 5 min and then chilled rapidly in a dry ice-ethanol bath. Samples were then centrifuged at max speed, and the aqueous layer was transferred to a new microcentrifuge tube. The sample was then PCA extracted and ethanol precipitated.

U6 RNA immunoprecipitated nonspecficially presumably through interactions with other methylated RNAs. To reduce this background signal, we purified U6 and U2 RNAs by gel purification prior to immunoprecipitiation. To do so, 30µg of total RNA was run on a 6% Urea Gel and bands from 90-110bp and 180-200bp were excised and incubated in G-50 buffer. The RNA was then PCA extracted and ethanol precipitated. Resulting RNA was cleaved with RNase H using specified oligonucleotides (*S. pombe* U6 5′, *S. pombe* U6 3′, *S. pombe* U2 5′) against U6 RNA or U2 RNA in order to disrupt RNA secondary structures that interfered with m^6A antibody recognition. M^6A IP was subsequently performed as described above.

Plasmids

To construct β-MAT-WT, the 3´ end of MAT2A gene was amplified using NC1145 and NC1146 (Oligonucleotide Table). All restriction enzymes were purchased from New England Biolabs. The PCR product was digested with EcoRI and BglII and inserted into the βΔ1(B-A) plasmid (Conrad et al., 2006) cut with the same enzymes using standard techniques. Importantly, all plasmids generated by PCR were sequence verified across the junctions and PCR insert.

The β-MAT-hp2-6m9 insert was ordered from GENEWIZ and digested with BsiWI and BglII and inserted into the β-MAT-WT cut with the same enzymes.

Deletion and mutations of MAT2A were made using SOEing PCR (Horton, 1995) with β-MAT-WT as the template, except β-MAT-hp1-6m9, which used β-MAT-hp2-6m9 as a template. In all cases, NC1576 was used as the 5′ primer and Sp6+ was used as the 3′ primer. β-MAT-Δhp1 used primers NC1653 and NC1654. β-MAT-hp1m9 used primers NC2014 and NC2015. β-MAT-hp1G3 used primers NC2137 and NC2138. β-MAT-hp1G4 used primers NC2203 and NC2204. β-MAT-hp1G4, 1xMS2 used primers NC2674 and NC2675. β-MAT-hp1U9 used primers NC2307 and NC2308. Inserts were then digested EcoRI-HF and XhoI and inserted into the β-MAT-WT cut with the same enzymes.

FL-MAT2A was generated by amplification of fully spliced MAT2A cDNA with NC1566 and NC1567. The PCR product was digested and ligated into pcDNA3-Flag cut with EcoRI and XhoI.

FLAG-tagged METTL16 was generated by amplification of fully spliced METTL16 cDNA with NC2425 and NC2426. The PCR product was digested and ligated into pcDNA3-Flag cut with BamHI-HF and XhoI. Si-resistant FLAG-METTL16 was amplified from the previous plasmid using SOEing PCR with the previous primers and NC2521 and NC2522. Mutations of METTL16 were made with SOEing PCR with si-resistant FLAG-METTL16 as the template with the primers NC2513 and NC2514 for PP185/186AA and NC2515 and NC2156 for F187G. Inserts were then digested BamHI-HF and XhoI. MS2-METTL16 and MS2-F187G were generated by digesting either FLAG-METTL16 or FLAG-F187G with BamHI-HF and XhoI. The insert was then ligated into the pcNMS2-NLS-Flag vector cut with the same restriction enzymes. MS2-M16 MTD was generated using primers NC2425 and NC2502 with FLAG-METTL16 as the template. MS2-M16 VCR was generated using primers NC2807 and NC2426

with FLAG-METTL16 as the template. Both were digested with BamHI-HF and XhoI and then ligated into the pcNMS2-NLS-Flag vector cut with the same restriction enzymes. The NMS2-Fl-hnRNP C1 construct was generated by inserting the hnRNP C1 coding sequence amplified with NC257 and NC258 into pcNMS2 using restriction enzymes BamHI and NotI.

The rM16-MTD expression plasmid was generated by amplification of fully spliced METTL16 cDNA with NC2499 and NC2502. The PCR product was digested and ligated into pE-SUMO cut with BsaI and XbaI. The mutations of this were made by using the same primers, but amplifying from the FLAG-tagged PP185/186AA and F187G plasmids.

Quantification and Statistical Analysis

Imagequant 5.2 was used to quantify northern blots. Bands were boxed, and equal size boxes were placed along the respective columns at sites of similar background. The signal from the background box was then subtracted from the signal from the sample box to quantify real signal.

Image Studio Ver 3.1 was used to quantify western blots. Bands were selected using the "Add Rectangle" feature, and background was automatically subtracted.

Each experiment was performed with a minimal of three biological replicates and the replicate number is given in the figure legends. Mean and standard deviation were calculated as indicated. For most experiments, statistical analyses used unpaired, Student's t-tests to test significance. For the m^6A-seq candidate/non-candidate experiments, p-values were determined with the Wilcoxon test. Where indicated, ns = not significant, * $p \leq 0.05$, ** $p \leq 0.01$, *** $p \leq 0.001$. In some cases, daggers (†) are used in place of asterisks to differentiate between comparisons with two different reference groups.

Data and Software Availability

The m^6A-seq data has been deposited to the NCBI GEO database under the accession number GSE90914.

Table 1. Quantitative RT-PCR Oligonucleotides

Quantitative RT-PCR oligonucleotides		
Target	Sequence	Efficiency
7SK Forward	TAAGAGCTCGGATGTGAGGGCGATCTG	94%
7SK Reverse	CGAATTCGGAGCGGTGAGGGAGGAAG	
MAT2A exon 1-3 Forward	CCACCCAGATAAGATTTGTGACC	95%
MAT2A exon 1-3 Reverse	GATGTAATTTCCCCAGCAAGAAG	
MAT2A exon 8-9 Forward	TCAGAAGAGTGAGAGAGAGCTAT	97%
MAT2A exon 8-9 Reverse	CCATAGGCTGCAGTCCTC	
MAT2A Intron 8 Forward	AAGTGGGTTGCTCAAGGTTT	90%
MAT2A Intron 8 Reverse	CCTGGCTCAACAAATACGAA	
MAT2A Exon 6 Forward	TGCGAAATACCTTGATGAGG	86%
MAT2A Exon 6 Reverse	AGGCCCACCAATAACAAATC	
MAT2A Intron 1 Forward	TTTCTGCCCTTAGGATGACC	72%
MAT2A Intron 1 Reverse	CAAGATCCTGGGTTTGTCCT	
MAT2A Hairpin 1 Forward	CATGGGAAGTGCCCAAAAAG	89%
MAT2A Hairpin 1 Reverse	CAGAGCTTGAAGGCTTCTCT	
MAT2A Hairpin Cluster Forward	ATTCTGGGGTATGGCGTAAG	94%
MAT2A Hairpin Cluster Reverse	TAAAAGCTGCCATCTGAGGT	
MALAT1 Forward	CCAGGTGCTACACAGAAGTG	99%
MALAT1 Reverse	TCTGCTGCTGTCTTCCTAGA	
β-Actin Forward	TCGTCCACCGCAAATGC	100%
β-Actin Reverse	TCAAGAAAGGGTGTAACGCAACT	
GAPDH Forward	AGCCTCAAGATCATCAGCAATG	81%
GAPDH Reverse	ATGGACTGTGGTCATGAGTCCTT	
METTL16 #1 Forward	TGGTATTTCCTCGCAACAGA	82%
METTL16 #1 Reverse	AAGAGCATCCATCAGGAGTG	
METTL16 #2 Forward	ACAGAAGACACTCCTGATGG	86%
METTL16 #2 Reverse	TTAACAGAACTAGGCGGAGG	
U1 Forward	CCATGATCACGAAGGTGGTTT	82%
U1 Reverse	ATGCAGTCGAGTTTCCCACAT	
U6 Forward	GCTTCGGCAGCACATATACTAAAAT	82%
U6 Reverse	CGCTTCACGAATTTGCGTGTCAT	
GNPTG Forward	GGAGTTTGTGACCTTGTGG	100%
GNPTG Reverse	GCTTCTCTGTAGGGCTCTC	
GMIP Forward	TGGCTTGCTAAAAGATGACTCC	95%
GMIP Reverse	GAAGTGGCCACGAGACTGT	
INPPL1 Forward	AACTCAGTGGGCGACCG	85%
INPPL1 Reverse	TAGGCTAGTTTGGAGGTGGTGT	
PTBP1 Forward	GTGAACTCGGTCCAGTCG	98%

PTBP1 Reverse	GGTCACAGGGTAGAAGAGGT	
PPP1R37 Forward	CCTCAAGGTGAACCACTCAC	95%
PPP1R37 Reverse	TCTTTCTTGGGTTCACGGTC	
MAN1B1 Forward	CCAGCAGACAGGCACAACC	
MAN1B1 Reverse	ACGCGGTACAGGTAGAACAGG	
ARAP1 Forward	CTGTCGGAGCAGCAGCTTG	
ARAP1 Reverse	GTCCACACAGCGGTACACGA	
WDR90 Forward	GCACAGACCTATGGCTGGCT	
WDR90 Reverse	GGTGGCAGGCATTGGGAAAC	
IFRD2 Forward	GCATGGGCTGACTGGAAAGC	
IFRD2 Reverse	AGCTCCTCACCCTTAGGTCCA	
FBXW5 Forward	GCATTGGACAGGGACCCTCA	
FBXW5 Reverse	GGTCATCTGGTGTGGCAGGA	
ANKRD13D Forward	GCCGTGTCTCTGGGAAACCT	
ANKRD13D Reverse	CCCACGTTGGCATTGTGTCG	
TRAF7 Forward	CCTCCCAGGTGTGGGACATT	
TRAF7 Reverse	TGGTCTGGCGTCGAGATGAC	
DGKZ Forward	ACCCACAGAGGCAACTCAGG	
DGKZ Reverse	CACCAGCACAGGCCTGAAAC	
CORO1B Forward	GGTGGCAGTACGTGGCTCT	
CORO1B Reverse	GCTCAAGGTCCTGGGCCTATC	
MAZ Forward	ACGAGAAGCCCTACCAGTGC	
MAZ Reverse	GTGGTAGCTCATGCGGTCCT	
XIST Forward	GGCAGAAGGTGGAAGGCTCA	
XIST Reverse	GGTCCAATTCAGGCCACCCT	
EEF2 Forward	CACAGCACCACGTCCTCGAA	
EEF2 Reverse	CGCTGTGTCGGGACAGTCT	
GLO1 Forward	GGGTCCCGTCGTCTGTGATA	
GLO1 Reverse	CGTCGGAGCAGCAACTGAG	
PARK7 Forward	AGGTGGCGGCTCAAGTGAAG	
PARK7 Reverse	GGATTCCTAACGGCCTGTTTCTCT	
PCBP1 Forward	TGACCACGTAACGAGCCCAA	
PCBP1 Reverse	CTTTCAGTCACACCGGCATCC	
DHCR24 Forward	ACGTGTGAGTGGTCAGGCAT	
DHCR24 Reverse	CCTGGAAGCCAGGAGGAAGG	
β-globin ex1:ex2 Forward	GGGCAAGGTGAACGTGGATG	
β-globin ex1:ex2 Reverse	GAGGTTGTCCAGGTGAGCCA	
β-globin ex2:ex3 Forward	AAGCTGCACGTGGATCCTGA	
β-globin ex2:ex3 Reverse	GCACACAGACCAGCACGTTG	
18s rRNA Forward	GGAGTATGGTTGCAAAGCTGA	96%
18s rRNA Reverse	ATCTGTCAATCCTGTCCGTGT	
Clk1 Exon 3 Forward	TCACATCGTCGTTCACATGG	
Clk1 Exon 5 Reverse	CCAAAAGCTCCTTCACCTAAAG	

Clk1 Intron 3 Reverse	AATTCAAGTTTCCCTGTTCCACA	
Clk1 Intron 4 Forward	TGTTTCCACTTCTTGATATGACTGA	
Clk1 Exon 5-6 Forward	TCGATCATAAAGCGGGAGGT	
Clk1 Exon 6 Reverse	GCGAGCAGCTTCACAGTATC	
Clk1 Intron 5 Forward	ATTGAGCATCATGTCTGTCATTCT	

Table 2. Northern Probe oligonucleotides

Northern Probe oligonucleotides	
Target	Sequence
MAT2A Gene Body T7	ATGAACGGACAGCTCAACGGC
	TAATACGACTCACTATAGGGACTTGGCTGTAGGTGGTAGAT
MAT2A 3' UTR T7	TGCACGTAAAGTACTTGTAGTTC
	TAATACGACTCACTATAGGGTGTTGGAATTGAGAACCAGACA
MAT2A Hairpin 1 T7	GCTTAAATATTGAAAGTGTTAGCCTTT
	TAATACGACTCACTATAGGGCAGGAAAATTTAGGAAGGAGGG
MAT2A Hairpin 1 DNA Probe	CAGAGCTTGAAGGCTTCTCTGTAGCCTACGCCAACAAGTCTGG GGAAAAA
MAT2A Retained Intron	GTCTTCCAACTGATTTGACTTCCACAGATCCAGCCAAACATCAT TTGCCAGAGCTCTTGA
	TAATACGACTCACTATAGGGCACTTTCAATATTTAAGCTTTTTG GGC
Human U6 DNA Probe	CGTGTCATCCTTGCGCAGGGGCCATGCTAATCTTCTCTGT
S. pombe U6 DNA Probe	GTCATCCTTGTGCAGGGGCCATGCTAATCTTCTCTGTATCGTTTC AATTT
S. pombe U2 DNA Probe	AACAGATACTACACTTGATCTAAGCCAAAA
GAPDH T7	CCTGCCGTCTAGAAAAACCTG
	CGCGTAATACGACTCACTATAGGGGGTTGAGCACAGGGTACTT TA

Table 3. RNaseH Oligonucleotides

RNaseH Oligonucleotides	
Target	Sequence
MAT2A Hairpin 1	CTTTTTGGGCACTTCCCATG
	CAGGAGCTGAAAGAGGACAGGAAAATTTAGGAAGGAGG
MAT2A 3′ UTR	TAACACTTTCAATATTTAAG
	AGCATAAGCACCAGGGAGAT
S. pombe U6 3′	GTGATCCGAAGATCATCAGAAA
S. pombe U6 5′	GGGTTTTCTCTCAATGTCGCAGT
S. pombe U2 5′	CCAAAAGGCCGAGAAGCGAT

Table 4. *In vitro* transcribed RNA

***In vitro* transcribed RNA**		
Target		Sequence
T7 MAT2A HP1	NC2207	TAATACGACTCACTATAGGGTGTTAGCCTTTTTTCCCCA
	NC1752	GGAAGGAGGGCCCTTTCCCT
T7 MAT2A HP1 Mut	NC2207	TAATACGACTCACTATAGGGTGTTAGCCTTTTTTCCCCA
	NC1752	GGAAGGAGGGCCCTTTCCCT
T7 U6	NC2212 NC2213	TAATACGACTCACTATAGGGGTGCTCGCTTCGGCAGCACA
		AAAATATGGAACGCTTCACG
T7 m^6A Consensus Sequence	NC2317	TAATACGACTCACTATAGGGACGAGTCCTGGACTGAAACGGACTTGTCCC
	NC2318	GGGACAAGTCCGTTTCAGTCCAGGACTCGTCCCTATAGTGAGTCGTATTA
T7 GNPTG	NC2742	TAATACGACTCACTATAGGGAGTTTGTGACCTTGTGGTG
	NC2743	CTCTGAGCACAAGCCTGGTC
T7 GMIP	NC2744	TAATACGACTCACTATAGGGAAGGTGAGTATGTTAGAGAGA
	NC2745	CGGCTGAAGTGGCCACGAGAC
T7 INPPL1	NC2746	TAATACGACTCACTATAGGGACAGTGACCATACCCCATGA
	NC2747	TAGTTTGGAGGTGGTGTGTGAG
T7 PTBP1	NC2748	TAATACGACTCACTATAGGGCGGACCCCAGCAGC
	NC2749	GACTGGACCGAGTTCACCG
T7 PPP1R37	NC2750	TAATACGACTCACTATAGGGTGAGACTGGACCTTCGGGAG
	NC2751	CTGCAGGACCGTCCCCT
NC2742		TAATACGACTCACTATAGGGAGTTTGTGACCTTGTGGTG
NC2743		CTCTGAGCACAAGCCTGGTC
NC2744		TAATACGACTCACTATAGGGAAGGTGAGTATGTTAGAGAGA
NC2745		CGGCTGAAGTGGCCACGAGAC
NC2746		TAATACGACTCACTATAGGGACAGTGACCATACCCCATGA
NC2747		TAGTTTGGAGGTGGTGTGTGAG
NC2748		TAATACGACTCACTATAGGGCGGACCCCAGCAGC
NC2749		GACTGGACCGAGTTCACCG
NC2750		TAATACGACTCACTATAGGGTGAGACTGGACCTTCGGGAG
NC2751		CTGCAGGACCGTCCCCT

Table 5. Splint Ligation

Splint Ligation	
Name	Sequence
Hp1-A2 (5´)	GCCUUUUUUCCCCAGACUUGUUGGCGUAGGCU
Hp1-A2 (3´)	ACAGAGAAGCCUUCAAGCUCUGAGGGAAAGGGC
Hp1-A4 (5´)	GCCUUUUUUCCCCAGACUUGUUGGCGUAGGCUAC
Hp1-A4 (3´)	AGAGAAGCCUUCAAGCUCUGAGGGAAAGGGC
Hp1-A6 (5´)	GCCUUUUUUCCCCAGACUUGUUGGCGUAGGCUACAG
Hp1-A6 (3´)	AGAAGCCUUCAAGCUCUGAGGGAAAGGGC
Hp1-A8 (5´)	GCCUUUUUUCCCCAGACUUGUUGGCGUAGGCUACAGAG
Hp1-A8 (3´)	AAGCCUUCAAGCUCUGAGGGAAAGGGC
Hp1-A9 (5´)	GCCUUUUUUCCCCAGACUUGUUGGCGUAGGCUACAGAGA
Hp1-A9 (3´)	AGCCUUCAAGCUCUGAGGGAAAGGGC
Hp1-wt splint; NC2535	GCCCTTTCCCTCAGAGCTTGAAGGCTTCTCTGTAGCCTACGCCAA CAAGTCTGGGGAAAAAAGGC
Hp1-C3G (5´)	GCCUUUUUUCCCCAGACUUGUUGGCGUAGGCUAG
Hp1-C3G splint; NC2537	GCCCTTTCCCTCAGAGCTTGAAGGCTTCTCTCTAGCCTACGCCAA CAAGTCTGGGGAAAAAAGGC
Hp1-A9U (3´)	AGAGAUGCCUUCAAGCUCUGAGGGAAAGGGC
Hp1-G(-6)C (5´)	GCCUUUUUUCCCCAGACUUGUUGGCCUAGGCUAC
Hp1-G(-6)C splint; NC2622	CCTCAGAGCTTGAAGGCTTCTCTGTAGCCTAGGCCAACAAGTC
Hp1-C3G:G(-6)C (5´)	GCCUUUUUUCCCCAGACUUGUUGGCCUAGGCUAG
Hp1-C3G:G(-6)C (5´) splint; NC2623	CCTCAGAGCTTGAAGGCTTCTCTCTAGCCTAGGCCAACAAGTC
Hp1-A2U (5´)	GCCUUUUUUCCCCAGACUUGUUGGCGUAGGCUUC
Hp1-A2U splint; NC2624	CCTCAGAGCTTGAAGGCTTCTCTGAAGCCTACGCCAACAAGTC
Hp1-U(-5)A (5´)	GCCUUUUUUCCCCAGACUUGUUGGCGAAGGCUAC
Hp1-U(-5)A splint; NC2625	CCTCAGAGCTTGAAGGCTTCTCTGTAGCCTTCGCCAACAAGTC
Hp1-A2U:U(-5)A (5´)	GCCUUUUUUCCCCAGACUUGUUGGCGAAGGCUUC
Hp1-A2U:U(-5)A (5´) splint; NC2526	CCTCAGAGCTTGAAGGCTTCTCTGAAGCCTTCGCCAACAAGTC
U6-wt (5´)	GUGCUCGCUUCGGCAGCACAUAUACUAAAAUUGGAACGAUAC
U6-wt (mid)	AGAGAAGAUUAGCAUGGCCCCUGCGCAAGGAU
U6-wt (3´)	GACACGCAAAUUCGUGAAGCGUUCCAUAUUUU
U6-wt splint; NC2638	AAAATATGGAACGCTTCACGAATTTGCGTGTCATCCTTGCGCAGG GGCCATGCTAATCTTCTCTGTATCGTTCCAATTTTAGTATAT

U6-G88C (3´)	GACACGCAAAUUCCUGAAGCGUUCCAUAUUUU
U6-G88C splint; NC2639	AAAATATGGAACGCTTCAGGAATTTGCGTGTCATCCTTGCGCAGG GGCCATGCTAATCTTCTCTGTATCGTTCCAATTTTAGTATAT
U6-UUC85-87AAG (3´)	GACACGCAAAAAGGUGAAGCGUUCCAUAUUUU
U6-UUC85-87AAG splint; NC2643	AAAATATGGAACGCTTCACCTTTTTGCGTGTCATCCTTGCGCAGG GGCCATGCTAATCTTCTCTGTATCGTTCCAATTTTAGTATAT
U6-C87G (3´)	GACACGCAAAUUGGUGAAGCGUUCCAUAUUUU
U6-UUC85-87AAG splint; NC2644	AAAATATGGAACGCTTCACCAATTTGCGTGTCATCCTTGCGCAGG GGCCATGCTAATCTTCTCTGTATCGTTCCAATTTTAGTATAT

Table 6. Plasmid Oligonucleotides

Plasmid Oligonucleotides		
Reporter	Primer Name	Sequence
β-MAT-WT	NC1145	ACCTACGAATTCGTCTCTTATGCTATTGGAGTTTC
	NC1146	GAACCTAGCATTTTATTTAGATCTTCAT
	NC1576	CTTATCTTCCTCCCACAGCT
	Sp6+	GCTCTAGCATTTAGGTGACACTATAG
β-MAT-Δhp1	NC1653	AAATTTAGGAAGGAGGGCCCTCAATATTTAAGCTTTTTGGGC
	NC1654	GCCCAAAAAGCTTAAATATTGAGGGCCCTCCTTCCTAAATTT
β-MAT-hp1m9	NC2014	CCAGACTTGTTGGCGTAGGCTCACTCCCCGCATTCAAGCTCTGAGGGAAAGG
	NC2015	CCTTTCCCTCAGAGCTTGAATGCGGGGAGTGAGCCTACGCCAACAAGTCTGG
β-MAT-hp1G3	NC2137	TGTTGGCGTAGGCTAGAGAG
	NC2138	CTCTCTAGCCTACGCCAACA
β-MAT-hp1G4	NC2203	TGTTGGCGTAGGCTACGGAG
	NC2204	CTCCGTAGCCTACGCCAACA
β-MAT-hp1G4, 1xMS2	NC2674	AAACATGAGGATCACCCATGTCGCTCTTTCAGCTCCTGACCAG
	NC2675	CGACATGGGTGATCCTCATGTTTGACAGGAAAATTTAGGAAGGAGG
β-MAT-hp1U9	NC2307	GCTACAGAGATGCCTTCAAGCTCTGAGGGA
	NC2308	TCCCTCAGAGCTTGAAGGCATCTCTGTAGC
β-MAT-hp2-6m9	CGTACGTAATAAGGTTTTAATTTAGTAAACCAATCCTATGCATGGTTTCAGCACTAGCCAAACCTCACCAACTCCTAGTTCTAGAAAAACAGGCACTTGGCAGCCTTGTGATGTCATCACTCCCCGTAACAGGGCAGTACCTGAGGGTCTGTAGGTTGCACACTTTGGTACCAGATAACTTTTTTTTTTCTTTATAAGAAAGCCTGAGTACTCCACACTGCACAATAACTCCTCCCAGGGTTTTAACTTTGTTTTATTTTCAAAACCAGGTCCAATGAGCTTTCTGAACAGCTGGTGTAGCTCACTCCCCACAAGCTTCCTTCAGAGAGCAGTGCTTTTGGCGGGGAGGAGGAAATCCCTTCATACTTGAACGTTTTCTAATTGCTTATTTATTGTATTCTGGGGTATGGCGTAAGTCACTCCCCGCAATCACCTCAGATGGCAGCTTTTAAAAGATTTTTTTTTTTTCTCTCAACACCATGATTCCTTTAACAACATGTTTCCAGCATTCCCAGGTAGGCCAAGGTGTCCTCACTCCCCAACTTGGGTTAGACCTACAGGGGGTCTGGCTGGTGTTAACAGAAGGGAGGGCAGAGCTGGTGCGGCTGGCCATGGAGAAAGCTGACTTGGCTGGTGTGGTCACTCCCCGCAAGCTTGTTTACATGCTTATTCCATGACTGCTTGCCCTAAGCAGAAAGTGCCTTTCAGGATCTATTTTTGGAGGTTTATTACGTATGTCTGGTTCTCAATTCCAACAGTTTAATGAAGATCT	
FLAG-	NC2425	CGCTTAGGATCCATGGCTCTGAGTAAATCAATGC

METTL16	NC2426	CGCTTACTCGAGCTAGTTAACTGCAACAAGCC
FLAG-METTL16 PP185/186AA	NC2513	CTTTTGCATGTGCAACGCTGCCTTTTTTGCCAATC
	NC2514	GATTGGCAAAAAAGGCAGCGTTGCACATGCAAAAG
FLAG-METTL16 F187G	NC2515	CTTTTGCATGTGCAACCCTCCCGGTTTTGCCAATC
	NC2516	GATTGGCAAAACCGGGAGGGTTGCACATGCAAAAG
FLAG-METTL16 siRNA Resistant	NC2521	ACCTTGAATGGCTGGTACTTTTTGGCTACCGAAGTGGATGATAT
	NC2522	ATATCATCCACTTCGGTAGCCAAAAAGTACCAGCCATTCAAGGT
FLAG-MAT2A	NC1566	GGCAAAGAATTCATGAACGGACAGCTCAACGG
	NC1567	ATAAAGCTCGAGTCAATATTTAAGCTTTTTGGGCACTTCC
rM16-MTD	NC2499	GAGGTCTCAAGGTATGGCTCTGAGTAAATCAATGC
	NC2502	GATCTAGATTACTAATCATAAAAACTCCAAGCTAAGG
MS2-M16 VCR	NC2807	CGCTTAGGATCCTATGATGATGTCACAGTACCATCAC
NMS2-hnRNPC1	NC257	AAGCCAGGATCCACCATGGACTACAAGGACGACGATGACAAGGCCAGCAACGTTACCAACAAG
	NC258	TCCGCTGCGGCCGCTCCTCCATTGGCGCTGTCTC

Table 7. Reagents and Resources

REAGENT or RESOURCE	SOURCE	IDENTIFIER
Antibodies		
Mouse monoclonal β-Actin	Abcam	Cat#ab6276
Rabbit polyclonal MAT2A	Abcam	Cat#ab77471
Rabbit polyclonal METTL16	Bethyl	Cat#A304-192A
Mouse monoclonal FLAG	Sigma	Cat#F3165
Rabbit polyclonal N^6-methyladenosine	Synaptic Systems	Cat#202003
Mouse monoclonal IgG1	Sigma	Cat#M5284
Chemicals, Peptides, and Recombinant Proteins		
rM16-MTD (aa1-291)	This paper	N/A
rPP185/186AA (aa1-291)	This paper	N/A
rF187G (aa1-291)	This paper	N/A
Critical Commercial Assays		
Deposited Data		
Human reference genome NCBI build 38, GRCh38	Genome Reference Consortium	http://www.ncbi.nlm.nih.gov/projects/genome/assembly/grc/human/
Experimental Models: Cell Lines		
Human: HEK293 cells	Dr. Joan A. Steitz (Yale University) (Conrad and Steitz, 2005)	
Human: HEK293T cells	Dr. Joshua Mendell (UT Southwestern Medical Center)	
Human: 293A-TOA cells	(Sahin et al., 2010)	N/A
Experimental Models: Organisms/Strains		
S. pombe ΔDuf890/SPAC27D7.08c	Bioneer	Cat#BG_H3843
S. pombe Background strain/ED666	Bioneer	Cat#BG_0000H8
Recombinant DNA		
Plasmid: β-MAT-WT	This paper	N/A
Plasmid: β-MAT-Δhp1	This paper	N/A
Plasmid: β-MAT-hp1m9	This paper	N/A
Plasmid: β-MAT-hp1G4	This paper	N/A
Plasmid: β-MAT-hp1G4, 1xMS2	This paper	N/A
Plasmid: β-MAT-hp1G3	This paper	N/A
Plasmid: β-MAT-hp1U9	This paper	N/A
Plasmid: β-MAT-hp2-6m9	This paper	N/A
Plasmid: β-MAT-hp1-6m9	This paper	N/A
Plasmid: β-MAT-hp1-6 A4G	This paper	N/A

Plasmid: FLAG-METTL16	This paper	N/A
Plasmid: FLAG-METTL16 PP185/186AA	This paper	N/A
Plasmid: FLAG-METTL16 F187G	This paper	N/A
Plasmid: pX459 (puromycin resistance)	(Ran et al., 2013)	Addgene #48139
Plasmid: pcDNA3	Thermo Fisher	V79020
Plasmid: pcDNA3-Flag	(Sahin et al., 2010)	N/A
Plasmid: FL-MAT2A	This paper	N/A
Plasmid: pE-SUMO	LifeSensors	Cat#1001K
Plasmid: pE-SUMO-M16-MTD	This paper	N/A
Plasmid: pcNMS2-NLS-Flag	(Sahin et al., 2010)	N/A
Plasmid: pcNMS2-NLS-Flag-MTD	This paper	N/A
Plasmid: MS2-METTL16	This paper	N/A
Plasmid: MS2-F187G	This paper	N/A
Plasmid: MS2-M16 MTD	This paper	N/A
Plasmid: MS2-M16 VCR	This paper	N/A
Plasmid: pcNMS2	(Lykke-Andersen et al., 2001)	N/A
Plasmid: MS2-hnRNP C1	This paper	N/A
Plasmid: MS2-hnRNP A1	(Lykke-Andersen et al., 2001)	N/A
Sequence-Based Reagents		
Primers for qRT-PCR, see Table S3	This paper	N/A
Primers for Northern probes, see Table S3	This paper	N/A
Primers for RNase H cleavage, see Table S3	This paper	N/A
Primers for *In vitro* RNA templates, see Table S3	This paper	N/A
Primers for Making Reporters, see Table S3	This paper	N/A
siRNA targeting sequence Silencer Select Negative Control #2	Thermo Fisher	Cat#4390846
siRNA targeting sequence Silencer Select siMETTL16 #1	Thermo Fisher	Cat#s35508
siRNA targeting sequence Silencer Select siMETTL16 #2	Thermo Fisher	Cat#s35507
siRNA targeting sequence Silencer Select siMAT2A	Thermo Fisher	Cat#s8526
Insert for β-MAT-hp2-6m9 (Table 6)	GENEWIZ	N/A
Software and Algorithms		
ImageQuant 5.2	GE Healthcare Life Sciences	
Image Studio Ver 3.1	LI-COR Biosciences	
bwa (v 0.7.9a-r786)	(Li and Durbin, 2009)	
StringTie (v1.1.2)	(Pertea et al., 2015)	

BedTools	(Quinlan and Hall, 2010)	
Analyst® 1.6.1	SCIEX	

CHAPTER FOUR
Results

THE U6 SNRNA M^6A METHYLTRANSFERASE METTL16 REGULATES SAM SYNTHEASE INTRON RETENTION

Introduction

SAM serves as methyl donor for nearly all cellular methylation reactions. The widespread use of methylation to regulate the activities of DNA, RNA, and proteins requires cells to precisely maintain SAM levels, but the mechanisms that control intracellular SAM abundance in mammalian cells are not well understood. Bacteria use riboswitches to directly link intracellular SAM levels with the production of the SAM synthetases that generate SAM from Met and ATP (Wang and Breaker, 2008). Several observations suggest that human SAM synthetase expression is also posttranscriptionally regulated. The human MAT2A gene encodes the SAM synthetase expressed in all cells except liver cells. Upon Met depletion, the stability of the cytoplasmic MAT2A mRNA increases (Martinez-Chantar et al., 2003b). Furthermore, the MAT2A 3´ UTR contains six hairpin structures that are evolutionarily conserved among vertebrates (Parker et al., 2011). While these do not bind SAM or function as a riboswitch, their conservation implies they are involved in MAT2A regulation. In addition, a significant fraction of the total MAT2A transcript accumulates in the nucleus in a retained intron isoform that is subject to nuclear degradation (Bresson et al., 2015). Intron retention in mammals is not well characterized, but recent studies suggest that it contributes to the regulation of thousands of mammalian RNAs (Boutz et al., 2015; Braunschweig et al., 2014; Yap et al., 2012). Together, these observations

suggest that cells control SAM homeostasis using undefined posttranscriptional mechanisms to regulate MAT2A.

For decades, N^6-methyladenosine (m^6A) has been recognized as a common mRNA modification, but only with the introduction of transcriptomics approaches (m^6A-seq) has the full scope of m^6A targets been defined (Dominissini et al., 2012; Meyer et al., 2012; Yue et al., 2015). The catalytic METTL3 protein in complex with a catalytically inactive METTL14 and the RNA-binding protein WTAP modify most m^6A sites in mRNA (Bokar et al., 1997; Liu et al., 2014; Ping et al., 2014; Schwartz et al., 2014; Sledz and Jinek, 2016; Wang et al., 2016a; Wang et al., 2016b). The METTL3 complex methylates mRNAs at RRACH motifs (R = A or G; H = A, C or U), often in 3´ UTRs (Dominissini et al., 2012; Ke et al., 2015; Meyer et al., 2012; Yue et al., 2015). Knockdown of the components of the METTL3 complex leads to changes in splicing patterns, alternative polyadenylation, RNA stability, transcriptional silencing, and translation (Dominissini et al., 2012; Ke et al., 2015; Lin et al., 2016; Meyer et al., 2015; Patil et al., 2016; Schwartz et al., 2014; Wang et al., 2016b; Zhou et al., 2015). Mechanistically, these changes in mRNA expression have been linked to RNA binding proteins whose affinity for a transcript is altered by m^6A modification (Alarcon et al., 2015; Dominissini et al., 2012; Du et al., 2016; Luo and Tong, 2014; Patil et al., 2016; Wang et al., 2014; Xiao et al., 2016; Zhou et al., 2015). In addition, methylation can alter protein binding by changing RNA structures (Liu et al., 2015).

Despite these advances, the understanding of m^6A pathways remains incomplete. It is unknown how, or even whether, the methylation of specific sites alters specific RNA processing events in response to intracellular or extracellular conditions. Furthermore, methyltransferases

other than METTL3 contribute to the overall m^6A profile. Notably, it has been over 35 years since the discovery that the U6 snRNA is m^6A modified (Epstein et al., 1980; Harada et al., 1980). The m^6A site lies in a sequence important for splicing catalysis and it is conserved (Brow and Guthrie, 1988; Gu et al., 1996; Nguyen et al., 2016). As such, this modification may contribute to U6 snRNA function, but the identity of the methyltransferase has remained unknown.

Here, we define a posttranscriptional regulatory mechanism involving a specific m^6A methylation site and the methyltransferase METTL16 that controls MAT2A intron retention in response to intracellular SAM levels. We show that splicing of the MAT2A retained intron is rapidly induced upon Met depletion, and this effect requires a conserved hairpin (hp1), which we further show is a METTL16 m^6A substrate. Importantly, knockdown of METTL16 abrogates induction of MAT2A splicing in Met-deprived conditions, while forced binding of METTL16 to the MAT2A 3′ UTR is sufficient to promote splicing in Met-replete conditions. We propose a model in which METTL16 occupancy on MAT2A hp1 promotes splicing of the retained intron. Under high SAM levels, METTL16 binds, methylates, and disassociates rapidly to favor intron retention. In SAM-limiting conditions, METTL16 cannot methylate efficiently, which increases its dwell time on hp1 and stimulates splicing of the retained intron. Finally, we show that METTL16 is the long-unknown U6 snRNA methyltransferase, and this function is conserved in *S. pombe*. We conclude that METTL16 is the conserved U6 snRNA methyltransferase, and it has evolved an additional function in vertebrates to control SAM homeostasis by posttranscriptionally regulating SAM synthetase gene expression.

Results

MAT2A Intron Retention Is Regulated

The MAT2A gene produces two RNA isoforms, a cytoplasmic mRNA and a nuclear retained-intron isoform (MAT2A-RI), across multiple cell types (Figure 6A and 7A)(Bresson et al., 2015). Because MAT2A mRNA levels increase in Met-free media (Martinez-Chantar et al., 2003b), we tested whether Met depletion regulates MAT2A intron retention. We observed a rapid decrease in MAT2A-RI and an increase in MAT2A mRNA upon Met withdrawal (Figure 6B). Nuclear run-on analysis confirmed that transcription rates of MAT2A are not enhanced upon Met depletion (Figure 7B). The MAT2A protein uses Met as a substrate to produce SAM, so the increase of MAT2A mRNA is unlikely to result directly from Met depletion. Instead, several observations suggest the response is due to loss of SAM. First, heterologous overexpression of MAT2A increased SAM levels (Figure 7C), which correlated with increases in intron retention (Figure 6C). Furthermore, this effect was reversed by Met depletion, except at the highest levels of MAT2A expression. In this case, excessive SAM buildup in these cells precluded SAM depletion during the 6-hr Met deprivation (Figure 7C). Second, the MAT2A inhibitor cycloleucine decreased intron retention in Met-replete media (Figure 7D)(Coulter et al., 1974). Third, transient permeabilization to allow entry of the otherwise cell-impermeable SAM restored basal levels of intron retention in Met-depleted cells (Figure 7E). Together, these data suggest that intracellular SAM levels regulate MAT2A intron retention. Finally, we confirmed that induction of MAT2A splicing results in changes in protein levels. Because depletion of Met removes an essential amino acid, we examined MAT2A RNA and protein over a series of Met concentrations. We observed a sharp shift to the spliced mRNA isoform between 11-33 μM extracellular Met and concomitant increases in protein levels of MAT2A (Figure 6D). We

conclude that MAT2A intron retention is regulated in response to SAM availability to control MAT2A protein production.

MAT2A Hairpin 1 Is Necessary for the Regulation of Intron Retention

The MAT2A 3´ UTR contains six hairpins with vertebrate-conserved sequence, structure, and placement (Parker et al., 2011). The hairpins are predicted to form a "duckbill"-like stem-loop with the nearly invariant sequence "UACAGAGAA" in the loop (Figure 8A). The first hairpin lies close to the stop codon and a cluster of three to five hairpins is located further downstream (Figure 6A and Figure 9A). Given its conservation and proximity to the retained intron, we hypothesized that MAT2A hp1 regulates intron retention.

We made a series of reporter constructs with the MAT2A exon 8, intron 8, exon 9, and 3´ UTR fused to β-globin with alterations the in hp1 or the hp2-6 cluster sequences (Figure 8B). Like the endogenous RNA, the wild-type (WT) reporter responded to Met depletion by reducing intron retention and increasing mRNA (Figure 8C). Alterations in hp1 impaired splicing induction as assessed by the percent intron retention (Figure 8C) and by the steady-state levels of the intron-retained reporter RNA (Figure 9B). Mutations in the hp2-6 cluster increased the mRNA isoform under Met-replete conditions without affecting intron retention (Figure 9C), potentially due to an increase in the stability of the otherwise unstable MAT2A mRNA. More importantly, a WT hp1 conferred regulated intron retention in the hp2-6 mutants (Figure 9C). To test if the hp cluster played a role in RNA stability, we measured RNA decay rates from transfected cells with either WT, hp1m9, or hp1-6m9 reporters in either the presence or absence of Met. In Met-replete conditions, the WT and hp1m9 were rapidly degraded at similar rates, though hp1-6m9 was significantly more stable and barely decreased. The hp1-6m9 Met-replete

stability mirrored the high stability of all three reporters in Met-free media (Figure 9D). These observations suggest that hp1 and the conserved UACAGAGAA play critical roles in the induction of splicing of the MAT2A retained intron, while the UACAGAGAA in the hp cluster is essential to promote degradation of the RNA under Met-replete conditions.

MAT2A Hairpin 1 Is M^{6}A Modified at a Site Identical to the U6 snRNA Methylation Site

The UACAGAGAA nonamer is identical to a sequence in U6 snRNA that is m^{6}A methylated by an unknown methyltransferase at position A4 (Figure 8A)(Epstein et al., 1980; Harada et al., 1980). Publically available m^{6}A-seq data suggest at least one METTL3-independent m^{6}A modification near MAT2A hairpins (Dominissini et al., 2012; Linder et al., 2015; Schwartz et al., 2014). To test hairpin methylation, we performed an m^{6}A-immunoprecipitation (m^{6}A-IP) using β-globin reporter RNAs (Figure 8D). We cleaved the 5´ end of β-globin using oligonucleotide-directed RNase H to eliminate a known β-globin m^{6}A site, and this fragment served as an m^{6}A-IP positive control (Figure 8D, bottom panel). We observed efficient m^{6}A-IP of the WT and hp1 mutant RNAs and reduced efficiency for the hp2-6 cluster mutant. Importantly, mutating all six hairpins resulted in the complete loss of m^{6}A-IP of the 3´ UTR without affecting the β-globin control (Figure 8D). Thus, the UACAGAGAA sequences in the MAT2A hairpins are important for the methylation of the MAT2A 3´ UTR.

Sequence identity suggests that MAT2A hp1 is methylated at position A4 by the same machinery that methylates U6 snRNA (Figure 8A). We examined hp1 methylation in an *in vitro* assay that supports U6 snRNA methylation but not methylation of METTL3 substrates (Shimba et al., 1995). We incubated uniformly adenosine-labeled substrates in nuclear extract and monitored m^{6}A modification by P1 nuclease treatment and thin layer chromatography

(TLC)(Figure 8E). Both U6 snRNA and the hp1 WT substrates were methylated in a SAM-dependent fashion. However, a substrate that mutates the predicted methylation site (hp1-A4G) was not methylated, nor was a METTL3 substrate (Figure 8E)(Liu et al., 2014). In addition, we site-specifically radiolabeled hp1 A2, A4, A6, A8, or A9, by splint ligation and only hp1-A4 was methylated (Figure 8F). Moreover, point mutants that interfere with splicing (Figure 8C) disrupted methylation *in vitro* (Figure 8G). We conclude that MAT2A hp1 is a substrate for m^6A modification at position A4 and that the U6 snRNA methyltransferase is likely responsible for the modification.

METTL16 Methylates MAT2A Hairpins and Contributes to Splicing Induction

In order to identify the methyltransferase that interacted with the MAT2A hairpins, we performed label transfer experiments and biotin-labeled RNA pull downs with an RNA substrate that repeated the UACAGAGAA motif five times. While these experiments appeared to give us specific bands on a silver stain compared to a mutated control (data not shown), mass spectrometry data failed to identify a methyltransferase. Later results suggest that secondary structure greatly aids in the binding protein's function (discussed in greater detail below and in Figure 15), and our RNA substrate lacked that secondary structure. So, despite thoughtful biochemistry, review of the literature resulted in discovering a protein candidate.

The conserved METTL16 protein contains a methyltransferase domain and two vertebrate-conserved regions (Figure 11A). The *E. coli* homolog of METTL16 m^6A methylates rRNA within a CAG motif, consistent with the site in U6 snRNA and MAT2A (Sergiev et al., 2008). Interestingly, *S. pombe* encodes a METTL16 homolog, and its U6 snRNA is m^6A methylated (Gu et al., 1996). However, *S. cerevisiae* does not encode a METTL16 homolog and, to our

knowledge, budding yeast U6 snRNA is not methylated. Moreover, METTL16 is nuclear, consistent with a role in regulation of MAT2A splicing and U6 methylation (Brown et al., 2016). For these reasons, we explored the possibility that METTL16 methylates MAT2A and U6 snRNA.

Several observations demonstrate that METTL16 is necessary for efficient MAT2A splicing and that this contributes to MAT2A activity. First, knockdown of METTL16 with siRNA (siM16) increases intron retention in the presence of Met (Figure 10A, 11B and 11C). Second, MAT2A-RI levels did not decrease significantly upon Met depletion and a highly attenuated increase in spliced mRNA was observed in the siM16-treated cells (Figure 10A and 11D). Third, MAT2A protein levels decreased ~26% upon METTL16 knockdown (Figure 11C). Fourth, as described in more detail below, SAM levels and m^6A/A ratios decreased upon METTL16 knockdown (Figure 6A and 6B). Thus, METTL16 is necessary for the regulation of MAT2A by intron retention.

We next tested whether METTL16 methylates MAT2A hp1. MAT2A contains a METTL3-dependent m^6A site upstream of the 3´ UTR (Linder et al., 2015). We liberated hp1 from this site by RNase H treatment of RNA from siCtrl or siM16-treated cells (Figure 10B, top). We performed m^6A-IP and found that MAT2A hp1 and coding sequence (CDS) efficiently immunoprecipitated from the siCtrl cells, but only the CDS immunoprecipitated in the siM16-treated cells (Figure 10B). We next confirmed a physical interaction between METTL16 and the MAT2A hairpins using formaldehyde-crosslinked RNA-immunoprecipitation (RIP)(Conrad, 2008). Cell lysates from crosslinked or non-crosslinked controls were briefly treated with nuclease and immunoprecipitated with anti-METTL16 antibody. Only hp1 and the hairpin

cluster region of MAT2A were enriched in the crosslinked METTL16 IP (Figure 10C, Figure 11E). Thus, METTL16 interacts with the MAT2A hairpin regions and is required for their methylation in cells.

To examine the biochemical activity of METTL16, we immunodepleted METTL16 from nuclear extract and tested methylation of hp1 (Figure 10D and 11F). We observed a nearly 6-fold decrease in methylation of hp1 in METTL16-immunodepleted extracts. Purified recombinant METTL16 methyltransferase domain (rM16-MTD; Figure 11G) increased activity in immunodepleted and control extracts. Furthermore, hp1 methylation activity was robust on the anti-METTL16 beads and virtually undetectable in the control beads. In addition, rM16-MTD was sufficient to specifically methylate hp1-A4, but none of the other hp1 adenosines (Figure 10E). Moreover, two recombinant proteins with mutations of highly conserved residues in the substrate-binding domain abrogated the activity (PP185/186AA and F187G)(Malone et al., 1995). Finally, rM16-MTD was unable to methylate two mutants that reduced splicing in reporter assays (Figure 10F). We conclude that METTL16 is required for induction of MAT2A splicing and it methylates the UACAGAGAA sequence in MAT2A 3´ UTR hairpins.

METTL16 Occupancy of Hairpin 1 Promotes MAT2A Splicing

Met depletion, hp1 mutation, or METTL16 knockdown reduce MAT2A hairpin modification (Figure 13A, 8D, and 9B), but the consequences of these treatments differ. Met depletion increases MAT2A mRNA (Figure 6B), while hp1 mutation or METTL16 knockdown results in loss of induction of splicing and mRNA production (Figure 8C and 10A). To rationalize this apparent contradiction, we hypothesized that the dwell time of METTL16 on hp1 dictates MAT2A splicing efficiency. In Met-rich conditions, SAM is plentiful, and METTL16

briefly occupies hp1 due to enzyme turnover. In Met-deprived conditions, the lack of SAM slows methylation and prolongs METTL16 occupation of hp1, which then drives splicing of MAT2A intron eight (Figure 18).

In this model, the methyltransferase activity regulates the dwell-time of METTL16 on MAT2A 3´ UTR, but methylation is not directly required for splicing. The model predicts that overexpressing wild-type or catalytically inactive METTL16 should drive hp1 binding and promote splicing even in Met-replete conditions, but an RNA-binding mutant should not induce splicing. Both the METTL16 PP185/186AA and F187G mutants are catalytically inactive (Figure 10E). In native RIP experiments, F187G does not bind MAT2A while the PP185/186AA mutant binds MAT2A, albeit less efficiently than wild-type METTL16 (Figure 13B, 13C). We knocked down endogenous METTL16 and overexpressed siRNA-resistant METTL16 wild-type, PP185/186AA, or F187G. As predicted, overexpression of wild-type METTL16 or PP185/186AA decreased intron retention in both Met-depleted and Met-rich media, whereas the RNA-binding mutant F187G did not affect intron retention (Figure 12A). Importantly, all three proteins were overexpressed to similar levels (Figure 13D). To verify the role of hp1, we performed a similar experiment with the β-MAT-WT or β-MAT-hp1-C3G reporters (Figure 12B). Once again, we observed decreased intron retention in the β-MAT-WT reporter upon METTL16 and PP185/186AA overexpression, but no change upon F187G overexpression. Overexpression of these proteins had little effect on intron retention in the β-MAT-hp1-C3G, demonstrating that hp1 is essential for splicing induction. These results suggest that METTL16 binding, but not methylation activity, is required for the induction of MAT2A splicing.

To further test the role of METTL16 occupancy on MAT2A splicing, we employed an MS2-tethering assay. We placed a binding site for the bacteriophage MS2 coat protein downstream of a mutant hp1 and co-expressed MS2 fusions to wild-type or F187G METTL16 (Figure 12C). Importantly, the point mutation, hp1-A4G, abrogates binding of METTL16 (Figure 13E). If METTL16 occupancy is the key to MAT2A splicing, tethering should be sufficient to induce splicing in the presence of Met and complement the lack of activity of the F187G and hp1 mutants (Figure 12A and 12B). Indeed, tethering of wild-type or F187G METTL16 was sufficient to drive splicing in a hp1 mutant reporter, but MS2-alone, MS2-hnRNP A1 and MS2-hnRNP C1 negative controls were not (Figure 12C). METTL16 homologs are found from *E. coli* to humans, but the MAT2A hairpins and two carboxyl-terminal METTL16 vertebrate conserved regions (VCRs) are restricted to vertebrates (Figures 11A). We reasoned that the METTL16-VCRs may promote splicing, while the methyltransferase domain regulates association with the transcript. Consistent with this hypothesis, tethering the METTL16-VCRs was sufficient to drive splicing, but the methyltransferase domain was not (Figure 12C). We conclude that METTL16 binding is sufficient to promote MAT2A splicing through the METTL16-VCR domains.

Finally, we performed a native RIP to monitor METTL16-MAT2A RNA association. As expected, METTL16 immunoprecipitated with MAT2A more efficiently after Met depletion (Figure 12D and 13F), further supporting the idea that METTL16 occupancy increases upon Met depletion to enhance MAT2A splicing. Taken together, these data strongly support the conclusion that METTL16 binding to hp1 drives splicing of the MAT2A retained intron.

Moreover, they suggest that the METTL16 methyltransferase domain controls binding to hp1, but the METTL16-VCRs promote splicing.

METTL16 Is the U6 m^6A-Methyltranfserase

The similarity between the MAT2A hairpin and U6 snRNA methylation sites suggest that METTL16 is the U6 snRNA methyltransferase. However, U6 snRNA adopts a variety of intermolecular and intramolecular structures, but none obviously resemble the MAT2A hairpin "duckbill" (e.g. Figure 15A). In principle, the duckbill may not be required for hp1 methylation, but individual mutation of each of the four bases that comprise the duckbill reduced methylation (Figure 14B compare lane 1 with lanes 2, 3, 5, and 6). However, compensatory mutations that restore base pairing did not restore activity (Figure 14B, lanes 4 and 7; Figure 15B), demonstrating that a two-nucleotide base pair at this position is not sufficient for activity. Instead, METTL16 may require a sequence-specific 2-nt base pair or the upstream GU may contribute to methylation as a sequence-specific single-stranded dinucleotide. If U6 snRNA is a METTL16 substrate, these findings suggest that it will have a similar upstream GU sequence or a two-nucleotide base paired structure adjacent to the methylated adenosine.

We first used biochemical assays to confirm that METTL16 is the U6 snRNA methyltransferase. We incubated rM16-MTD with U6 snRNA radiolabeled at position A43, which corresponds to A4 in the UACAGAGAA sequence (Figure 14A, 15A). As predicted, rM16-MTD methylates U6 snRNA A43, while PP185/186AA and F187G do not (Figure 14C). In METTL16 immunodepletion experiments, we observed reduced methylation, complementation by rM16-MTD, and robust activity on the anti-METTL16 beads (Figure 14D) further confirming that METTL16 methylates U6 snRNA at A43. Unlike hp1, there is no GU

dinucleotide upstream of the methylation site. However, the AC preceding the m^6A site is base paired with G88 and U89 similar to G(-6) and U(-5) in hp1 (Figure 14A and 15A)(Mougin et al., 2002). We observed no methylation of G88C substrates with rM16-MTD or nuclear extract (Figure 14C and Figure 15C). In addition, mutation of the bases immediately preceding G88 did not affect methylation, demonstrating the specificity of the G88C mutation (Figure 15C). Thus, both G88 in U6 snRNA and G(-6) in hp1 are essential for methylation by METTL16. Their primary sequence positions relative to the site of methylation are quite different, but the secondary sequences are similar (Figure 14A). Taken together, these data suggest that METTL16 prefers a substrate in which the AC flanking of the methylated adenosine is base-paired with GU.

In addition to these biochemical data, we observed an interaction between METTL16 and U6 snRNA in cells, but not U1 snRNA or 7SK RNA controls (Figure 14E, Figure 15D). Surprisingly, we observed no change in U6 snRNA m^6A-IP efficiency upon METTL16 knockdown (data not shown). We reasoned that the long half-life of U6 snRNA and residual METTL16 activity after knockdown masked differences in steady-state U6 snRNA methylation. A published CRISPR screen and our failed attempts to knockout METTL16 suggest that METTL16 is essential in mammalian cells (Wang et al., 2015a). However, deletion of the *S. pombe* METTL16 homolog, Duf890, produces viable, albeit slow-growing, yeast. M^6A-IP of U6 snRNA was lost on RNA from two independent ΔDuf890 colonies, but m^6A-IP of the U2 snRNA control was unaltered (Figure 14F). We conclude that METTL16 and its eukaryotic homologs are U6 snRNA m^6A methyltransferases.

Identification of METTL16-dependent m^6A sites

The METTL3 complex is responsible for the majority of mRNA methylation on the degenerate consensus RRACH. In contrast, methylation of U6 snRNA and MAT2A apparently requires both the UACAGAGAA nonamer and a specific RNA structure. These observations suggest that METTL16 is not a widely used mRNA m^6A methyltransferase. However, we observed an ~20% drop in m^6A to A ratios upon METTL16 knockdown (Figure 16A). In principle, METTL16 could frequently target UACAGAGAA sequences, or its activity could be expanded to non-UACAGAGAA targets by unknown cellular co-factors. Alternatively, METTL16 knockdown may lower m^6A by decreasing MAT2A activity. In fact, SAM levels were reduced in siM16-treated cells (Figure 16B). In the latter case, METTL16 contributes globally to m^6A methylation through its role in SAM biosynthesis.

To explore these potential broader roles for METTL16, we performed m^6A-seq and identified 2,715 peaks in 1533 genes that decrease upon METTL16 knockdown (Table S1). In contrast to typical m^6A sites commonly found in 3´ UTRs, 82% of the METTL16-dependent peaks were in introns or spanned intron-exon boundaries (Figure 16C). Compared to introns as a whole, this subset had a higher GC content, were shorter, and they skewed slightly to the 3´ ends of the RNAs (Figure 17A). Thus, the METTL16-sensitive peaks represent a distinct subset of m^6A modifications.

Only MAT2A and two additional peaks overlapped an UACAGAGAA site (GNPTG and GMIP; Figure 16D). Unlike MAT2A, we observed no METTL16 binding in cells and no methylation of these additional sites in nuclear extract (Figure 16E and 16F, lanes 1-3). Furthermore, the UACAGAGAA sequences are not conserved (Figure 17B), and there is a verified RRACH methylation site within the GNPTG peak (Linder et al., 2015). In addition, we

examined the m^6A IP efficiency of all windows that contain UACAGAGAA sites and have reads in the siCtrl m^6A-IP sample (Table S2). We observed no differences upon METTL16 knockdown between this dataset and two randomized control groups (Figure 17C). We conclude that UACAGAGAA element is not widely methylated by METTL16.

To test whether METTL16-dependent peaks respond to SAM levels, we knocked down or overexpressed MAT2A and performed m^6A-IP on several METTL16-dependent and METTL16-independent m^6A sites (Figures 16G, 16H, 17D, 17E). Upon MAT2A knockdown, the m^6A-IP efficiency of the METTL16-dependent sites decreased compared to the METTL16-independent sites (Figure 16G), while MAT2A overexpression increased METTL16-dependent m^6A-IP efficiency (Figure 16H). These data support the conclusion that METTL16-dependent m^6A sites are sensitive to SAM levels. Surprisingly, MAT2A overexpression was not able to complement METTL16 depletion (Figure 16I), suggesting that their METTL16-dependence is not exclusively the result of depressed SAM levels. However, we observed no binding to METTL16 (Figure 16J) and no methylation of three strong candidates in vitro (Figure 17F and 16F, lanes 4-7), suggesting they are not direct targets (see Discussion). Regardless of whether these are direct or indirect targets of METTL16, these data show that METTL16 is required for normal m^6A methylation profiles beyond its direct effects on the methylation of U6 snRNA and MAT2A.

Discussion

Precise control of SAM levels is important for a variety of cell functions, but SAM regulation is not well understood. Our data suggest a model in which METTL16 occupancy of hp1 controls production of SAM by inducing splicing of the MAT2A retained intron in SAM-limiting conditions (Figure 18). When SAM is available (top), METTL16 binds hp1, methylates

it, and then disassociates. Although limited basal splicing likely occurs, the short dwell time of METTL16 is insufficient for robust splicing induction. The nuclear MAT2A-RI is then degraded by PABPN1-PAPα/γ mediated RNA decay (Bresson et al., 2015). In SAM-limiting conditions (bottom), METTL16 binds to hp1, but stalls due to the lack of a methyl donor. The resulting increased occupancy on hp1 stimulates splicing of the MAT2A retained intron through the METTL16-VCRs. For simplicity, the diagram depicts posttranscriptional splicing induction, but we favor a model in which METTL16 promotes co-transcriptional splicing induction. We propose that METTL16 is a central factor in a feedback loop that links SAM levels to expression of the SAM synthetase.

Methylation of mRNA affects RNA processing at multiple stages of gene expression. Generally, m^6A mechanisms involve methylation "writers" (e.g. METTL3) that add the modification and "readers" (e.g. YTH family proteins) that differentially bind methylated RNA to induce changes in RNA metabolism (Yue et al., 2015). This work expands the mechanistic understanding of m^6A modification in two important ways. First, it has been difficult to directly link an intracellular or extracellular signal to a change at a specific m^6A site that in turn alters the expression of the modified mRNA. Here we link intracellular SAM levels with methylation of a specific adenosine in MAT2A that subsequently regulates intron retention. Second, in contrast to the two-component writer-reader paradigm, METTL16 serves as both m^6A writer and reader. Interestingly, METTL3 binding to 3´ UTRs can promote translation independent of m^6A methylation (Lin et al., 2016). Thus, while m^6A generally affects RNA metabolism through methylation readers, direct contributions of methyltransferases on RNA processing should not be overlooked.

Precisely how METTL16 promotes splicing remains unknown and unidentified co-factors certainly contribute to splicing induction. The UACAGAGAA element in U6 snRNA is critical for pre-mRNA splicing (Brow and Guthrie, 1988; Gu et al., 1996; Nguyen et al., 2016), so it is tempting to speculate that this sequence is used as a U6 mimic to regulate splicing of the retained intron. In principle, the methylation of U6 snRNA could be linked to splicing induction, but this seems unlikely, as the steady-state U6 snRNA methylation state does not change rapidly enough to account for the quick changes in splicing of MAT2A. Regardless of the potential roles for U6 snRNA, our data show that stable association of METTL16 is a key point of regulation of MAT2A splicing. The tethering assays further show that the METTL16-VCRs are sufficient to promote splicing, consistent with the vertebrate co-evolution of the hairpins and these domains. Future studies will seek to define the mechanisms of METTL16-induced MAT2A splicing.

METTL16 homologs are found in organisms ranging from *E. coli* to humans, but little is known about their functions. With the exception of rRNA targeting by *E. coli* ybiN/rlmF, no substrates for METTL16 family members have previously been identified (Sergiev et al., 2008). The *C. elegans* METT-10 restricts germ cell proliferation and is important for development of several organs (Dorsett et al., 2009), and *A. thaliana* FIONA1 is essential for maintaining plant circadian rhythms (Kim et al., 2008). The *C. elegans* and *A. thaliana* SAM synthetase genes have no UACAGAGAA elements, so these phenotypes are likely attributable to loss of U6 snRNA methylation, methylation of an unidentified target(s), or even other unknown functions of METTL16. METTL16 was also reported to bind a structured 3´-end triple helix structure of the nuclear noncoding MALAT1 RNA, apparently independent of its methyltransferase activity (Brown et al., 2016). The substrate specificities of METTL16 family members suggest that they

evolved initially to be rRNA methyltransferases and subsequently were co-opted by eukaryotes to target U6 snRNA. Later, vertebrate METTL16 gained a second function in the regulation of SAM using the METTL16-VCRs and the hairpin loops in MAT2A.

Our m^6A-seq identified a large number of METTL16-dependent m^6A sites. We cannot determine conclusively from our data whether METTL16 directly targets these sites or they are strictly regulated by the loss of intracellular SAM (Figure 16B). Consistent with the sites being indirect, the UACAGAGAA consensus was not enriched, METTL16-dependent m^6A sites are sensitive to SAM levels (Figure 16G, 16H, 17E), no interaction was observed by RIP (Figure 16J), and putative targets were not methylated *in vitro* (Figure 16F). However, METTL16 knockdown was not complemented by increasing SAM levels by overexpression of MAT2A, supporting a more direct role for METTL16 in these m^6A peaks (Figure 16I, 17E). Therefore, our data do not rule out the model that METTL16 methylates these sites, perhaps using different cellular co-factors that direct its activity to sites lacking the UACAGAGAA sequence. Importantly, even if the sites identified here are indirect, other direct targets of METTL16 may exist. For example, our poly(A)-selection step excludes detection of non-polyadenylated RNAs, and our bioinformatic pipeline filters any peaks lost in the METTL16 knockdown samples that are also down-regulated in the input samples.

Regardless of whether the METTL16-dependent peaks are indirect or direct METTL16 targets, our analysis revealed a distinct subset of m^6A sites. Unlike the m^6A sites commonly found in UTRs, the METTL16-dependent sites were primarily localized to introns or intron-exon boundaries. Because we selected for poly(A), these are likely intron-retained RNAs. Moreover, the introns themselves were on average shorter and more GC-rich. Interestingly, short, GC-rich

introns have been reported to be more subject to intron retention and may be spliced by intron definition (Amit et al., 2012). Whether METTL16-dependent m^6A methylation is mechanistically linked to these splicing characteristics remains unknown. We also cannot rule out confounding effects that loss of U6 snRNA methylation may have on splicing or biogenesis of methylated pre-mRNAs. In any case, further definition of the mechanisms METTL16 will lead to insights into SAM homeostasis and RNA biogenesis.

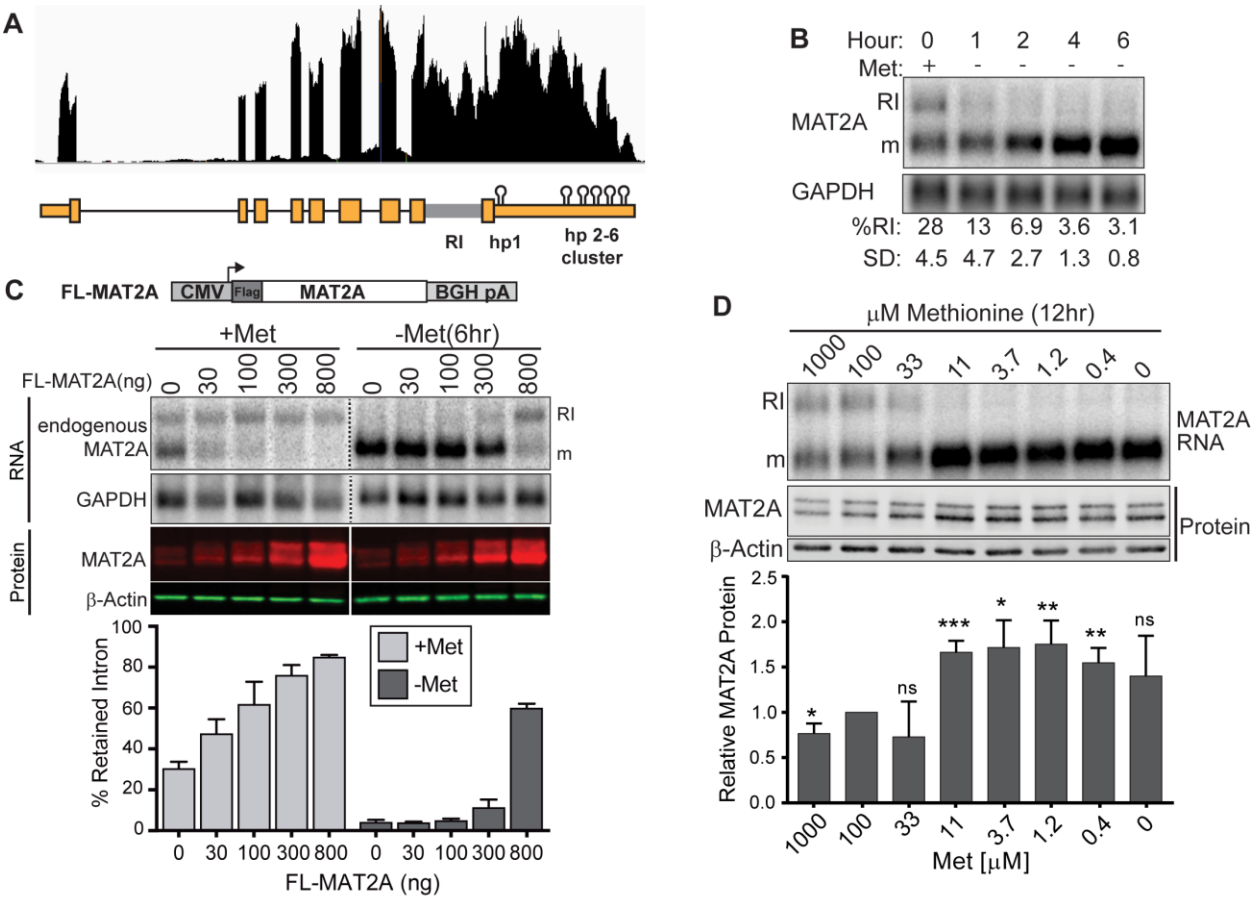

Figure 6. MAT2A Intron Retention Is Regulated

(A) RNA-seq trace of MAT2A from poly(A)-selected total RNA. The retained intron (RI) is highlighted in gray. (B) MAT2A northern blot from Met depletion time course. Data are mean ± standard deviation (SD); *n*=3. GAPDH serves as loading control. RI and m are MAT2A-RI and mRNA isoforms, respectively. These experiments were performed by Olga Hunter. (C) *Top,* Endogenous MAT2A and GAPDH northern blots with RNA from MAT2A overexpressing cells. Intervening lanes were removed (dashed lines), but the same exposure is shown. *Middle,* Western blot of MAT2A. The antibody recognizes both endogenous and overexpressed MAT2A. The doublet reflects two posttranslationally modified protein isoforms (α2 and α2′)(Halim et al., 1999). *Bottom*, quantification of the northern blots; data are mean ± SD; *n*=3. (D) Northern and

western blot analyses after a 12-hr shift to the indicated Met concentrations. Protein is quantified below as mean ± SD; n=3. Unless otherwise noted, all statistical analyses are unpaired Student's t-tests and significance is annotated as not significant (ns), $p \leq 0.05$ (*), $p \leq 0.01$ (**), or $p \leq 0.001$ (***). Here, comparisons were made to the 100 μM sample.

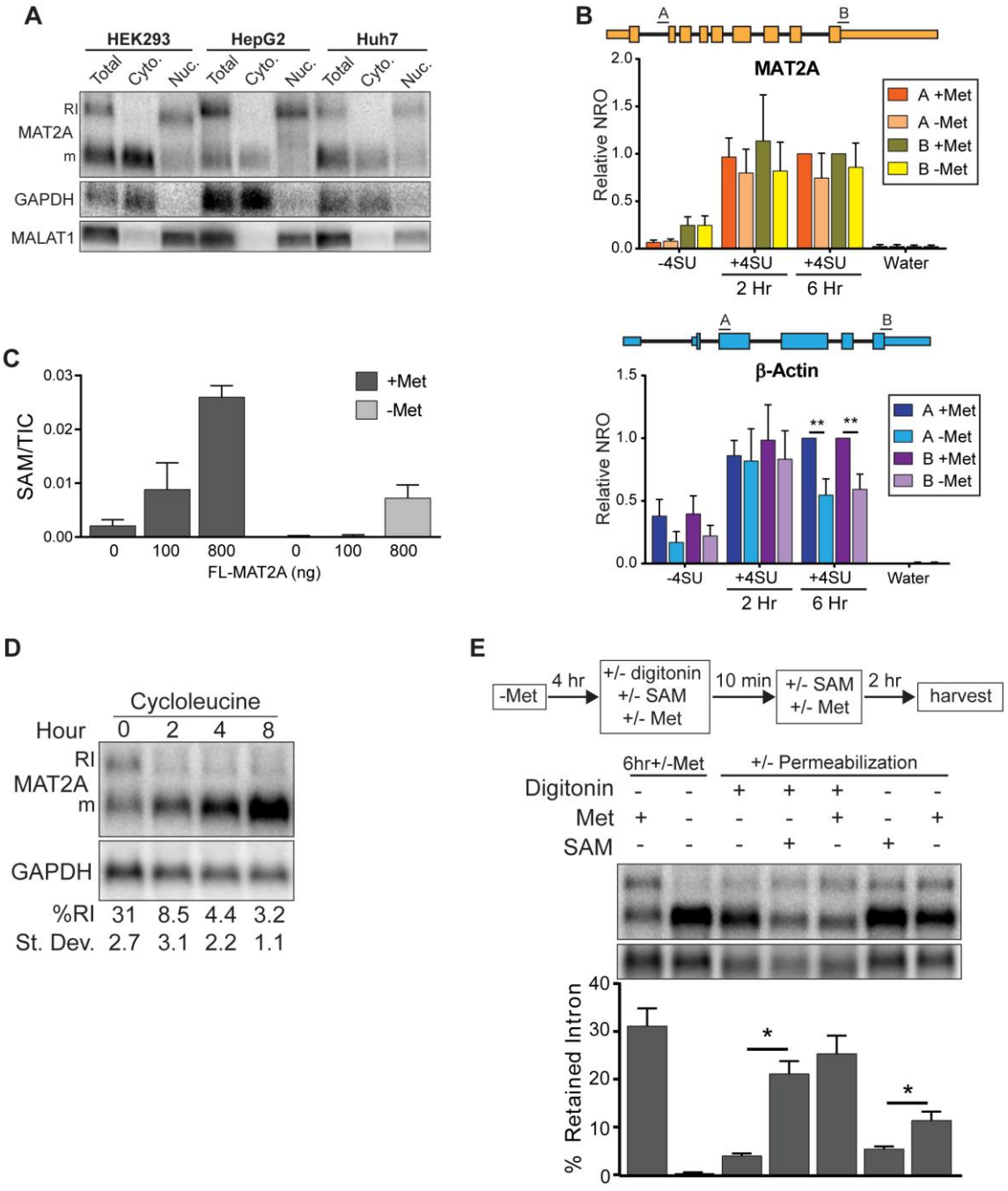

Figure 7. Induced Splicing of MAT2A Retained Intron is Driven by Intracellular SAM

(A) Northern blot of MAT2A with total, cytoplasmic, or nuclear RNA from the indicated cell lines. GAPDH and MALAT1 are cytoplasmic and nuclear markers, respectively. (B) Nuclear

run-on analysis measuring MAT2A and β-Actin transcription +/- Met for 2 and 6 hours. Nuclear run-on was performed in the presence of 4-thiouridine triphosphate (4SU) to allow selection of the run-on transcripts, so -4SU samples are included as a negative controls (see Materials and Methods). Transcription was monitored by RT-qPCR of two amplicons for each gene shown on the diagrams above the data (labeled A and B). For each experiment the +4SU/+Met 6H sample was set to 1. Data represented as mean ± SD; $n \geq 5$. (C) SAM measurements relative to total ion counts (TIC) for cells transfected as indicated. To detect SAM, the experiment was scaled up to 6-well plates, but the axis shows transfection amounts relative to a 12-well plates for easy comparison with Figure 1C. Data represented as mean ± SD; $n=4$. Mass spec analysis was performed by Kuanqing Liu. (D) Northern blot with quantification from cells treated with the MAT2A inhibitor cycloleucine for the indicated amounts of time. Data represented as mean ± SD; $n=3$. Experiment was performed by Olga Hunter. (E) *Top,* schematic of the digitonin permeabilization experiment. Cells were grown in Met-free media for 4hr and treated with Met or SAM in the presence or absence of digitonin for 10 minutes. After digitonin washout cells were grown for an additional 2hr in media supplemented with Met or SAM as indicated. Lanes 1 and 2 are cells grown in +/- Met media for 6 hr as controls. RNA was analyzed by northern blot and quantified. Data represented as mean ± SD; $n=3$.

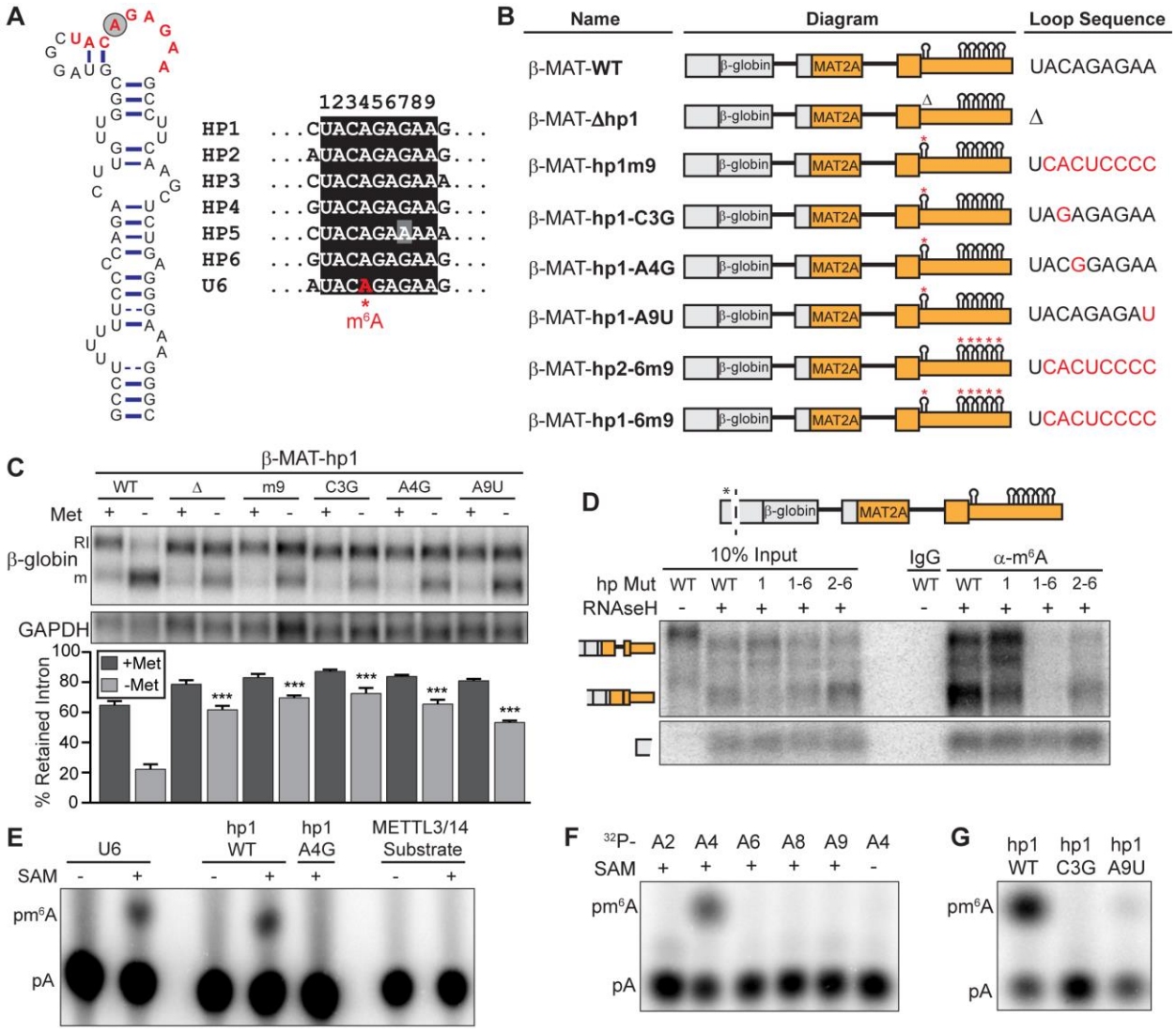

Figure 8. MAT2A Hairpin 1 Is Necessary for Regulation of Intron Retention and Has an N^6-Methyladenosine Modification

(A) *Left*, Structure of MAT2A hp1. Red, conserved nonamer; gray circle, predicted m^{6}A (A4). *Right*, Alignment of MAT2A conserved nonamers and U6 snRNA m^{6}A site. (B) Diagram of β-globin-MAT2A reporters. Red asterisks, mutation sites. (C) Northern blot and quantification of β-globin reporter assay. Data are mean ± SD; *n*=4. Statistical analysis compared all –Met samples to the WT-Met control (lane 2). (D) M^{6}A-IP experiment with indicated β-globin

reporters. RNase H cleavage site is shown as dashed lines. (E) TLC from an *in vitro* methylation assay in nuclear extract with uniformly labeled substrates. (F) Same as (E) except the hp1 RNA substrates were radiolabeled at specific adenosines. (G) Same as (F) with A4-labeled WT, C3G, or A9U substrates. For (E-G), experiments were performed by Olga Hunter and Nicholas Conrad.

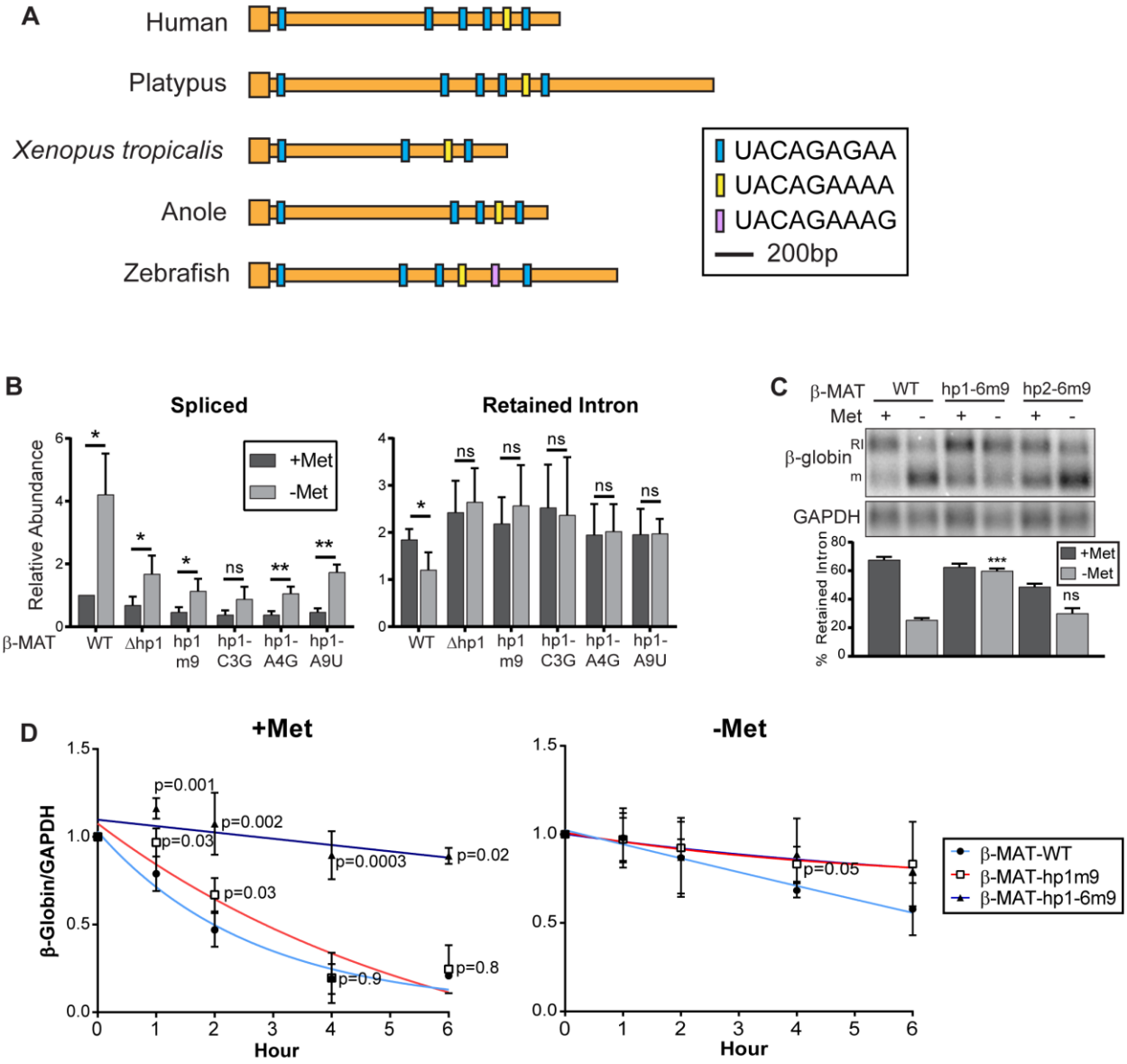

Figure 9. Conservation of MAT2A 3′ UTR and Hairpin Effects on Splicing and Stability

(A) Diagram of the last exon of SAM synthetase genes from various organisms including coding sequence (large box) and 3´ UTR. The conserved sequences are indicated by colored boxes. The diagram is approximately to scale. (B) Steady-state levels of spliced and unspliced β-globin reporter RNAs normalized to GAPDH and expressed relative to spliced WT +Met. Data represented as mean ± SD; *n*=4. (C) Northern blot of transfected β-globin reporters. Percent

retained intron is quantified from the northern blots, and statistical analysis compares WT –Met to other –Met samples. Data represented as mean ± SD; *n*=4. (D) RNA decay curves of different β-globin reporters normalized to GAPDH from Actinomycin D (ActD) treated cells. Cells were treated with either +/- Met media for four hours prior to hour 0, and then kept in the same media when ActD was added. Cells were fractionated, and only the cytoplasmic, spliced mRNA fraction was measured by Northern blot. P-values are compared to the WT at corresponding times. Data represented as mean ± SD; For hours 0, 1, 2, and 4, *n*=4. For hour 6, *n*=2.

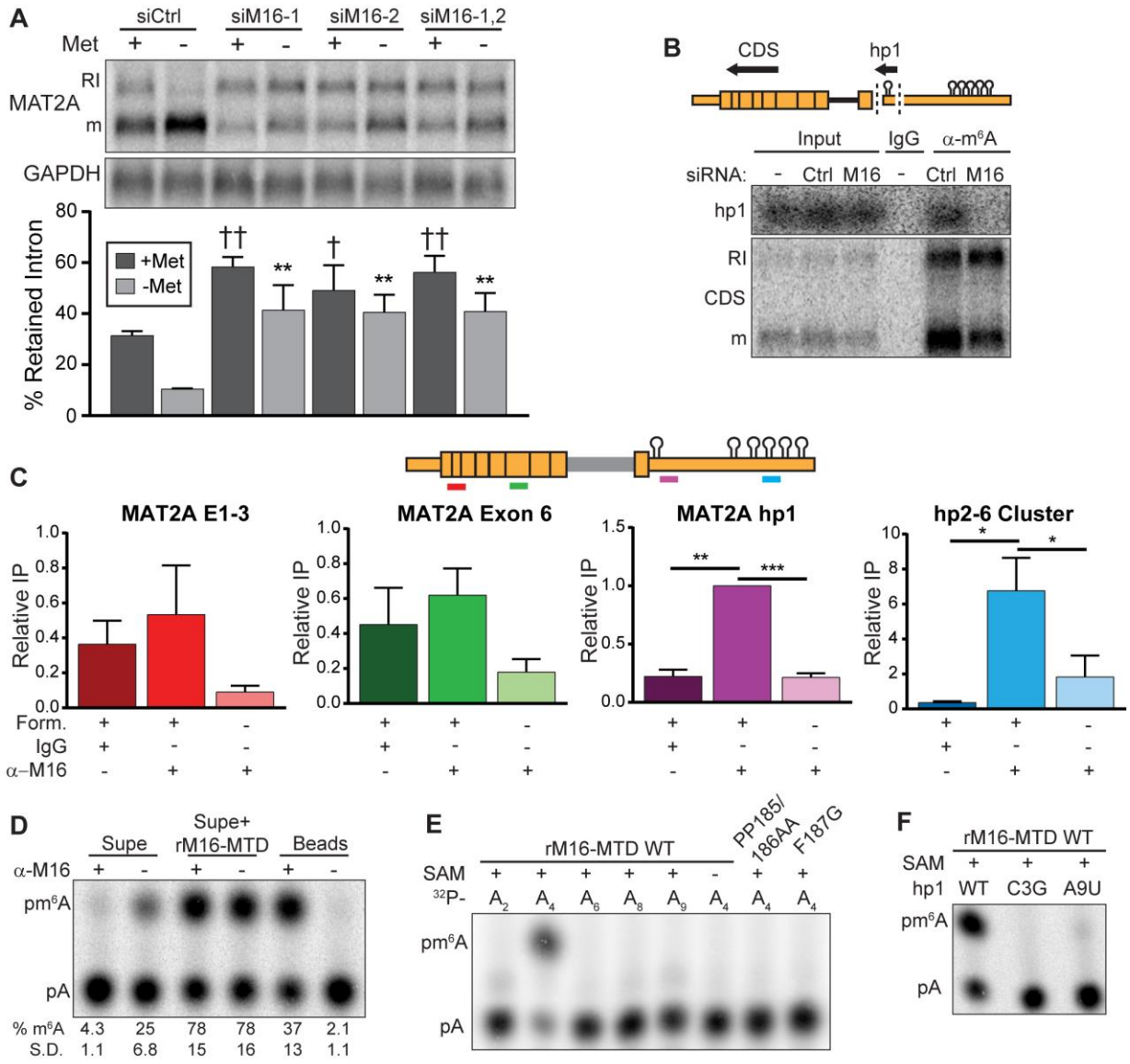

Figure 10. METTL16 Methylates the MAT2A Hairpins and Is Required for Splicing Induction

(A) Northern blot of MAT2A after knockdown with control siRNAs (siCtrl), or two METTL16 siRNAs transfected individually or together. Met was depleted for 4 hours. Quantification is mean ± SD; *n*=4. Statistical analysis compared –Met samples to siCtrl–Met (asterisks), and +Met samples to siCtrl+Met (daggers). (B) *Top*, Schematic of the MAT2A probes (arrows) and sites of

RNase H cleavage (dashed lines). *Bottom*, Northern blot of m^6A-IP with poly(A)-selected, RNase H-treated RNA from cells after the indicated siRNA treatments. (C) Formaldehyde RIP of METTL16 with MAT2A RNA. RT-qPCR amplicons are shown; the anti-M16/+Form value for hp1 was set to 1. Data are mean ± SD; *n*=3. (D) TLC from METTL16 immunodepletion experiment using hp1 radiolabeled at position A4 as substrate. Data are mean ± SD; *n*=3. (E) *In vitro* methylation assay using wild-type or mutant rM16-MTD with site-specific radiolabeled hp1 substrates. (F) *In vitro* methylation assay using wild-type rM16-MTD with A4-labeled WT or mutant substrates. For (D-F), experiments were performed by Olga Hunter and Nicholas Conrad.

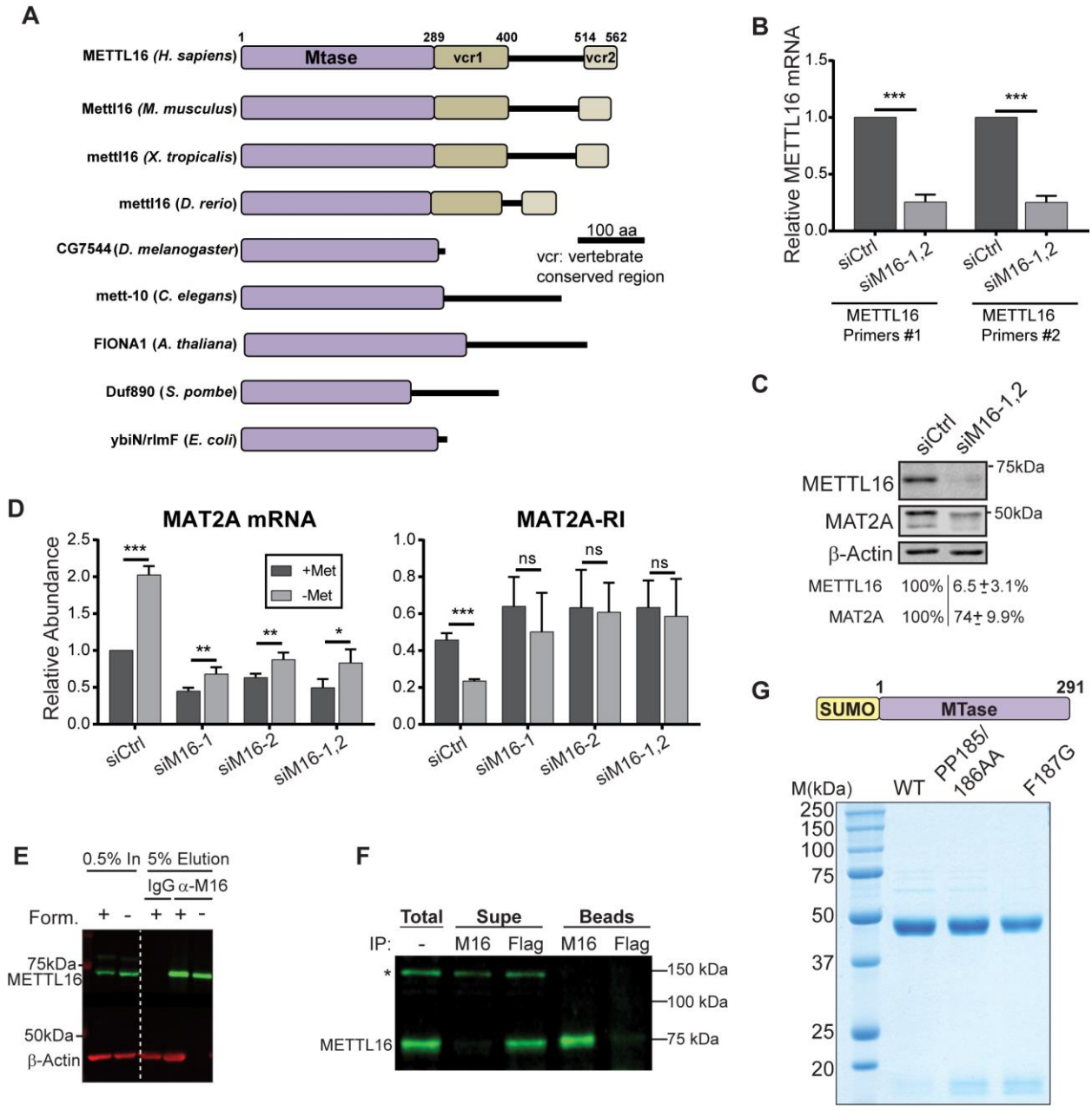

Figure 11. METTL16 Conservation and Additional Controls for METTL16 Knockdown and *In Vitro* Assays

(A) Diagram of METTL16 homologs. The methyltransferase and two vertebrate conserved regions (vcr) are shown. The diagrams are approximately to scale. (B) Quantitative RT-PCR of METTL16 mRNA with two different primer sets to show knockdown efficiency. Knockdown

experiments proceeded for 96 hrs. The values were normalized to GAPDH and expressed relative to siCtrl. Data represented as mean ± SD; $n \geq 7$. (C) Western blot of METTL16, MAT2A, and β-Actin after METTL16 knockdown. Relative levels of METTL16 and MAT2A after normalization to β-Actin are indicated. Data represented as mean ± SD; $n \geq 3$. (D) Levels of MAT2A mRNA and MAT2A-RI in METTL16 knockdown calculated from the northern blots (Figure 3A); values normalized to GAPDH and expressed relative to siCtrl +Met. Data represented as mean ± SD. $n=4$. (E) Western blot of protein from RIP experiment. β-Actin precipitates nonspecifically in crosslinked cells, providing a loading control for these lanes. (F) Western blot of METTL16 immunodepletion from nuclear extract. *Indicates a nonspecific band detected by the antibody that controls for sample loading. (G) Coomassie stain of recombinant METTL16 proteins purified from *E. coli*. This experiment was performed by Olga Hunter.

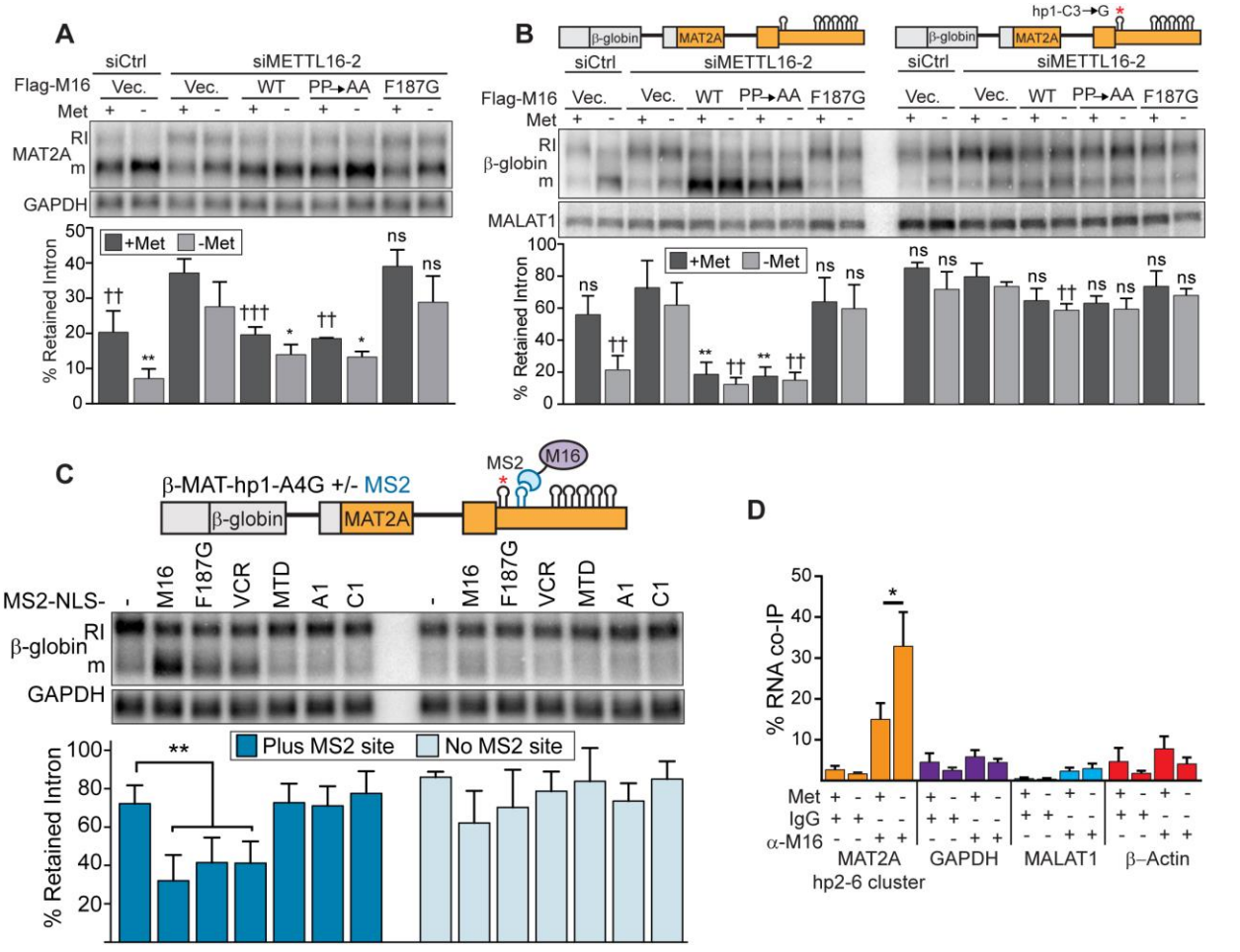

Figure 12. METTL16 Dwell Time on Hairpin 1 Regulates MAT2A Intron Retention

(A) Northern blot of MAT2A after knockdown of METTL16 and overexpression with Flag-tagged siRNA resistant METTL16 proteins (Vec., empty vector; WT, FLAG-METTL16; PP→AA, FLAG-PP185/186AA; F187G, FLAG-F187G). Data are mean ± SD; *n*=4. Statistical analysis compared all –Met samples to -Met/vector (asterisks), and all +Met samples to +Met/vector (daggers). (B) Same as (A) except β-globin reporters, β-MAT-WT or β-MAT-hp1-C3G, were assayed. Data represented as mean ± SD; $n \geq 3$. (C) Diagram of MS2 tethering strategy, representative northern blot, and quantification of intron retention (dark blue, with MS2 binding sites; light blue, no MS2 binding site). The MS2 fusions include a nuclear localization

signal (NLS). Data are mean ± SD; *n*=4. (D) METTL16 native RIP with extracts from cells grown for 3 hr +/-Met. Limited RNA digestion was performed and the MALAT1 amplicon is over 5 kb from the METTL16 binding site, so it serves as a negative control along with GAPDH and β-actin (Brown et al., 2016). Data are mean ± SD; *n*=3.

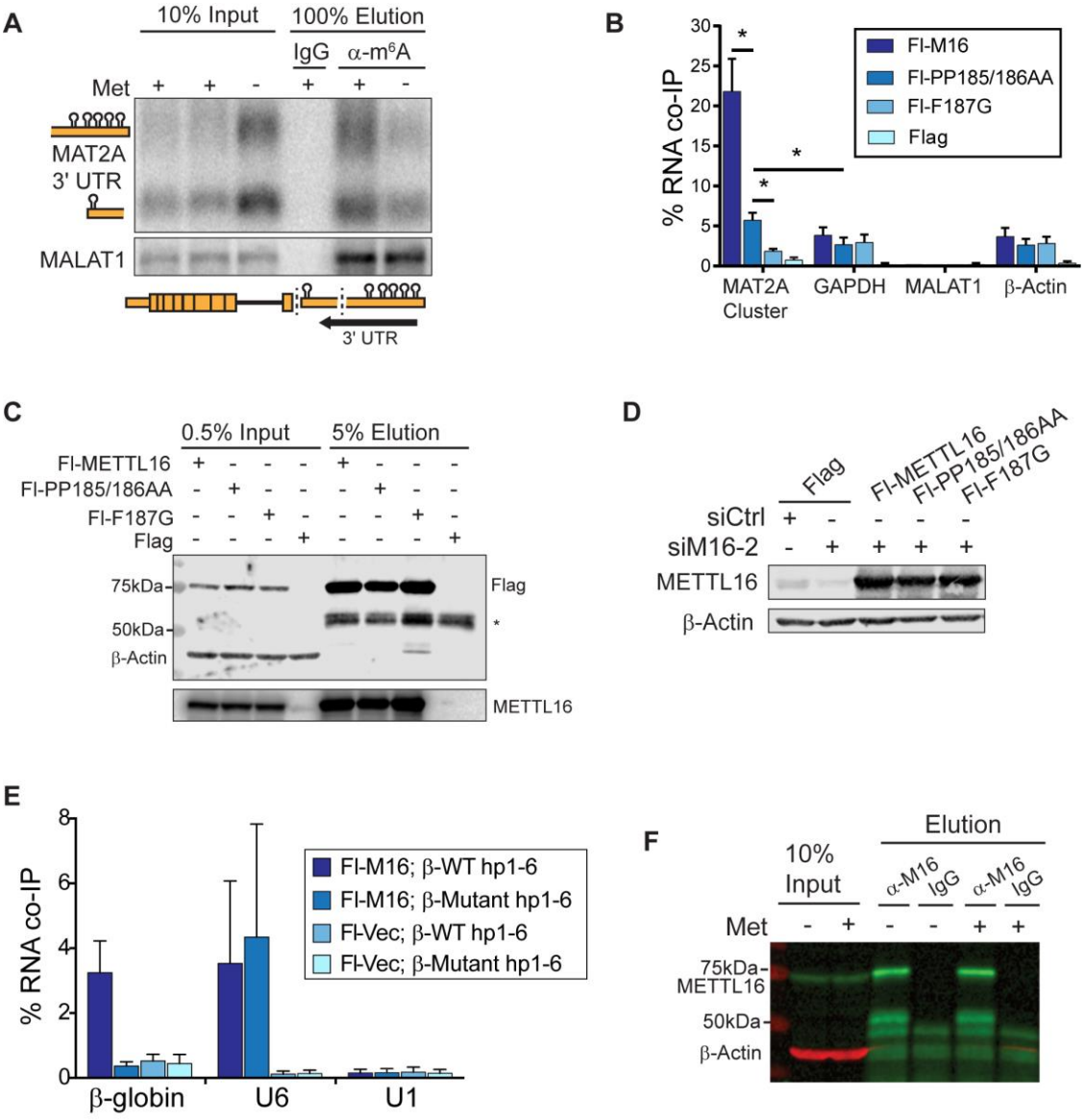

Figure 13. METTL16 Binding to Hairpin 1 Regulates MAT2A Intron Retention

(A) M^{6}A-IP with RNA from cells +/- 4 hours of Met depletion. Diagram shows RNase H sites as dashed lines and position of 3´ UTR probe (arrow). Note that the IP efficiency in Met-depleted conditions is lower even though the input MAT2A RNA levels are much higher. (B) Native RIP with anti-Flag antibodies using extracts from cells transfected with Flag vector, Fl-METTL16, Fl-PP185/186AA, and Fl-F187G. Met-free media was added 3 hrs prior to harvesting to ensure

METTL16 binding. Quantitative RT-PCR was used to measure RIP as a percentage of the input. GAPDH, MALAT1, and β-Actin are abundant transcripts used as negative controls. Data represented as mean ± SD; *n*=3. (C) Western blot of protein from native RIP as in (B). Asterisk indicates heavy chain antibody band. (D) Western blot with extracts from the indicated knockdown and transiently overexpressing cells. (E) Native RIP with anti-Flag antibodies using extracts from cells transfected with Fl-METTL16 (Fl-M16) or an empty vector control (Vec). Cells were co-transfected with β-globin-MAT2A reporter with all six hairpins either wild-type or A4G mutant sequence. Met-free media was added 2.5 hr prior to harvesting to ensure METTL16 binding. Quantitative RT-PCR was used to measure RIP as a percentage of the input. U6 snRNA is a positive control while U1 snRNA is a negative control. Data represented as mean ± SD; *n*=3. This experiment was performed by Olga Hunter. (F) Western blot of protein from native RIP of endogenous METTL16 +/- Met.

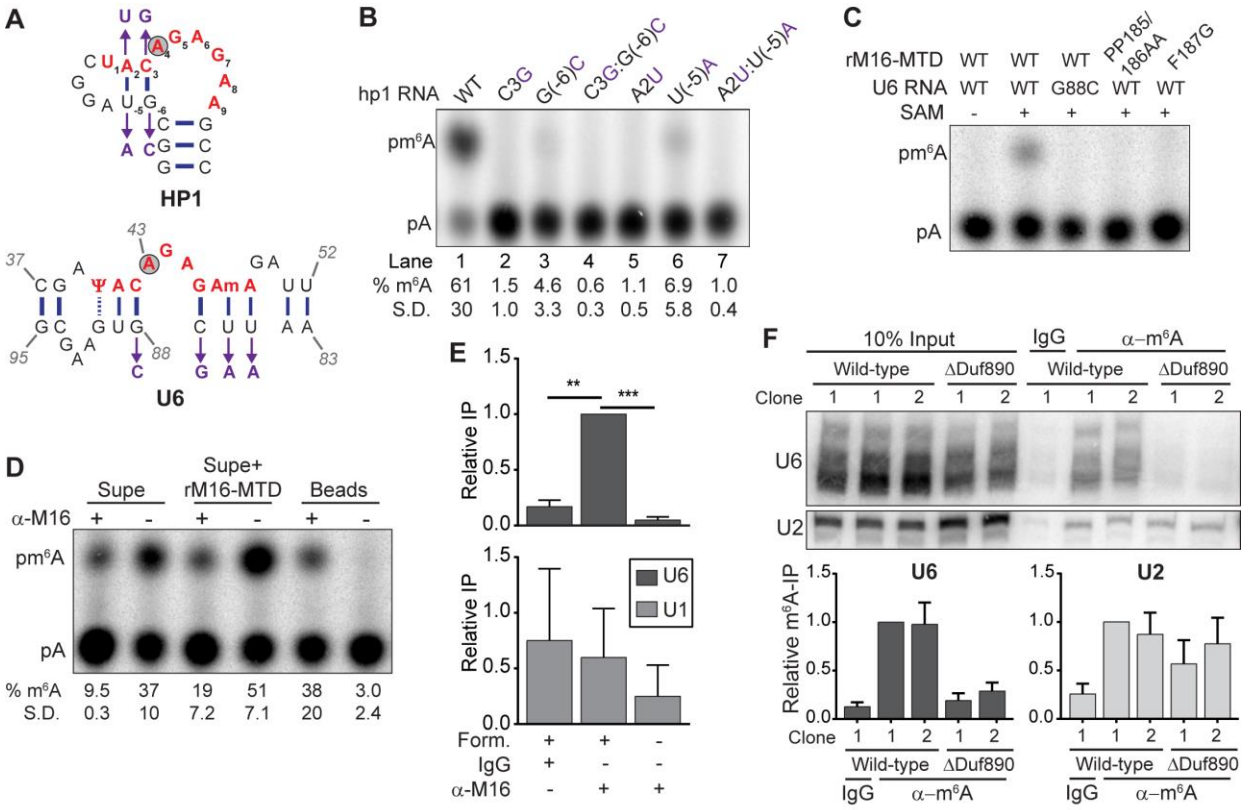

Figure 14. METTL16 Is the U6 snRNA N^6-Methyltranfserase

(A) Predicted structures surrounding the MAT2A hp1 and U6 snRNA methylation sites (gray circles). Red, conserved nonamer; Purple, mutants. (B) *In vitro* methylation with rM16-MTD and indicated hp1 substrates. Data are mean ± SD; *n*=3. (C) *In vitro* methylation assay using a site-specifically radiolabeled full-length WT or G88C U6 RNA substrates with rM16-MTD, PP185/186AA, or F187G. For (B-D), experiments were performed by Olga Hunter and Nicholas Conrad. (D) Immunodepletion assay (Figure 10D) using a U6 snRNA substrate. Quantification is mean ± SD; *n*=3. (E) Formaldehyde RIP of METTL16 with U6 and U1 snRNAs. The anti-M16/+Form for U6 was set to 1. Data are mean ± SD; *n*=3. (F) M^{6}A-IP of RNA from two independent colonies of wild-type or ΔDuf890 *S. pombe* strains. The IP efficiency for the wild-type clone 1 was set to 1. Data are mean ± SD; *n*=5.

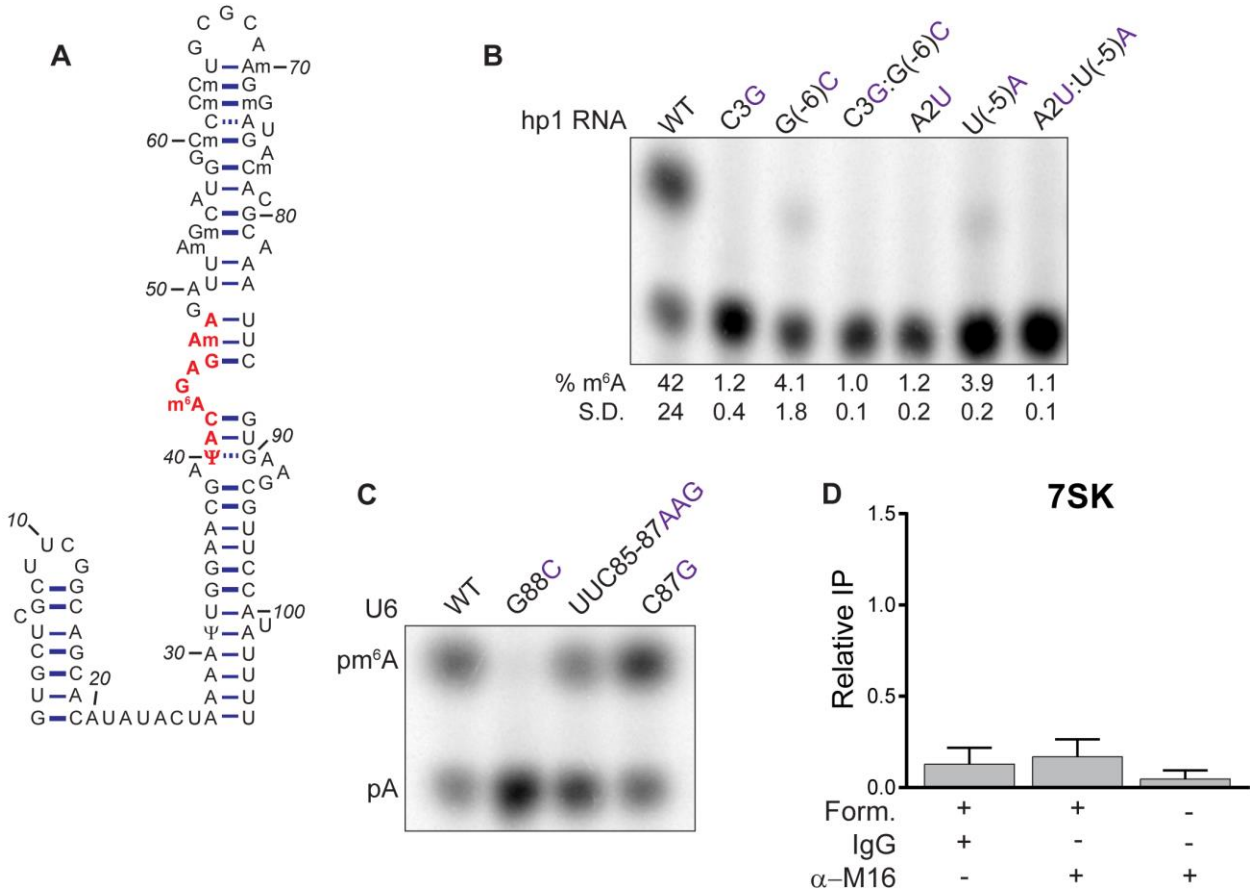

Figure 15. Further Validation that METTL16 Is the U6 snRNA N^6-Methyltranferase

(A) Structure of the free U6 snRNA (Mougin et al., 2002). (B) *In vitro* methylation assay using substrates as in Figure 16D, except the methylation activity was assessed in nuclear extract. (C) *In vitro* methylation assay in nuclear extract with U6 WT, G88C, UUC85-87AAG mutant, and C87G mutants. Label is at U6 snRNA position A43. For (B-C), experiments were performed by Olga Hunter and Nicholas Conrad. (D) Formaldehyde RIP assessing METTL16 IP of 7SK RNA as performed in Figure 14E. Data represented as mean ± SD; *n*=3.

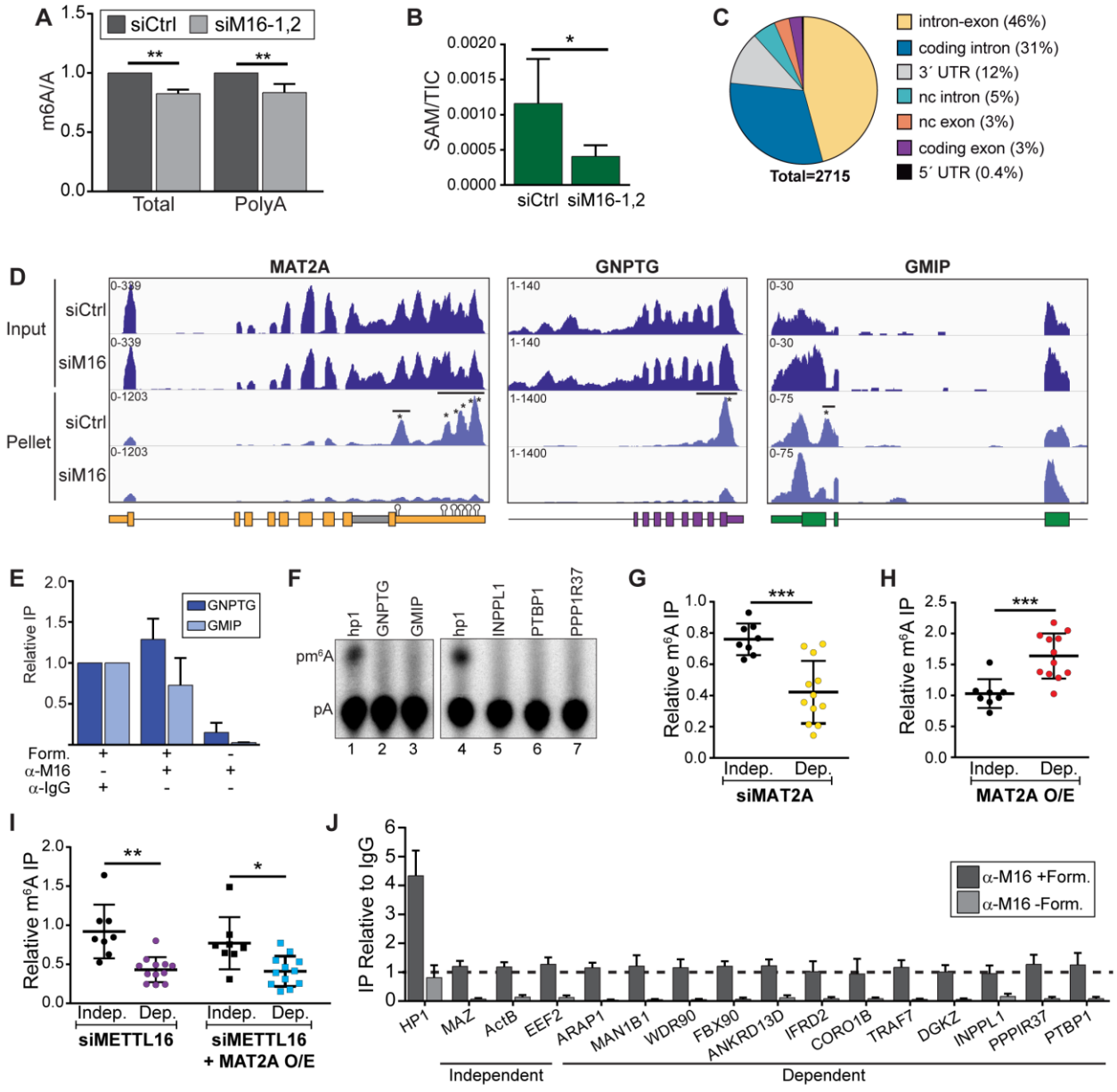

Figure 16. Global Analysis of M^{6}A after METTL16 Knockdown

(A) Ratio of m^{6}A to A in total and poly(A)-selected RNA after METTL16 knockdown; siCtrl was set to 1. Data are mean ± SD; $n \geq 4$. (B) Intracellular SAM levels normalized to total ion count (TIC) after METTL16 knockdown. Data are mean ± SD; $n=6$. For (A-B) experiments, mass spec analysis was performed by Kuanqing Liu. (C) Pie chart depicting the annotations of

the m^6A peaks that decrease upon METTL16 knockdown. (D) RNA-seq traces from the m^6A-seq. The peaks and UACAGAGAA sites are indicated by bars and asterisks, respectively. For (C-D) experiments, sequencing data analysis was performed by Beibei Chen. (E) Formaldehyde RIP as in Figure 10C; the IgG control was set to 1. Data are mean ± SD; *n*=3. (F) *In vitro* methylation assay as in Figure 8E. Experiment performed by Olga Hunter and Nicholas Conrad. (G) M^6A-IP was performed on RNA from cells in which MAT2A was knocked down. The m^6A-IP efficiency was compared to siCtrl samples for a panel of twelve METTL16-dependent and nine METTL16-independent m^6A peaks (Figure 15E). Each point is the average m^6A-IP efficiency for a specific peak. (H) Same as (G) except MAT2A was overexpressed. (I) Same as (G) except RNA from siM16-treated cells was assessed +/- MAT2A overexpression. (J) Formaldehyde RIP as in (E). The IP efficiency of the IgG control was set to one, but is not shown.

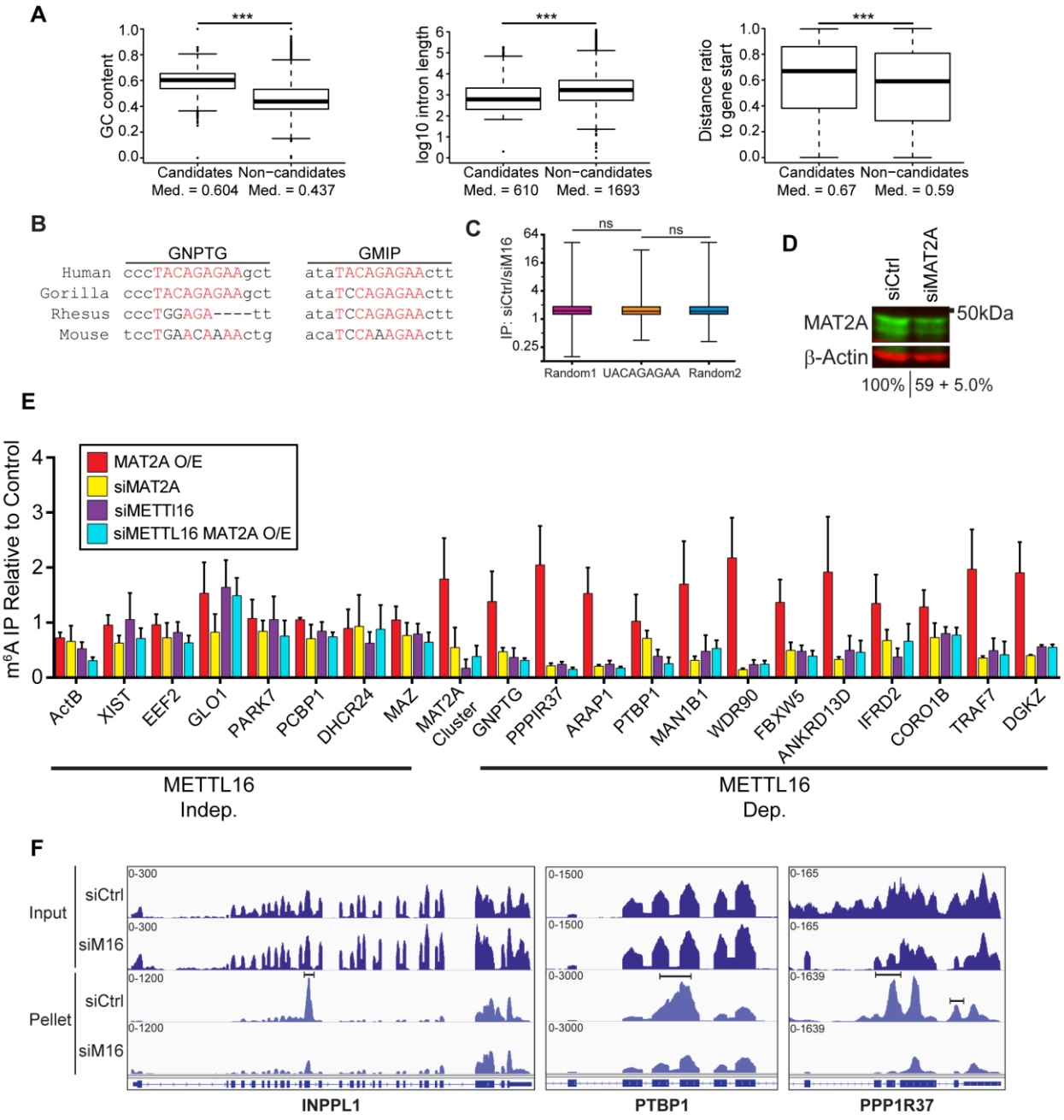

Figure 17. Global analysis of METTL16-dependent m^{6}A sites

(A) Comparison of the GC-content, intron length and distance to gene start of the introns overlapping the METTL16-dependent peaks (candidates; n=1943) identified by m^{6}A-seq with the total population of introns (non-candidates; n=162,259). The distance to gene start is

calculated as a fraction of the entire gene length. Statistical significance was $p<2.2 \times 10^{-16}$ determined using the Wilcoxon test. Mean values are listed below each sample. Sequencing data analysis performed by Beibei Chen. (B) The TACAGAGAA elements in GNPTG and GMIP are not conserved. Alignments show the TACAGAGAA element in upper case and its conservation in red. Note that mutation of A2 inhibits methylation (Figure 14 and 15), so the single A to C change in Gorilla and Rhesus GMIP likely inhibits methylation. (C) All windows containing reads on UACAGAGAA elements in the siCtrl m^6A-IP sample were pooled and the relative IP in siCtrl compared to siM16 is shown as a box-and whiskers plot (n=753). The data were compared to two independent random sets of windows that passed the same threshold of reads in the anti-m^6A siCtrl pellets (n=753 and n=757). The box is the 25^{th}—75^{th} percentile, the horizontal line is the median and the whiskers are the upper and lower 25 percent. Sequencing data analysis performed by Beibei Chen. (D) Western blot showing MAT2A knockdown efficiency compared to β-Actin loading controls (*n*=3) (E) Quantification of the m^6A IP efficiency of nine METTL16-independent peaks, twelve METTL16-dependent peaks, and MAT2A. The m^6A-IP efficiency of MAT2A overexpression is relative to empty vector control, while siRNA treatments are relative to the siControl. (F) RNA-seq traces of INPPL1, PTBP1, and PPP1R37 from an m^6A-seq experiment. Both inputs (dark blue) and pellets (light blue) are shown; the scale is shown in the upper left corner. The bars approximate the position of the METTL16-dependent m^6A peaks.

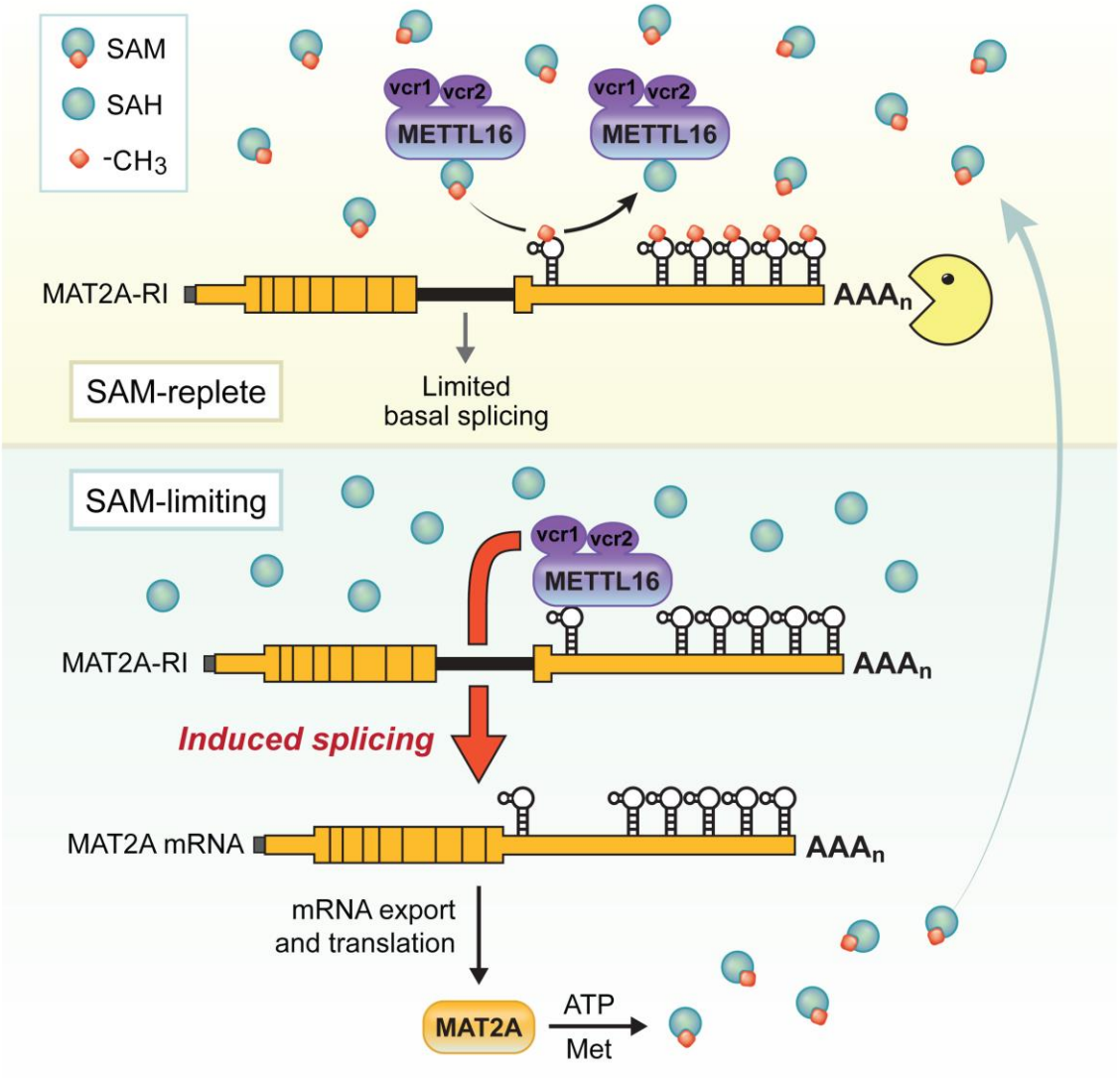

Figure 18. Model for METTL16 Activation of MAT2A Splicing in Response to SAM Levels

We propose that SAM abundance controls the dwell-time of METTL16 on the MAT2A hp1 by modulating its methylation efficiency. In turn, METTL16 occupancy promotes efficient splicing. See text for details. The diagram depicts posttranscriptional splicing induction, but our data are also consistent with METTL16 promoting co-transcriptional splicing. Figure drawn by Angela Diehl.

CHAPTER FIVE
Results

MAT2A MRNA LEVELS ARE REGULATED BY CO-TRANSCRIPTIONAL SPLICING OF A RETAINED INTRON

Introduction

Intron retention is an alternative splicing event where an mRNA is fully processed, except at least one intron remains unspliced. While intron retention is known to be a form of regulation in other organisms, it was long thought to be rare and often non-regulatory in mammals (Keren et al., 2010). However, more recent studies and extensive bioinformatic analysis have shown that intron retention is fairly common; roughly 50% of genes express a retained intron form in at least 10% of their transcripts in at least one cell type (Boutz et al., 2015; Braunschweig et al., 2014; Galante et al., 2004; Sakabe and de Souza, 2007; Yap et al., 2012). Retained intron (RI) transcripts for most genes are nuclear (Bergeron et al., 2015; Boutz et al., 2015; Braunschweig et al., 2014; Yap et al., 2012), though some reports suggest that certain genes produce RI transcripts that can be exported to the cytoplasm (Braunschweig et al., 2014; Wong et al., 2013). Interestingly, RIs are often highly conserved in mammals (Boutz et al., 2015; Braunschweig et al., 2014), suggesting that there is likely something within the intron sequence to promote its retention or conditional splicing, though no common sequence has been identified. RIs also often have weaker splice sites, are more biased towards the 3′ ends of transcripts, are shorter than average, and are more GC rich (Boutz et al., 2015; Braunschweig et al., 2014; Sakabe and de Souza, 2007).

Despite these commonalities, mechanistic information for regulation of these RI RNAs is lacking. Though studies have found that downregulation or overexpression of splicing components can affect intron retention (Guo et al., 2014; Wong et al., 2013; Yap et al., 2012), few addressed how this regulation occurred in response to regulatory cues. For example, the SR protein kinase Clk1 expresses predominantly an RI isoform under normal conditions. Upon treatment with a Clk1 inhibitor, CB19, the RI form of Clk1 can be post-transcriptionally spliced to produce an mRNA (Boutz et al., 2015; Ninomiya et al., 2011). This work proposes a model in which RI transcripts can act as reservoirs for mRNAs of their respective genes when prompted by a regulatory cue. However, more examples of regulated intron retention are needed to understand if this type of regulation is broadly applicable.

We identified that the gene MAT2A also expresses a nuclear RI transcript, with the intron 8 of MAT2A retained (Figure 6A, 7A) (Chapter 4) (Bresson and Conrad, 2013). MAT2A expresses a SAM synthetase, which takes Met and ATP and converts it into SAM. Depletion of Met, which depletes cellular SAM, regulates the mRNA expression of MAT2A (Martinez-Chantar et al., 2003b). Upon Met depletion, the MAT2A RI isoform decreases, while the fully spliced form increases (Figure 6B). Other methods of modulating SAM levels within the cell also affect the relative expression of the MAT2A RI isoform to the mRNA (Figure 6C, 7C, 7D, and 7E), and we have previously identified that this regulation is caused by interaction of a highly conserved 3′ UTR hairpin with the m^6A methyltransferase METTL16 (Pendleton et al., 2017). However, the fate of the RI isoform of MAT2A remained undefined.

To further define mechanisms of intron retention, we studied the regulatory switch that modulates levels of MAT2A RNA. We find that upon Met depletion, the MAT2A RI isoform is

not spliced and exported as an mRNA, but is degraded. The shift into the mRNA isoform is instead driven by increased co-transcriptional splicing of the RI. Overexpression of METTL16 can also promote increased co-transcriptional splicing of the MAT2A RI. Furthermore, we validated post-transcriptional splicing of the Clk1 RI isoform, but also determined that an increase of co-transcriptional splicing for its RI occurs upon inducing conditions. These data suggest that not all RI transcripts act as mRNA precursors, but an increase of co-transcriptional splicing might be a shared mechanism regardless of RI isoform fate.

Results

Splicing of the RI Isoform of MAT2A Is Not Induced upon Met Depletion

While there are a variety of potential roles for RI transcripts, we focused on testing the two most obvious models for their regulation. The first model is the dead end model (Figure 19A, *left*), in which the RI isoforms produced undergo degradation. This model suggests that levels of an mRNA are determined during co-transcriptional splicing and that genes may use intron retention to influence their mRNA levels without modifying their transcription rates. The second model is the reservoir model (Figure 19A, *right*); the RI isoform serves, essentially, as a source for rapid production of more mRNA. If a signal indicates that more of its gene is necessary, the RI isoform can be spliced to rapidly produce more mRNA. The previously identified Clk1 transcript was reported to behave according to this model (Boutz et al., 2015; Ninomiya et al., 2011).

In order to test these models, we first performed transcription inhibition with either ActD or flavopiridol, and then induced with the stimuli responsible for decreasing the RI isoform and increasing the mRNA. As previously described (Boutz et al., 2015), when the cells were treated

with flavopiridol and then CB19, the Clk1 kinase inhibitor, we observed a decrease of the RI isoform and an increase of the fully spliced isoform (Figure 19B). Surprisingly, when we treated the cells with ActD then CB19, we did not observe this splicing response. Instead, we observed degradation of both the RI and the fully spliced isoforms at a similar rate with or without CB19 treatment. Thus, though the Clk1 retained intron can be spliced, it seems that the transcription inhibitor used affects its induced splicing response.

When we performed the transcription inhibition and then Met depletion, we observed a different result (Figure 19C). First, the MAT2A mRNA isoform never increases over time, though it persists longer in Met-free conditions. This persistence is consistent with previously observed improved cytoplasmic stability upon Met depletion (Martinez-Chantar et al., 2003b). Second, we observed no substantial decrease of the MAT2A RI isoform in the Met-free conditions compared to the Met-replete conditions. This observation does not support the idea that splicing of the MAT2A RI form induces upon Met depletion. Third, as previously reported, the MAT2A RI and nuclear MAT2A mRNA become hyperadenylated upon transcription inhibition (Bresson et al., 2015). This artificial effect could potentially interfere with normal splicing regulation of the transcript, so we are cautious about the interpretation of the results. Nonetheless, these data do not support a precursor-product relationship between MAT2A RI and the mRNA.

To eliminate the side effects of transcription inhibitors, we performed a pulse chase assay with 4-thiouridine (4SU) to monitor MAT2A levels. We added 4SU to the cell media for two hours, performed a brief washout period to ensure complete incorporation, and then changed the media to either Met-replete or Met-free. Initial results of endogenous MAT2A were inconclusive

(Figure 19D). While we clearly observed that the MAT2A mRNA is more stable under Met-free conditions, initial low levels of the RI isoform made it difficult to determine if decreases in the RI levels corresponded with increases with the mRNA. To address this problem, we overexpressed an exogenous MAT2A to drive the endogenous MAT2A into mostly the RI isoform (Figure 6C), and then performed the pulse chase experiment. Though we started with considerably more of the RI isoform, we did not observe an increase in the fully spliced mRNA that corresponds with the decrease in the RI isoform upon either Met-free or Met-replete media conditions (Figure 19E). While these results do not conclusively prove that the MAT2A RI isoform can never undergo splicing, they favor the dead end model.

MAT2A RI Regulation Is Driven by Increased Efficiency of Co-transcriptional Splicing

Because we found no evidence to support the reservoir model for MAT2A, we investigated if splicing of the RI was co-transcriptionally regulated. We used both nuclear run-on assays and 4SU "quick pulse" experiments to measure co-transcriptional splicing. In nuclear run-on assays, nuclei are isolated under conditions where polymerases in the elongation phase can still function, but splicing components are non-functional. The nuclei are subjected to conditions where the polymerase elongation is allowed to briefly progress in the presence of labeled nucleotides to allow labeling of the nascent RNA. In the 4SU "quick pulse" experiment, RNA is briefly labeled in the cell, and the cells are harvested. While this procedure mostly captures nascent RNA, RNA processing can still occur. For both of these experiments, if co-transcriptional splicing occurs, RT-qPCR can detect signal across the exon junction. This signal would increase upon inducing conditions. If post-transcriptional splicing of the RI was responsible for the switch to mRNA,

then no change in the RI exon junction signal would be expected upon inducing conditions (Figure 20A).

We found that isolated, labeled RNA from both nuclear run-on assays (Figure 20B) and 5-minute 4SU pulse experiments (Figure 20C) show an increase of only the MAT2A RI exon junction upon Met depletion. Other exon junctions and intronic regions show no significant change relative to Met-replete conditions. Furthermore, we tested if the previously established interaction with METTL16 could also drive increased co-transcriptional splicing. We overexpressed Flag-tagged empty vector, METTL16, PP185/186AA, or F187G. METTL16 and PP185/186AA both have been previously shown to promote more of the spliced MAT2A isoform, while F187G does not affect MAT2A isoform expression (Figure 12A and B). We performed a 10-minute 4SU pulse, and found increased signal for the RI exon 8-9 junction upon both METTL16 and PP185/186AA, though not for F187G, overexpression (Figure 20D). This result suggests that METTL16 helps to drive co-transcriptional splicing of the MAT2A RI.

Though others identified that the Clk1 RI isoform can be post-transcriptionally spliced (Boutz et al., 2015; Ninomiya et al., 2011), we observed differences in the splicing response dependent upon the transcription inhibitor. To further explore the previous result, we investigated if co-transcriptional splicing plays a role in the induction of the Clk1 mRNA. After pre-treating our cells with CB19 for one hour, we performed a 5-minute 4SU pulse, and then measured the resulting labeled RNA through RT-qPCR (Figure 20E). While expression of the housekeeping gene GAPDH and other Clk1 intron and exon junctions do not change, the Clk1 RI exon junction increases in CB19-treated cells compared to DMSO-treated cells. This data

suggests that co-transcriptional splicing of the RNA plays a role in responding to the Clk1 splicing stimulus.

Discussion

The abundance of RI transcripts suggests that they likely play regulatory roles in the cell, but their regulatory mechanisms are still poorly understood. In this work, we demonstrated that conditions that induce more MAT2A mRNA and decrease the RI isoform do not appear to do so through post-transcriptional splicing of the RI. Rather, the previously described interaction of METTL16 with a regulatory element in the MAT2A 3′ UTR induces increased co-transcriptional splicing upon Met depletion (Figure 21). The co-transcriptional splicing, as well as increased stability of the MAT2A mRNA under Met-free conditions, is responsible for the dramatic shift to the accumulation of only the fully spliced mRNA.

The regulation of the MAT2A RI isoform adds another example of regulated intron retention to the field and provides evidence that not all RI transcripts act as reservoirs. Though previous work showed that some RI transcripts are exported to the cytoplasm and undergo NMD (Braunschweig et al., 2014; Wong et al., 2013), our data suggests that there might be nuclear subsets of RI transcripts that are processed differently. An interesting difference to be noted between the MAT2A RI and the Clk1 RI is their response to transcription inhibitor treatment. The MAT2A RI became hyperadenylated and stable (Bresson and Conrad, 2013), though this stability was not seen in a pulse chase experiment. This observation, coupled with previous work that suggested the transcription inhibitor induced hyperadenylation decouples the transcripts from nuclear degradation (Bresson et al., 2015), supports the idea that the hyperadenylation and stability of some nuclear transcripts is an artifact of the transcription inhibitors. The Clk1 RI did

not undergo the hyperadenylation or increased stability effect. Another paper also noticed that many of the RI transcripts were highly stable after transcription inhibition (Boutz et al., 2015), though if they behave similarly to MAT2A, this could be an artefactual result.

In addition, induced splicing for Clk1 was only seen with flavopiridol, not ActD, treatment. These observed differences could be explained by the different methods of transcription inhibition. ActD intercalates DNA and blocks further progression of the RNA polymerase. Flavopiridol works by inhibiting CDK9, and therefore blocks RNA polymerase from entering elongation. It's possible the induced splicing seen in flavopiridol is actually just splicing of nascent transcripts from the already elongating RNA polymerase. If true, then it suggests that co-transcriptional splicing also might be the main regulatory mechanism of the Clk1 RI.

Nevertheless, the observation that MAT2A and Clk1 behave differently upon treatment with transcription inhibitors could provide evidence of different populations of nuclear RI transcripts. Further exploration is necessary to be confident in this difference, though if it proves to be true, it will be interesting to identify if there are any variances between the populations.

Furthermore, our work emphasizes the importance of induced co-transcriptional splicing of the normally poorly splicing RI transcripts (Boutz et al., 2015; Braunschweig et al., 2014; Sakabe and de Souza, 2007). Co-transcriptional splicing is by far the most common splicing method (Ameur et al., 2011; Bhatt et al., 2012; Khodor et al., 2011), and our data suggests that cells will switch to this method when more of an mRNA is necessary. However, a more widespread study with a stimulus that induces the splicing of a broad range of RI transcripts is necessary to confirm this hypothesis.

Overall, a greater understanding of RI regulatory mechanisms helps substantiate that intron retention is a legitimate form of RNA regulation, and not just aberrant splicing. The identification of more regulatory cues and the study of more individual transcripts will be necessary to better understand the variety of intron retention mechanisms that cells utilize. Given the increase of intron retention in certain cancers (Dvinge and Bradley, 2015; Hsu et al., 2015; Jung et al., 2015), mechanistic knowledge of intron retention could prove therapeutically useful.

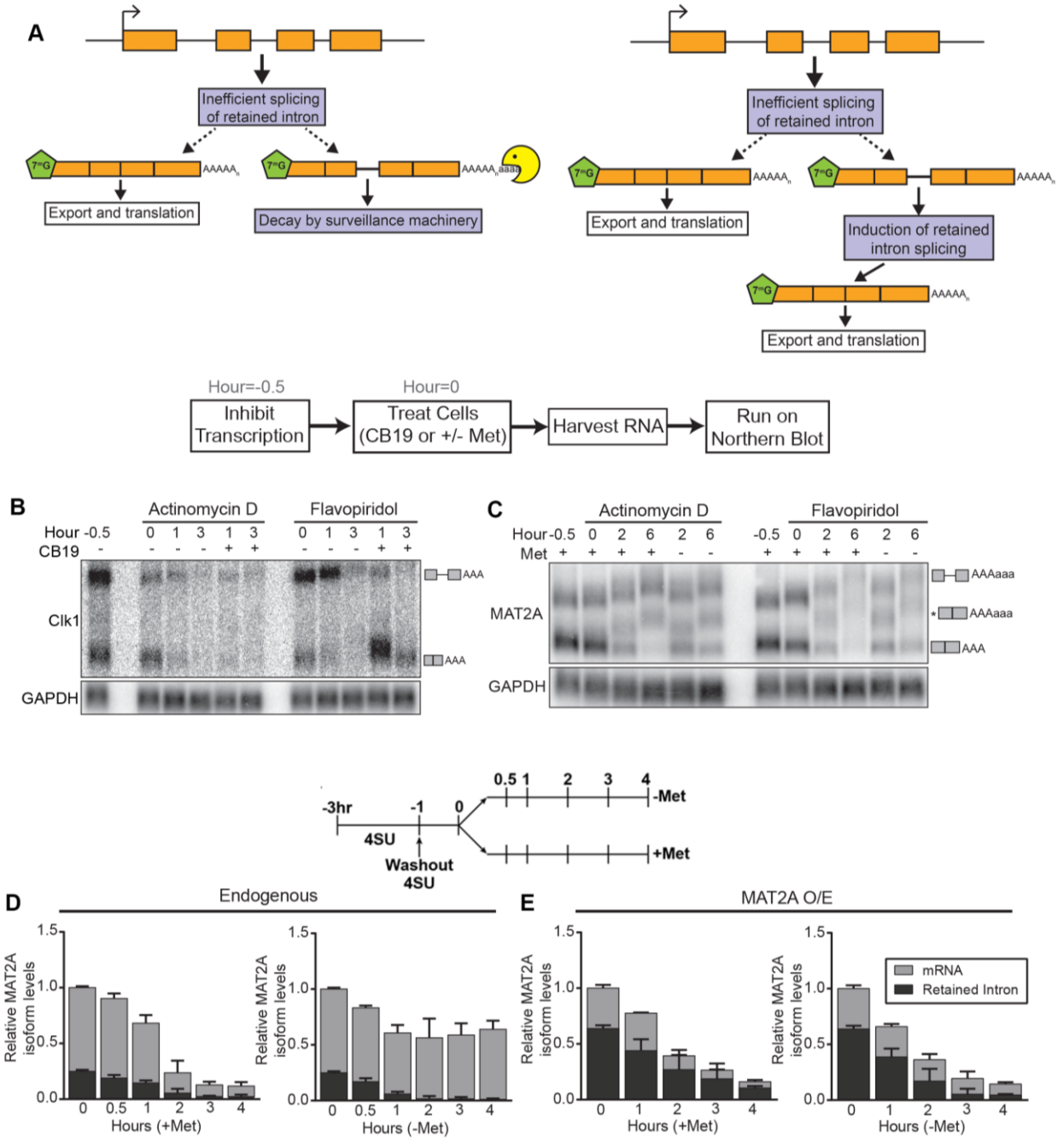

Figure 19. Splicing of the RI Isoform of MAT2A Is Not Induced upon Met Depletion

(A) Models depicting potential fates of RI RNAs. The "dead-end" model (*left*) depicts that the RI isoform is always degraded. The "reservoir" model (*right*) depicts that a signal can induce post-transcriptional of the RI transcript. (B) Northern blot of Clk1 RNA after treatment with ActD or

flavopiridol, then the Clk1 kinase inhibitor CB19 or DMSO. (C) Northern blot of MAT2A RNA after treatment with either ActD or flavopiridol, then Met-free or complete media. GAPDH serves as a loading control. (D) 4SU labeling assay to assess the precursor-product relationship between the MAT2A RI isoform and mRNA with endogenous MAT2A. Quantified by northern blot. Data represented as mean ± SD; *n*=3. Experiment performed by Nicholas Conrad. (E) MAT2A mRNA was exogenously overexpressed before the 4SU labeling assay as in (D). Data represented as mean ± SD; *n*=3. Experiment performed by Nicholas Conrad.

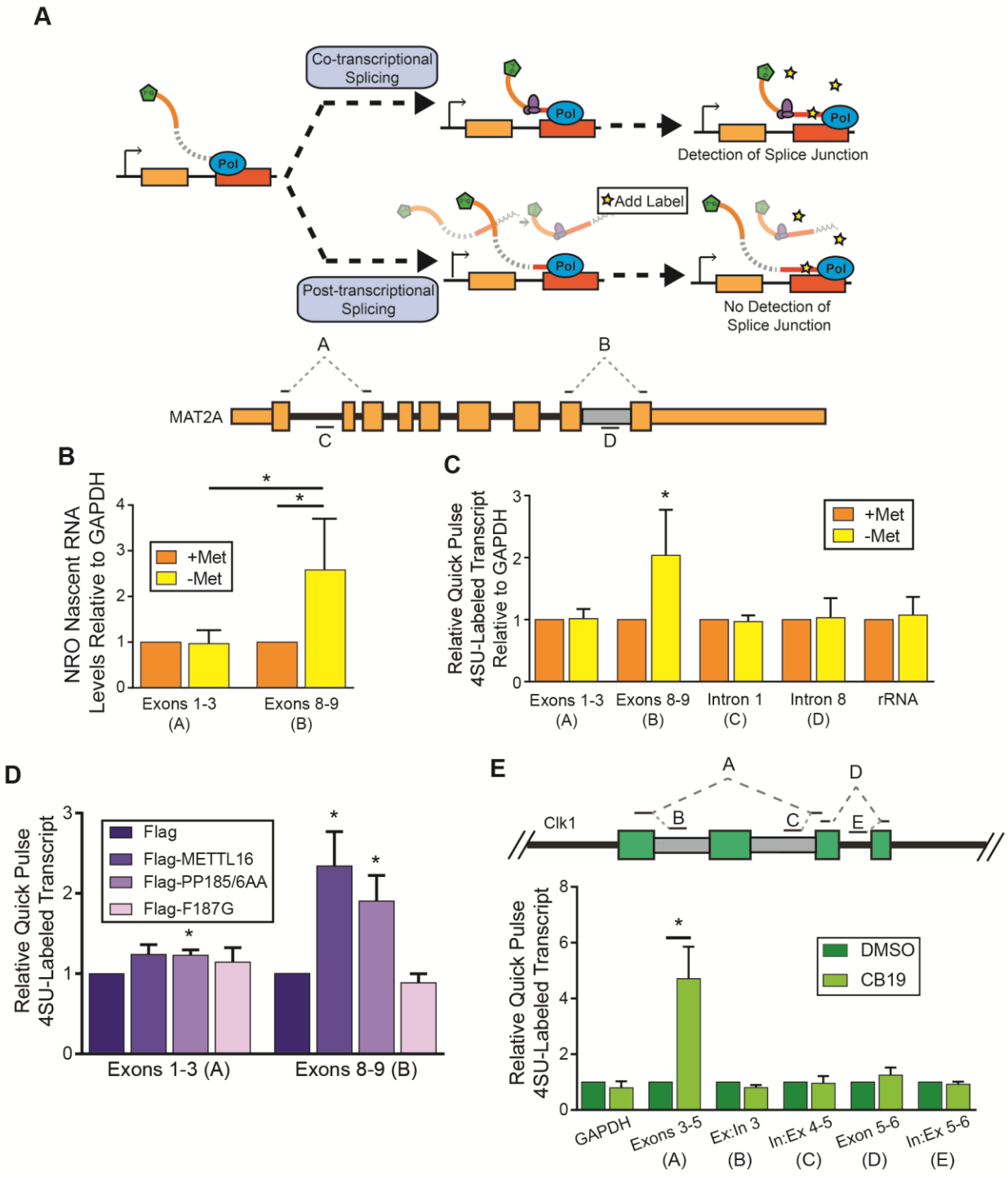

Figure 20. MAT2A RI Regulation Is Driven by Increased Efficiency of Co-transcriptional Splicing

(A) Diagram of co-transcriptional splicing assays. (B) Nuclear run-on with 4SU labeling of nascent transcripts for MAT2A. Nuclei were harvested after 6 hours +/- Met and the procedure performed. Labeled RNA was measured by RT-qPCR. Because –Met conditions generally decrease transcription, we standardized all samples relative to the levels of GAPDH. Data represented as mean ± SD; $n \geq 5$. (C) Quick pulse assays were performed after 1 hour +/- Met, and the labeled RNA was measured by RT-qPCR. Because –Met conditions generally decrease transcription, we standardized all samples relative to the levels of GAPDH. Data represented as mean ± SD; $n \geq 4$. (D) Quick pulse assays were performed after 24 hour overexpression of empty Flag vector, METTL16, PP185/186AA, or F187G, and the labeled RNA was measured by RT-qPCR. Samples were standardized to the empty Flag vector. Data represented as mean ± SD; $n=3$. (E) Quick pulse assays after 1 hour CB19 treatment, and the labeled RNA was measured by RT-qPCR. Samples were standardized to the DMSO control. Data represented as mean ± SD; $n=3$.

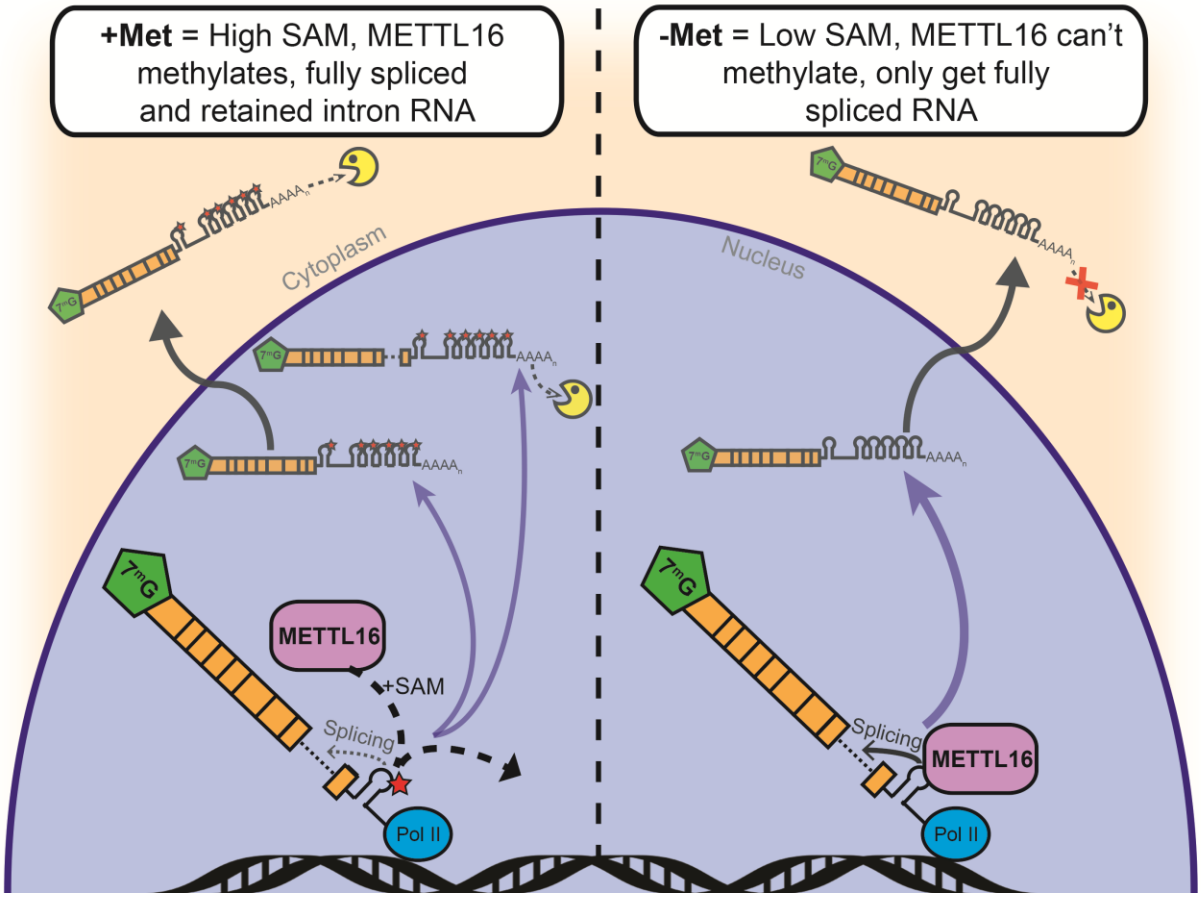

Figure 21. MAT2A Undergoes Co-transcriptional Splicing Regulated by METTL16 Interaction

We propose that MAT2A intron retention is regulated by the METTL16 through co-transcriptional splicing of the retained intron. SAM abundance controls the dwell-time of METTL16 on the MAT2A hp1 by modulating its methylation efficiency. Increased METTL16 interaction drives co-transcriptional splicing, which produces more fully spliced mRNA.

CHAPTER SIX
Conclusions and Future Directions

Conclusions

This work describes a unique pathway that regulates SAM through a relatively understudied mechanism of alternative splicing. We have described that MAT2A expresses both a fully spliced mRNA and an RI isoform, and that intracellular SAM levels modulate the expression and stability of these isoforms. In conditions of high SAM, the cell favors the expression of the RI isoform; in conditions of low SAM, it favors the fully spliced mRNA. We demonstrated that this change in isoform expression is dependent upon hairpins in the MAT2A 3′ UTR. While the hp2-6 cluster towards the end of the 3′ UTR plays a role in stability, the hp1 at the very beginning of the 3′ UTR is critical for the increased splicing upon low cellular SAM levels. Furthermore, a highly conserved UACAGAGAA sequence located in the loop of each hairpin is necessary for this activity.

We showed that this UACAGAGAA sequence is conserved in the U6 snRNA and has an m^6A methylation at the Cm^6AG in both MAT2A and U6. When this sequence is mutated, the methylation no longer occurs. We found that METTL16 is the m^6A methyltransferase for this modification in both MAT2A and U6 and confirmed that it has separate activity from the previously identified METTL3 m^6A methyltransferase. We searched for additional mRNA targets of METTL16 through m^6A-seq by comparing sites in the siCtrl that disappear upon METTL16 knockdown. We found only two potential mRNAs with METTL16-sensitive m^6A sites near a UACAGAGAA motif. We also identified several thousand METTL16-sensitive m^6A

sites, but we could not confirm a physical interaction of METTL16 with any of these sites. In addition, many of these sites also decrease upon partial MAT2A knockdown. This decrease could suggest that these sites are more sensitive to intracellular SAM levels. We confirmed that METTL16 knockdown also decreases intracellular SAM levels.

We demonstrated that METTL16 regulates MAT2A intron retention. First, we showed that METTL16 associates better with the MAT2A hairpins upon low SAM levels. Second, using METTL16 mutants or RNA-protein tethering experiments, we displayed that the interaction of METTL16 with the MAT2A hp1 is necessary to drive the splicing of the MAT2A RI. Furthermore, the VCRs of the METTL16 protein are necessary and sufficient to drive this splicing activity. These observations together suggest a model. The METTL16 MTD recognizes the MAT2A hairpin sequence, and this association is dependent upon cellular SAM levels. The METTL16 VCR drives the splicing of the MAT2A RI. This SAM sensing mechanism is one of the first examples of a specific m^6A site regulating the levels of an mRNA.

Finally, we showed that MAT2A intron retention is regulated on the level of co-transcriptional splicing. We coupled either transcription inhibition or RNA labeling experiments with Met depletion to induce more of the fully spliced mRNA, and neither method was able to demonstrate that the MAT2A RI isoform could be post-transcriptionally spliced. We then used other assays to measure co-transcriptional splicing, and found that both Met depletion and METTL16 overexpression increased the measured co-transcriptional splicing of the retained intron. These experiments add an additional example of regulated intron retention, where few exist.

Future Directions

While this dissertation details several interesting discoveries, numerous questions remain unanswered. Because this project encompassed SAM metabolic regulation, the m^6A modification, and intron retention, a variety of follow-up projects are necessary to better understand the regulation described.

First, more work is needed to detail the role of MAT2A as a SAM sensor. As described in the literature review, MAT2A's cellular expression is highly regulated and intertwined with the expression of MAT2B and MAT1A. It would be interesting to study how the expression and stability of the MAT2B and MAT1A proteins are affected in METTL16 knockdown. In addition, it is currently unknown how the conserved sequence in the MAT2A RI relates to its intron retention. While looking at the intron sequence conservation was initially a goal of this project, it was difficult to distinguish between what could be regulatory or what could be disrupting spliceosomal interactions. Now that we know that METTL16 plays an important role in inducing the RI splicing, and we have adequate RNA-protein tethering assays, we might be better able to identify what intronic sequence elements are important through additional deletion analysis. Furthermore, our hp1 mutant experiments were all done with transfected reporters. We should try to use CRISPR to delete hp1 in mammalian cells, though if MAT2A can no longer splice under these conditions and the cells are inviable, we should try an inducible deletion. Regardless, it will be interesting to see how the endogenous MAT2A expresses and responds to intracellular SAM levels without hp1.

Second, MAT2A uses a different m^6A consensus sequence than the METTL3 RRACH, but others' CLIP-seq data (Patil et al., 2016; Wang et al., 2014; Xu et al., 2014) suggests that many of the m^6A binding proteins still interact with the MAT2A hairpins. It will be interesting to use

the MAT2A hairpins to expand upon the known knowledge of the m^6A readers. Most previous studies indicated that they likely only interacted with lncRNAs and mRNAs, not regulatory RNAs (rRNAs, snRNAs) with m^6A modifications, since the RRACH motif is enriched in the CLIP-seq data. Based on the interactions with MAT2A, however, this bias does not seem to be sequence based. Studies that look at kinetics of the m^6A readers binding to the UACAGAGAA motif compared to the RRACH motif could elucidate if those interactions differ, and if so, if that affects the usual function of the m^6A readers. If there are no significant changes, then it might suggest that RNA structure or additional protein interactions at regulatory RNA m^6A sites prevent additional association with the m^6A readers. Furthermore, most of the work for the m^6A demethylases has also focused on their interactions with the RRACH sites. Overexpression of the demethylases or *in vitro* reconstitution with the MAT2A modified hairpins and other RNAs could test if these demethylases have any sequence specificity, or if they demethylate all m^6A modified sequences with similar efficiency.

Third, we would benefit from a greater understanding of METTL16's ability to sense SAM. For METTL16 to act as a SAM sensor, it would need to be fairly sensitive to cellular SAM levels. We have noticed in our *in vitro* experiments that the concentration of SAM must be >200µM in order to detect methylation activity for the MAT2A hairpins, and SAH must have a similar concentration to SAM to inhibit METTL16 (data not shown). This observation is surprising given that most methyltransferases have a K_m of less than 100µM for SAM (Marjon et al., 2016). More detailed *in vitro* kinetics are necessary to understand METTL16's role as SAM sensor. A knockout of METTL16 in mammalian cells might also aid in understanding what happens to SAM when METTL16 is absent. Though we failed at obtaining a knockout in

HCT116 cells, we could try to do the knockout in mouse embryonic stem cells, as was achieved with METTL3 and METTL14 (Batista et al., 2014; Geula et al., 2015). We could also use CRISPR to add a SMASh-tag to the endogenous METTL16, enabling us to induce its degradation. These methods might give us a better idea of what happens to SAM levels in mammalian cells when METTL16 is fully absent.

Fourth, our studies do not conclusively prove whether or not METTL16 modifies other RNAs besides MAT2A and U6. In order to improve our confidence in this model, we would need to perform CLIP-seq, or some variation of it, to see if METTL16 binds near any of the m^6A sites that we see change in our METTL16 knockdown m^6A-seq. Currently, background issues have made CLIP with METTL16 difficult, but we are actively troubleshooting this method. If we can confirm that METTL16 targets additional mRNA m^6A sites, then we need to further identify if they are modified at a different sequence than MAT2A and U6, as our data suggests. If so, then we will need to explore if METTL16 needs additional interacting proteins to modify at different sequences and attempt to reconstitute that activity *in vitro*. We will also need to test if METTL16 m^6A sites drive any different functions than those associated with the RRACH sites. Our data suggested that knockdown of METTL16 promoted the greatest changes in m^6A sites near weak introns, so it's possible that the hypothetical METTL16 m^6A sites play a role in splicing. Alternatively, additional data might reveal that METTL16 does not m^6A modify the sites that decrease in the m^6A-seq. If so, we can investigate why the loss of METTL16 affects these m^6A sites. While we know that the sites are somewhat SAM sensitive, we cannot rescue them by overexpressing MAT2A during METTL16 knockdown. Additional regulation of these m^6A sites is likely necessary.

Fifth, we need to identify interacting factors of METTL16. As mentioned previously, if METTL16 can methylate additional sequences, it might utilize interacting factors to identify a variety of targets. In addition, while we showed that the METTL16 VCR is necessary and sufficient for splicing of the MAT2A RI, it has no homology to any known splicing proteins, so it could likely be recruiting and interacting with some sort of splicing factor. We have performed some initial affinity chromatography followed by mass spectrometry on METTL16 and have found some RNA binding proteins, though we have not yet identified their roles. We are currently trying to perform mass spectrometry with the METTL16 VCR to discern if any protein specifically interacts with that region. For any promising candidate, we will need to perform knockdowns and observe if the splicing of MAT2A changes or if m^6A levels are affected.

Sixth, while we confirmed that METTL16 methylates U6 snRNA, we have no idea what the m^6A modification on U6 does. Now that we know the U6 m^6A methyltransferase, we can utilize the *S. pombe* ΔDuf890 strain to identify if the modification plays a role in U6 stability, protein interaction, folding, or role in splicing. The U6 modification is highly conserved, and the *S. pombe* ΔDuf890 grows almost three times slower than the wild-type and produces less RNA. This observation suggests that something is going awry with its RNA, and we will likely need to perform RNA-seq to understand how loss of the U6 m^6A modification affects other RNAs.

Seventh, MAT2A has been suggested as a potential target for MTAP-deficient cancers (Marjon et al., 2016; Mavrakis et al., 2016), though it has proven difficult to inhibit. Because METTL16 acts upstream of MAT2A to control its expression, it's possible that loss of METTL16 activity could prove lethal for MTAP-deficient cancers. We will need to knockdown

METTL16 in MTAP-deficient cell lines with matched controls to see if this hypothesis is true, but if so, we could look for specific METTL16 inhibitors with small molecule screens.

Eighth, a recent report suggests that METTL16 non-catalytically binds to the MALAT1 triple helix (Brown et al., 2016). We also confirmed this interaction (data not shown). Neither we nor the group that reported it understand what the function of this interaction is. MALAT1 is a highly expressed lncRNA, but its function is not well-defined. It will be interesting in the future to investigate if METTL16 knockdown affects MALAT1 RNA levels or localization, and perhaps a better understanding of the METTL16-MALAT1 interaction will delineate the role of MALAT1 in the cell.

Finally, though the vast majority of m^6A sites in the cell are likely modified by METTL3, it is possible that there are additional m^6A methyltransferases besides METTL16. Single-nucleotide-resolution m^6A mapping correctly identified one of the m^6A sites on the MAT2A hairpins (Linder et al., 2015), and studies that looked at m^6A site change upon knockdown of METTL3, METTL14, and WTAP did not report any changes with the MAT2A hairpins (Schwartz et al., 2014). By comparing these two data sets, it might be possible to identify sites similar to the MAT2A hairpins that suggest a modification not performed by the RRACH machinery. Measuring changes in m^6A levels after knockdown or knockout of potential m^6A methyltransferases might also suggest if other m^6A methyltransferases exist. Identifying additional m^6A machinery could provide insight into important RNA regulation.

Our lab has many options to explore in terms of METTL16 regulation, both in terms of specific mechanism and broad functionality. While we have done a tremendous amount of work

to confirm how METTL16 regulates MAT2A, it is humbling to reflect on the many questions that remain unanswered and the many experiments that have yet to be done.

APPENDIX
Splice Junction Nuclear Run-on Assay Protocol

(Black is standard transcriptional protocol, red indicates modifications for either low expression or exon junctions)

Taken from (Davidson et al., 2012) and (Core et al., 2008). Normalization for NROs is not always straightforward, so be careful and get close to equal recovery at all harvesting steps, PCA, EtOH precip, etc.

Nuclear Run-On

1. Trypsinize cells as usual. One 10-cm plate per sample. Make sure to include one sample (at least) as a "no-4sU" control) Quench trypsin with **ice-cold media** instead of warm media and place on ice. **Keep on ice** for rest of protocol except as noted.
2. Count cells.
3. Centrifuge ~ 1-3 x 10^7 cells per sample at 1800rpm/3min/4°
    - Within a single experiment, be sure to equilibrate cell number between your samples. That is, take the sample with lowest cell number and equilibrate to it.
    - For transcription measurement experiments, 1-2 HEK293 10 cm plates or 2-3 ATOA plates at near 100% confluence have the desirable cell number.
    - For the co-transcriptional splicing (exon junction measuring) experiments, I have increased to 2 HEK293 15cm plates per sample. Increasing beyond this did not result in a significant improvement of results because of background issues.
4. Resuspend pellets in 5 mL ice-cold PBS.

- Alt. for greater cell number, resuspend pellets in 10mL ice-cold PBS, then divide into two 15mL tubes into 5mL each (each sample now subdivided into 2 tubes. I keep 2 tubes per sample for the rest of the experiment—I've tried combining them at later steps, but I think it makes my samples dirtier).

5. Transfer to 15 mL conical tubes and centrifuge at 1800rpm/3min/4°.
6. ***Gently (avoid bubbles) but thoroughly*** resuspend each pellet in 1 mL of HLB supplemented with 0.5% IGEPAL and 1mM DTT. (add IGEPAL and DTT fresh for each experiment)
7. 5 min/ice
8. During the 5 min, remove 50 uL for steady-state analysis→1 mL TriReagent
9. Underlay ***carefully*** with 1mL HLB-Suc with 0.5%IGEPAL and 1mM DTT

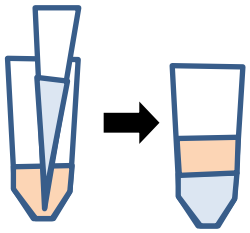

10. Centrifuge at 600x g (1700 rpm in Legend Sorvall) 5min/4°
11. Carefully remove supe and discard.
    - I use vacuum to remove ~90%, but pipette to remove the remaining supe.
12. Resuspend pellet ***gently*** in 60 uL 2x TXN Buffer plus 1 uL RNAsin and 5mM DTT and transfer to eppe tube
    - Final volume should be ~120uL. If not, add H_2O to 120 uL
    - If final volume is over 120 (this can be true at highest cell levels), adjust nucleotide and sarkosyl accordingly.

- For the higher cell number, I usually use around 110uL of 2x TXN Buffer.

13. Add 3 uL of nucleotide mix +/- 4sUTP (see below for concentrations)
    - So, 5.5uL of nucleotide mix +/- 4sUTP
14. Mix ***gently, avoid bubbles, but thoroughly.***
15. Add 3 uL of 20% Sarkosyl
    - I try and distribute the Sarkosyl when I add it (pipette w/swirling motion) because it's hard to mix due to histones release from DNA.
    - For the exon junction experiments, I omit the Sarkosyl because of an extra wash step after the reaction.
16. Mix ***gently by flicking tube,*** but realize the solution will get viscous: do not pipette up and down!
17. 30°/5 min
18. Add 1mL of HLB-150 (150mM NaCl) supplemented with 0.1% Triton, 1mM DTT.
19. Spin at 600xg at 4^{o}C for 5min. Pull off the supernatant before adding 1mL Trizol.
20. Add 1 mL Tri-REAGENT to eppe tube to stop reaction
21. Transfer to 3mL in a 15 mL conical (4mL Trizol total)
    - ***Be careful:*** the pellets stay viscous in the 1mL of Trizol and stick to the walls of the pipette tip→ you need to pipette up and down with the same tip to get **all** of the goopy stuff off the walls and into the 4 mL of trizol and to get it to dissolve upon transfer.
22. Trizol extraction of RNA.

DNase Treatment

23. Resuspend pellet in 159 uL H2O, add 1 uL RNasin, 20 uL DNase Buffer, 20 uL RQ1 DNase
24. 37°/60min
25. Stop with 10 uL 500 mM EDTA and 10 uL 300 mM EGTA
    - This is important to chelate divalent cations→if they carryover they may alter hydrolysis conditions as they can catalyze that reaction.
26. Add 20 uL 10M NH_4OAc/PCA/ETOH as usual.

Hydrolysis – Do NOT perform for co-transcriptional splicing (exon junctions) experiments. It dramatically decreases signal. If a gene is not highly expressed, it is not necessary to perform for transcription experiments, though it does introduce a bias towards the 5' end of genes, and you lose any information about differential polymerase density on the gene.

1. Precip/wash RNA and thoroughly resuspend in 40 uL H_2O
2. Nanodrop and adjust to 1 mg/ml
    - I have been doing from ~40 ug, but this has not been optimized formally. Given low signal-to-noise I suspect more is better.
3. Start with 40 uL of 1 mg/mL RNA→on ice!
4. Add 10 uL 1M NaOH on ice.
    - The 1M NaOH stock should be ***made fresh*** by diluting 1:10 from our 10M stock.
5. 4 min on ice: Time this as precisely and reproducibly between the samples as possible!

- You may want to check hydrolysis efficiency in your hands; it seems to vary and it's important that the average length is long enough for efficient qRT-PCR, but short enough to resolve the place on the DNA that txn occurred.
- I've had luck with ~400-1000 as seen on a nondenaturing gel (so they may be bigger in reality)
- Previous versions called for 30min, but this was empirically determined to be too much for RT-qPCR based detection.

6. To stop hydrolysis: add 61 uL of neutralizing solution.
7. Add 300 uL EtOH and precipitate as usual.

Biotinylation, Streptavidin Selection, and RT-qPCR

- Perform as in the "large-scale 4sU" protocol.
- Remember to perform a PCA then a chloroform step after elution to ensure samples are clean for qRT-PCR.
- I have not been running the biotinylated inputs (ie the 3 ul you take out during the SA selection step). However, I sometimes analyze the steady-state (taken out during NRO as described above) depending on experimental design. If you do this, remember to DNAse this sample as well.
- RT-qPCR as usual. Make sure you use random hexamers for priming. Also, I've been doing a 1:20 dilution of the cDNA (our standard RT RXN yields 20 uL of cDNA stock) for the qPCR reaction.

BUFFERS

HLB (Filter sterilize for long-term storage—add DTT and IGEPAL day of experiment)

	Amount	Stock	Final
TrisHCl (7.5)	0.5 mL	1M	10 mM
NaCl	125 uL	4M	10 mM
MgCl2	125 uL	1M	2.5mM
	50 mL		

HLB-Suc: HLB with 10% sucrose (w/v; I make this fresh each time using a filtered stock of 25% sucrose; add DTT and IGEPAL as necessary.)

H2O	3 mL
25% Sucrose	2 mL
1M TrisHCl (7.5)	50 uL
1M MgCl2	12.5
4M NaCl	12.5
	~5 mL (Add IGEPAL and DTT to 0.5% and 1 mM)

2x TXN Buffer (Store for < 2 weeks at RT, can store small aliquots long-term at -20; no DTT)**

TrisHCl (8.0)	200 uL	1M	20 mM
KCl	900 uL	2M	180 mM
MgCl2	100 uL	1M	10 mM
Glycerol	8.3 mL	60%	50% (v/v)
H_2O	0.5 mL		
DTT*			5 mM
	10 mL		

*ADD DTT IMMEDIATELY BEFORE USE

**Add 1 uL RNasin per sample.

Neutralizing Solution:

1M TrisHCl (pH 6.8)	50 uL
3M NaOAc (pH 5.2) KCl	10 uL
Glyco-Blue	1 uL
	61 uL

Nucleotide Mixes:

10 mM each A, G, C plus 40 □M of either UTP (-4sU control only) or 40 □M 4S-UTP

(TriLink); make ~ 50-100 uL and store at -20°. ALWAYS INCLUDE A "-4SU CONTROL"!

Day-of-experiment checklist:
Thaw/Warm: Trypsin, 1M DTT, Trizol, NTP mixes, 30° heat block,
Chill on ice: TC centrifuge, media (for trypsin quenching), PBS, HLB (+DTT/IGEPAL), HLB-suc (+DTT/IGEPAL), 2X TXN buffer (+DTT/RNAsin/H2O)
Prep: HLB-Suc (+IGEPAL/DTT), 2X TXN (+DTT/RNAsin/H2O), HLB (+DTT/IGEPAL)

4-thiouridine (4sU) for RT-qPCR/NB

This protocol is for doing pulse (+/-chase) analysis with 4sU with detection by qRT-PCR or northern blot (NB). We also use it for NROs with 4S-UTP. It is based on the protocols of (Zeiner et al., 2008) and (Dolken et al., 2008). We have made many changes to increase signal to noise.

Biotinylate samples

1. Biotinylate RNA with HPDP-biotin:
    1. Mix (In the following order; make sure reagents RNase-free!):

Reagent	Amount	Stock	Final
RNA/H_2O**	varies		0.2-0.4 mg/mL
H_2O	varies		
NaOAc (pH 5.2)	1.33 uL	3M	20 mM
EDTA	0.4 uL	500 mM	1 mM
SDS	1 uL	20%	0.1%
Biotin-HPDP	100 uL	0.4 mg/mL	0.2 mg/mL
	200 uL**		

    2. Order of addition: 1) RNA 2) Aqueous master mix 3) Biotin-HPDP/DMF mix
    3. 3 hr/25° (not RT, but a 25° heat block/water bath)
    4. Extract once with 200 uL chloroform
        - Note because of large volume of DMF, recovery of aqueous will be less than 200.
    5. Add 20 uL 10M NH_4OAc, 1 uL glycoblue, and 80 uL H_2O
    6. Extract TWICE with chloroform by vortexing/centrifuging at 12K for 3 min.
        - In my hands, this leads to ~ 200 uL aqueous recovery.
    7. Add 500 uL EtOH and precipitate (usually o/n at -20)

*** Note: We've been doing ~40-80 ug RNA per 200 uL reaction volume. The reaction can be scaled up/down. (typically: 40 ug for NRO, 80 ug for NB, or 20 ug for RT-PCR)*

For lower expressed genes, or co-transcriptional splicing experiments, I tend to use 90µg of RNA.

Streptavidin (SA) select:

1. Wash and block Dynal MyOne Streptavidin T1 beads:
    - For each sample remove 20 uL of bead slurry (e.g. 5 samples, take 100 uL slurry: make sure to resuspend well prior to taking your aliquot, the beads tend to stick to the bottom). *NOTE: 20 uL is linear up to ~80 ug (exp#102513), so we could probably do less for some experiments, but I've never tested.*
    - Wash 3 times in MPG 1:10-I (using magnetic stand, do not centrifuge except briefly at low speeds if you need to collect beads stuck to the top of tube).
    - After final wash resuspend in 1mL MPG 1:10-I per sample number (e.g. 5 samples=5 mL).
    - Add competitors/detergent to final concentrations below and mix well:
        - 0.1 ug/uL poly(A) (Sigma)
        - 0.1 ug/uL ssDNA
        - 0.1 ug/uL cRNA
        - 0.1% SDS
    - Nutate at RT/60 min

2. Pellet biotinylated RNA, wash, and resuspend in 100 uL H_2O.
    - Check concentration of RNA before proceeding. If the concentrations have changed from the biotinylation process, readjust them so that they are all equal.
3. 65°/5 min
4. Add 950 uL of washed Dynal Streptavidin T1 beads/blocker mix.
    - For the co-transcriptional splicing experiments, to reduce background, I add this ~1mL mixture to 3mL of MPG 1:10-I, supplemented appropriately with competitors, in 15mL conical tubes.
5. Nutate/60min/RT
6. Centrifuge 300g/5-10 sec (do not use "short", this overrides speed settings). (I don't do this for the 15mL conicals—it's not necessary)
7. Wash (500 uL each wash)
    - *Note: Perform washes by first placing tubes on magnetic stand for ~30-60 sec, remove solution, then take the tubes away from the magnet and add wash solution. Add the wash solution directly to the side where the beads are to agitate them to make sure all the beads get washed. We also alternate sides of the tubes on the magnetic stand to make sure different beads are in contact with wash solutions. Do these steps quickly enough to keep the beads from drying. We never put more than 8 tubes on the stand at a time.* The wash solutions are:
        - MPG 1:10-I, RT

- MPG 1:10, 55° (pre-warm wash buffer and add immediately to beads; we don't actually place the beads at 55°; note: no detergent)
- MPG 1:10-I, RT
- MPG-I, RT
- MPG-I, RT
- MPG-I, RT
- MPG 1:10-I, RT
- MPG-I, no salt, RT
- MPG-I, no salt, RT
- MPG 1:10-I, RT

8. Elute (200 uL each): (vortex briefly at half speed or pipette to mix thoroughly)
    - MPG 1:10-I with 5% β-mercaptoethanol, RT/5 min
    - MPG 1:10-I with 5% β-mercaptoethanol, RT/5 min
    - Combine eluted fractions, add 1.5 uL glyblue, 40 uL 3M NaOAc
    - PCA extract (PCA is sufficient for NB)
    - Chloroform extract twice (this step is necessary for RT-qPCR)
    - Add 1 mL EtOH and precipitate (usually o/n at -20)

Perform RT-qPCR or NB as usual

Buffers:

Note: We make all buffers without Igepal and store them. We do not store the igepal-containing buffers. (Although that would almost certainly be fine for shorter periods of time).

MPG (make 50 mL, long-term storage is ok)

Reagent	Amount	Stock	Final
NaCl	12.5 mL	4M	1M
EDTA	1 mL	500 mM	10 mM
TrisHCl (7.5)	5 mL	1M	100 mM
H2O	31.5 mL		

MPG-I: MPG + 0.1% igepal (make a small volume; don't store)

MPG 1:10: MPG diluted 10-fold in H_2O

MPG 1:10-I: MPG 1:10 with 0.1% Igepal

MPG-I, no salt: (100 mM Tris, 10 mM EDTA, 0.1% IGEPAL)

Biotin-HPDP is from Pierce. Resuspend in DMF to a concentration of 1 mg/ml. Store at 4°. Use within 1 month (make sure you put the date on the tube and store as a "lab stock" at 4° in ClickIT box, so we don't waste.

BIBLIOGRAPHY

Agrawal, V., Alpini, S.E., Stone, E.M., Frenkel, E.P., and Frankel, A.E. (2012). Targeting methionine auxotrophy in cancer: discovery & exploration. Expert Opin. Biol. Ther. *12*, 53-61.

Alarcon, C.R., Goodarzi, H., Lee, H., Liu, X., Tavazoie, S., and Tavazoie, S.F. (2015). HNRNPA2B1 Is a Mediator of m(6)A-Dependent Nuclear RNA Processing Events. Cell *162*, 1299-1308.

Ameur, A., Zaghlool, A., Halvardson, J., Wetterbom, A., Gyllensten, U., Cavelier, L., and Feuk, L. (2011). Total RNA sequencing reveals nascent transcription and widespread co-transcriptional splicing in the human brain. Nat. Struct. Mol. Biol. *18*, 1435-1440.

Amit, M., Donyo, M., Hollander, D., Goren, A., Kim, E., Gelfman, S., Lev-Maor, G., Burstein, D., Schwartz, S., Postolsky, B., *et al.* (2012). Differential GC content between exons and introns establishes distinct strategies of splice-site recognition. Cell reports *1*, 543-556.

Andersson, R., Enroth, S., Rada-Iglesias, A., Wadelius, C., and Komorowski, J. (2009). Nucleosomes are well positioned in exons and carry characteristic histone modifications. Genome Res. *19*, 1732-1741.

Anko, M.L. (2014). Regulation of gene expression programmes by serine-arginine rich splicing factors. Semin. Cell Dev. Biol. *32*, 11-21.

Barash, Y., Calarco, J.A., Gao, W., Pan, Q., Wang, X., Shai, O., Blencowe, B.J., and Frey, B.J. (2010). Deciphering the splicing code. Nature *465*, 53-59.

Batista, P.J., Molinie, B., Wang, J., Qu, K., Zhang, J., Li, L., Bouley, D.M., Lujan, E., Haddad, B., Daneshvar, K., *et al.* (2014). m(6)A RNA modification controls cell fate transition in mammalian embryonic stem cells. Cell stem cell *15*, 707-719.

Batsche, E., Yaniv, M., and Muchardt, C. (2006). The human SWI/SNF subunit Brm is a regulator of alternative splicing. Nat. Struct. Mol. Biol. *13*, 22-29.

Bergeron, D., Pal, G., Beaulieu, Y.B., Chabot, B., and Bachand, F. (2015). Regulated Intron Retention and Nuclear Pre-mRNA Decay Contribute to PABPN1 Autoregulation. Mol. Cell. Biol. *35*, 2503-2517.

Bhatt, D.M., Pandya-Jones, A., Tong, A.J., Barozzi, I., Lissner, M.M., Natoli, G., Black, D.L., and Smale, S.T. (2012). Transcript dynamics of proinflammatory genes revealed by sequence analysis of subcellular RNA fractions. Cell *150*, 279-290.

Bokar, J.A., Shambaugh, M.E., Polayes, D., Matera, A.G., and Rottman, F.M. (1997). Purification and cDNA cloning of the AdoMet-binding subunit of the human mRNA (N6-adenosine)-methyltransferase. RNA (New York, N.Y.) *3*, 1233-1247.

Boutz, P.L., Bhutkar, A., and Sharp, P.A. (2015). Detained introns are a novel, widespread class of post-transcriptionally spliced introns. Genes Dev. *29*, 63-80.

Braunschweig, U., Barbosa-Morais, N.L., Pan, Q., Nachman, E.N., Alipanahi, B., Gonatopoulos-Pournatzis, T., Frey, B., Irimia, M., and Blencowe, B.J. (2014). Widespread intron retention in mammals functionally tunes transcriptomes. Genome Res. *24*, 1774-1786.

Bresson, S.M., and Conrad, N.K. (2013). The human nuclear poly(a)-binding protein promotes RNA hyperadenylation and decay. PLoS Genet. *9*, e1003893.

Bresson, S.M., Hunter, O.V., Hunter, A.C., and Conrad, N.K. (2015). Canonical Poly(A) Polymerase Activity Promotes the Decay of a Wide Variety of Mammalian Nuclear RNAs. PLoS Genet. *11*, e1005610.

Bringmann, P., and Luhrmann, R. (1987). Antibodies specific for N6-methyladenosine react with intact snRNPs U2 and U4/U6. FEBS Lett. *213*, 309-315.

Brosnan, J.T., and Brosnan, M.E. (2006). The sulfur-containing amino acids: an overview. The Journal of nutrition *136*, 1636s-1640s.

Brow, D.A., and Guthrie, C. (1988). Spliceosomal RNA U6 is remarkably conserved from yeast to mammals. Nature *334*, 213-218.

Brown, J.A., Kinzig, C.G., DeGregorio, S.J., and Steitz, J.A. (2016). Methyltransferase-like protein 16 binds the 3'-terminal triple helix of MALAT1 long noncoding RNA. Proc. Natl. Acad. Sci. U. S. A. *113*, 14013-14018.

Bujnicki, J.M., Feder, M., Radlinska, M., and Blumenthal, R.M. (2002). Structure prediction and phylogenetic analysis of a functionally diverse family of proteins homologous to the MT-A70 subunit of the human mRNA:m(6)A methyltransferase. J. Mol. Evol. *55*, 431-444.

Cantoni, G.L. (1975). Biological methylation: selected aspects. Annu. Rev. Biochem. *44*, 435-451.

Carroll, S.M., Narayan, P., and Rottman, F.M. (1990). N6-methyladenosine residues in an intron-specific region of prolactin pre-mRNA. Mol. Cell. Biol. *10*, 4456-4465.

Cho, S., Hoang, A., Sinha, R., Zhong, X.Y., Fu, X.D., Krainer, A.R., and Ghosh, G. (2011). Interaction between the RNA binding domains of Ser-Arg splicing factor 1 and U1-70K snRNP protein determines early spliceosome assembly. Proc. Natl. Acad. Sci. U. S. A. *108*, 8233-8238.

Clancy, M.J., Shambaugh, M.E., Timpte, C.S., and Bokar, J.A. (2002). Induction of sporulation in Saccharomyces cerevisiae leads to the formation of N6-methyladenosine in mRNA: a potential mechanism for the activity of the IME4 gene. Nucleic Acids Res. *30*, 4509-4518.

Conrad, N.K. (2008). Chapter 15. Co-immunoprecipitation techniques for assessing RNA-protein interactions in vivo. Methods Enzymol. *449*, 317-342.

Conrad, N.K., Mili, S., Marshall, E.L., Shu, M.D., and Steitz, J.A. (2006). Identification of a rapid mammalian deadenylation-dependent decay pathway and its inhibition by a viral RNA element. Mol. Cell *24*, 943-953.

Conrad, N.K., and Steitz, J.A. (2005). A Kaposi's sarcoma virus RNA element that increases the nuclear abundance of intronless transcripts. The EMBO journal *24*, 1831-1841.

Core, L.J., Waterfall, J.J., and Lis, J.T. (2008). Nascent RNA sequencing reveals widespread pausing and divergent initiation at human promoters. Science (New York, N.Y.) *322*, 1845-1848.

Coulter, A.W., Lombardini, J.B., Sufrin, J.R., and Talalay, P. (1974). Structural and conformational analogues of L-methionine as inhibitors of the enzymatic synthesis of S-adenosyl-l-methionine. 3. Carbocyclic and heterocyclic amino acids. Mol. Pharmacol. *10*, 319-334.

Daguenet, E., Dujardin, G., and Valcarcel, J. (2015). The pathogenicity of splicing defects: mechanistic insights into pre-mRNA processing inform novel therapeutic approaches. EMBO reports *16*, 1640-1655.

Davidson, L., Kerr, A., and West, S. (2012). Co-transcriptional degradation of aberrant pre-mRNA by Xrn2. The EMBO journal *31*, 2566-2578.

De Conti, L., Baralle, M., and Buratti, E. (2013). Exon and intron definition in pre-mRNA splicing. Wiley interdisciplinary reviews. RNA *4*, 49-60.

Deng, X., Chen, K., Luo, G.Z., Weng, X., Ji, Q., Zhou, T., and He, C. (2015). Widespread occurrence of N6-methyladenosine in bacterial mRNA. Nucleic Acids Res. *43*, 6557-6567.

Dermody, J.L., Dreyfuss, J.M., Villen, J., Ogundipe, B., Gygi, S.P., Park, P.J., Ponticelli, A.S., Moore, C.L., Buratowski, S., and Bucheli, M.E. (2008). Unphosphorylated SR-like protein Npl3 stimulates RNA polymerase II elongation. PLoS One *3*, e3273.

Desrosiers, R., Friderici, K., and Rottman, F. (1974). Identification of methylated nucleosides in messenger RNA from Novikoff hepatoma cells. Proc. Natl. Acad. Sci. U. S. A. *71*, 3971-3975.

Dettmer, K., Nurnberger, N., Kaspar, H., Gruber, M.A., Almstetter, M.F., and Oefner, P.J. (2011). Metabolite extraction from adherently growing mammalian cells for metabolomics studies: optimization of harvesting and extraction protocols. Anal. Bioanal. Chem. *399*, 1127-1139.

Dignam, J.D., Lebovitz, R.M., and Roeder, R.G. (1983). Accurate transcription initiation by RNA polymerase II in a soluble extract from isolated mammalian nuclei. Nucleic Acids Res. *11*, 1475-1489.

Dina, C., Meyre, D., Gallina, S., Durand, E., Korner, A., Jacobson, P., Carlsson, L.M., Kiess, W., Vatin, V., Lecoeur, C., *et al.* (2007). Variation in FTO contributes to childhood obesity and severe adult obesity. Nat. Genet. *39*, 724-726.

Do, R., Bailey, S.D., Desbiens, K., Belisle, A., Montpetit, A., Bouchard, C., Perusse, L., Vohl, M.C., and Engert, J.C. (2008). Genetic variants of FTO influence adiposity, insulin sensitivity, leptin levels, and resting metabolic rate in the Quebec Family Study. Diabetes *57*, 1147-1150.

Dolken, L., Ruzsics, Z., Radle, B., Friedel, C.C., Zimmer, R., Mages, J., Hoffmann, R., Dickinson, P., Forster, T., Ghazal, P., *et al.* (2008). High-resolution gene expression profiling for simultaneous kinetic parameter analysis of RNA synthesis and decay. RNA (New York, N.Y.) *14*, 1959-1972.

Dominissini, D., Moshitch-Moshkovitz, S., Salmon-Divon, M., Amariglio, N., and Rechavi, G. (2013). Transcriptome-wide mapping of N(6)-methyladenosine by m(6)A-seq based on immunocapturing and massively parallel sequencing. Nat. Protoc. *8*, 176-189.

Dominissini, D., Moshitch-Moshkovitz, S., Schwartz, S., Salmon-Divon, M., Ungar, L., Osenberg, S., Cesarkas, K., Jacob-Hirsch, J., Amariglio, N., Kupiec, M., *et al.* (2012). Topology of the human and mouse m6A RNA methylomes revealed by m6A-seq. Nature *485*, 201-206.

Dorsett, M., Westlund, B., and Schedl, T. (2009). METT-10, a putative methyltransferase, inhibits germ cell proliferative fate in Caenorhabditis elegans. Genetics *183*, 233-247.

Du, H., Zhao, Y., He, J., Zhang, Y., Xi, H., Liu, M., Ma, J., and Wu, L. (2016). YTHDF2 destabilizes m(6)A-containing RNA through direct recruitment of the CCR4-NOT deadenylase complex. Nature communications *7*, 12626.

Dvinge, H., and Bradley, R.K. (2015). Widespread intron retention diversifies most cancer transcriptomes. Genome Med. *7*, 45.

Eggert, C., Chari, A., Laggerbauer, B., and Fischer, U. (2006). Spinal muscular atrophy: the RNP connection. Trends Mol. Med. *12*, 113-121.

Engel, J.D., and von Hippel, P.H. (1978). Effects of methylation on the stability of nucleic acid conformations. Studies at the polymer level. J. Biol. Chem. *253*, 927-934.

Epstein, P., Reddy, R., Henning, D., and Busch, H. (1980). The nucleotide sequence of nuclear U6 (4.7 S) RNA. J. Biol. Chem. *255*, 8901-8906.

Finkelstein, J.D. (1990). Methionine metabolism in mammals. J. Nutr. Biochem. *1*, 228-237.

Fontecave, M., Atta, M., and Mulliez, E. (2004). S-adenosylmethionine: nothing goes to waste. Trends Biochem. Sci. *29*, 243-249.

Fox-Walsh, K.L., Dou, Y., Lam, B.J., Hung, S.P., Baldi, P.F., and Hertel, K.J. (2005). The architecture of pre-mRNAs affects mechanisms of splice-site pairing. Proc. Natl. Acad. Sci. U. S. A. *102*, 16176-16181.

Frayling, T.M., Timpson, N.J., Weedon, M.N., Zeggini, E., Freathy, R.M., Lindgren, C.M., Perry, J.R., Elliott, K.S., Lango, H., Rayner, N.W., *et al.* (2007). A common variant in the FTO gene is associated with body mass index and predisposes to childhood and adult obesity. Science (New York, N.Y.) *316*, 889-894.

Galante, P.A., Sakabe, N.J., Kirschbaum-Slager, N., and de Souza, S.J. (2004). Detection and evaluation of intron retention events in the human transcriptome. RNA (New York, N.Y.) *10*, 757-765.

Garcia-Trevijano, E.R., Latasa, M.U., Carretero, M.V., Berasain, C., Mato, J.M., and Avila, M.A. (2000). S-adenosylmethionine regulates MAT1A and MAT2A gene expression in cultured rat hepatocytes: a new role for S-adenosylmethionine in the maintenance of the differentiated status of the liver. FASEB journal : official publication of the Federation of American Societies for Experimental Biology *14*, 2511-2518.

Geula, S., Moshitch-Moshkovitz, S., Dominissini, D., Mansour, A.A., Kol, N., Salmon-Divon, M., Hershkovitz, V., Peer, E., Mor, N., Manor, Y.S., *et al.* (2015). Stem cells. m6A mRNA methylation facilitates resolution of naive pluripotency toward differentiation. Science (New York, N.Y.) *347*, 1002-1006.

Glaudemans, A.W., Enting, R.H., Heesters, M.A., Dierckx, R.A., van Rheenen, R.W., Walenkamp, A.M., and Slart, R.H. (2013). Value of 11C-methionine PET in imaging brain tumours and metastases. Eur. J. Nucl. Med. Mol. Imag. *40*, 615-635.

Gomes Trolin, C., Ekblom, J., and Oreland, L. (1998). Regulation of methionine adenosyltransferase catalytic activity and messenger RNA in SH-SY5Y human neuroblastoma cells. Biochem. Pharmacol. *55*, 567-571.

Gornemann, J., Kotovic, K.M., Hujer, K., and Neugebauer, K.M. (2005). Cotranscriptional spliceosome assembly occurs in a stepwise fashion and requires the cap binding complex. Mol. Cell *19*, 53-63.

Gu, J., Patton, J.R., Shimba, S., and Reddy, R. (1996). Localization of modified nucleotides in Schizosaccharomyces pombe spliceosomal small nuclear RNAs: modified nucleotides are clustered in functionally important regions. RNA (New York, N.Y.) *2*, 909-918.

Guo, R., Zheng, L., Park, J.W., Lv, R., Chen, H., Jiao, F., Xu, W., Mu, S., Wen, H., Qiu, J., *et al.* (2014). BS69/ZMYND11 reads and connects histone H3.3 lysine 36 trimethylation-decorated chromatin to regulated pre-mRNA processing. Mol. Cell *56*, 298-310.

Halim, A.B., LeGros, L., Geller, A., and Kotb, M. (1999). Expression and functional interaction of the catalytic and regulatory subunits of human methionine adenosyltransferase in mammalian cells. J. Biol. Chem. *274*, 29720-29725.

Harada, F., Kato, N., and Nishimura, S. (1980). The nucleotide sequence of nuclear 4.8S RNA of mouse cells. Biochem. Biophys. Res. Commun. *95*, 1332-1340.

Haussmann, I.U., Bodi, Z., Sanchez-Moran, E., Mongan, N.P., Archer, N., Fray, R.G., and Soller, M. (2016). m6A potentiates Sxl alternative pre-mRNA splicing for robust Drosophila sex determination. Nature *540*, 301-304.

Hernandez, N., and Weiner, A.M. (1986). Formation of the 3' end of U1 snRNA requires compatible snRNA promoter elements. Cell *47*, 249-258.

Hongay, C.F., and Orr-Weaver, T.L. (2011). Drosophila Inducer of MEiosis 4 (IME4) is required for Notch signaling during oogenesis. Proc. Natl. Acad. Sci. U. S. A. *108*, 14855-14860.

Horikawa, S., Sasuga, J., Shimizu, K., Ozasa, H., and Tsukada, K. (1990). Molecular cloning and nucleotide sequence of cDNA encoding the rat kidney S-adenosylmethionine synthetase. J. Biol. Chem. *265*, 13683-13686.

Hsu, T.Y., Simon, L.M., Neill, N.J., Marcotte, R., Sayad, A., Bland, C.S., Echeverria, G.V., Sun, T., Kurley, S.J., Tyagi, S., *et al.* (2015). The spliceosome is a therapeutic vulnerability in MYC-driven cancer. Nature *525*, 384-388.

Huang, Z.Z., Mao, Z., Cai, J., and Lu, S.C. (1998). Changes in methionine adenosyltransferase during liver regeneration in the rat. The American journal of physiology *275*, G14-21.

Huff, J.T., Plocik, A.M., Guthrie, C., and Yamamoto, K.R. (2010). Reciprocal intronic and exonic histone modification regions in humans. Nat. Struct. Mol. Biol. *17*, 1495-1499.

Irimia, M., and Blencowe, B.J. (2012). Alternative splicing: decoding an expansive regulatory layer. Curr. Opin. Cell Biol. *24*, 323-332.

Jia, G., Fu, Y., Zhao, X., Dai, Q., Zheng, G., Yang, Y., Yi, C., Lindahl, T., Pan, T., Yang, Y.G., *et al.* (2011). N6-methyladenosine in nuclear RNA is a major substrate of the obesity-associated FTO. Nat. Chem. Biol. *7*, 885-887.

Jung, H., Lee, D., Lee, J., Park, D., Kim, Y.J., Park, W.Y., Hong, D., Park, P.J., and Lee, E. (2015). Intron retention is a widespread mechanism of tumor-suppressor inactivation. Nat. Genet. *47*, 1242-1248.

Ke, S., Alemu, E.A., Mertens, C., Gantman, E.C., Fak, J.J., Mele, A., Haripal, B., Zucker-Scharff, I., Moore, M.J., Park, C.Y., *et al.* (2015). A majority of m6A residues are in the last exons, allowing the potential for 3' UTR regulation. Genes Dev. *29*, 2037-2053.

Keith, J.M., Ensinger, M.J., and Mose, B. (1978). HeLa cell RNA (2'-O-methyladenosine-N6-)-methyltransferase specific for the capped 5'-end of messenger RNA. J. Biol. Chem. *253*, 5033-5039.

Keren, H., Lev-Maor, G., and Ast, G. (2010). Alternative splicing and evolution: diversification, exon definition and function. Nature reviews. Genetics *11*, 345-355.

Khodor, Y.L., Rodriguez, J., Abruzzi, K.C., Tang, C.H., Marr, M.T., 2nd, and Rosbash, M. (2011). Nascent-seq indicates widespread cotranscriptional pre-mRNA splicing in Drosophila. Genes Dev. *25*, 2502-2512.

Kim, J., Kim, Y., Yeom, M., Kim, J.H., and Nam, H.G. (2008). FIONA1 is essential for regulating period length in the Arabidopsis circadian clock. The Plant cell *20*, 307-319.

Kornblihtt, A.R., Schor, I.E., Allo, M., Dujardin, G., Petrillo, E., and Munoz, M.J. (2013). Alternative splicing: a pivotal step between eukaryotic transcription and translation. Nature reviews. Molecular cell biology *14*, 153-165.

Kotb, M., and Kredich, N.M. (1985). S-Adenosylmethionine synthetase from human lymphocytes. Purification and characterization. J. Biol. Chem. *260*, 3923-3930.

Lacadie, S.A., and Rosbash, M. (2005). Cotranscriptional spliceosome assembly dynamics and the role of U1 snRNA:5'ss base pairing in yeast. Mol. Cell *19*, 65-75.

Laxman, S., Sutter, B.M., Wu, X., Kumar, S., Guo, X., Trudgian, D.C., Mirzaei, H., and Tu, B.P. (2013). Sulfur amino acids regulate translational capacity and metabolic homeostasis through modulation of tRNA thiolation. Cell *154*, 416-429.

Lee, Y., and Rio, D.C. (2015). Mechanisms and Regulation of Alternative Pre-mRNA Splicing. Annu. Rev. Biochem. *84*, 291-323.

Lerner, M.R., Boyle, J.A., Mount, S.M., Wolin, S.L., and Steitz, J.A. (1980). Are snRNPs involved in splicing? Nature *283*, 220-224.

Li, A., Chen, Y.S., Ping, X.L., Yang, X., Xiao, W., Yang, Y., Sun, H.Y., Zhu, Q., Baidya, P., Wang, X., *et al.* (2017). Cytoplasmic m6A reader YTHDF3 promotes mRNA translation. Cell Res. *27*, 444-447.

Li, H., and Durbin, R. (2009). Fast and accurate short read alignment with Burrows-Wheeler transform. Bioinformatics (Oxford, England) *25*, 1754-1760.

Lin, S., Choe, J., Du, P., Triboulet, R., and Gregory, R.I. (2016). The m(6)A Methyltransferase METTL3 Promotes Translation in Human Cancer Cells. Mol. Cell *62*, 335-345.

Linder, B., Grozhik, A.V., Olarerin-George, A.O., Meydan, C., Mason, C.E., and Jaffrey, S.R. (2015). Single-nucleotide-resolution mapping of m6A and m6Am throughout the transcriptome. Nat. Methods *12*, 767-772.

Liu, J., Yue, Y., Han, D., Wang, X., Fu, Y., Zhang, L., Jia, G., Yu, M., Lu, Z., Deng, X., *et al.* (2014). A METTL3-METTL14 complex mediates mammalian nuclear RNA N6-adenosine methylation. Nat. Chem. Biol. *10*, 93-95.

Liu, N., Dai, Q., Zheng, G., He, C., Parisien, M., and Pan, T. (2015). N(6)-methyladenosine-dependent RNA structural switches regulate RNA-protein interactions. Nature *518*, 560-564.

Liu, N., Parisien, M., Dai, Q., Zheng, G., He, C., and Pan, T. (2013). Probing N6-methyladenosine RNA modification status at single nucleotide resolution in mRNA and long noncoding RNA. RNA (New York, N.Y.) *19*, 1848-1856.

Liu, N., Zhou, K.I., Parisien, M., Dai, Q., Diatchenko, L., and Pan, T. (2017). N6-methyladenosine alters RNA structure to regulate binding of a low-complexity protein. Nucleic Acids Res.

Liu, Q., Wu, K., Zhu, Y., He, Y., Wu, J., and Liu, Z. (2007). Silencing MAT2A gene by RNA interference inhibited cell growth and induced apoptosis in human hepatoma cells. Hepatology research : the official journal of the Japan Society of Hepatology *37*, 376-388.

Long, J.C., and Caceres, J.F. (2009). The SR protein family of splicing factors: master regulators of gene expression. The Biochemical journal *417*, 15-27.

Lopez-Bigas, N., Audit, B., Ouzounis, C., Parra, G., and Guigo, R. (2005). Are splicing mutations the most frequent cause of hereditary disease? FEBS Lett. *579*, 1900-1903.

Lu, S.C., and Mato, J.M. (2005). Role of methionine adenosyltransferase and S-adenosylmethionine in alcohol-associated liver cancer. Alcohol (Fayetteville, N.Y.) *35*, 227-234.

Ludwig, M.L., and Matthews, R.G. (1997). Structure-based perspectives on B12-dependent enzymes. Annu. Rev. Biochem. *66*, 269-313.

Luo, S., and Tong, L. (2014). Molecular basis for the recognition of methylated adenines in RNA by the eukaryotic YTH domain. Proc. Natl. Acad. Sci. U. S. A. *111*, 13834-13839.

Lykke-Andersen, J., Shu, M.D., and Steitz, J.A. (2001). Communication of the position of exon-exon junctions to the mRNA surveillance machinery by the protein RNPS1. Science (New York, N.Y.) *293*, 1836-1839.

Maddocks, O.D., Labuschagne, C.F., Adams, P.D., and Vousden, K.H. (2016). Serine Metabolism Supports the Methionine Cycle and DNA/RNA Methylation through De Novo ATP Synthesis in Cancer Cells. Mol. Cell *61*, 210-221.

Malone, T., Blumenthal, R.M., and Cheng, X. (1995). Structure-guided analysis reveals nine sequence motifs conserved among DNA amino-methyltransferases, and suggests a catalytic mechanism for these enzymes. J. Mol. Biol. *253*, 618-632.

Marjon, K., Cameron, M.J., Quang, P., Clasquin, M.F., Mandley, E., Kunii, K., McVay, M., Choe, S., Kernytsky, A., Gross, S., *et al.* (2016). MTAP Deletions in Cancer Create Vulnerability to Targeting of the MAT2A/PRMT5/RIOK1 Axis. Cell reports *15*, 574-587.

Martinez-Chantar, M.L., Garcia-Trevijano, E.R., Latasa, M.U., Martin-Duce, A., Fortes, P., Caballeria, J., Avila, M.A., and Mato, J.M. (2003a). Methionine adenosyltransferase II beta subunit gene expression provides a proliferative advantage in human hepatoma. Gastroenterology *124*, 940-948.

Martinez-Chantar, M.L., Latasa, M.U., Varela-Rey, M., Lu, S.C., Garcia-Trevijano, E.R., Mato, J.M., and Avila, M.A. (2003b). L-methionine availability regulates expression of the methionine adenosyltransferase 2A gene in human hepatocarcinoma cells: role of S-adenosylmethionine. J. Biol. Chem. *278*, 19885-19890.

Martinez-Contreras, R., Cloutier, P., Shkreta, L., Fisette, J.F., Revil, T., and Chabot, B. (2007). hnRNP proteins and splicing control. Adv. Exp. Med. Biol. *623*, 123-147.

Matera, A.G., and Shpargel, K.B. (2006). Pumping RNA: nuclear bodybuilding along the RNP pipeline. Curr. Opin. Cell Biol. *18*, 317-324.

Mato, J.M., Alvarez, L., Ortiz, P., and Pajares, M.A. (1997). S-adenosylmethionine synthesis: molecular mechanisms and clinical implications. Pharmacol. Ther. *73*, 265-280.

Mato, J.M., Martinez-Chantar, M.L., and Lu, S.C. (2013). S-adenosylmethionine metabolism and liver disease. Ann. Hepatol. *12*, 183-189.

Mauer, J., Luo, X., Blanjoie, A., Jiao, X., Grozhik, A.V., Patil, D.P., Linder, B., Pickering, B.F., Vasseur, J.J., Chen, Q., *et al.* (2017). Reversible methylation of m6Am in the 5' cap controls mRNA stability. Nature *541*, 371-375.

Mavrakis, K.J., McDonald, E.R., 3rd, Schlabach, M.R., Billy, E., Hoffman, G.R., deWeck, A., Ruddy, D.A., Venkatesan, K., Yu, J., McAllister, G., *et al.* (2016). Disordered

methionine metabolism in MTAP/CDKN2A-deleted cancers leads to dependence on PRMT5. Science (New York, N.Y.) *351*, 1208-1213.

Meyer, K.D., Patil, D.P., Zhou, J., Zinoviev, A., Skabkin, M.A., Elemento, O., Pestova, T.V., Qian, S.B., and Jaffrey, S.R. (2015). 5' UTR m(6)A Promotes Cap-Independent Translation. Cell *163*, 999-1010.

Meyer, K.D., Saletore, Y., Zumbo, P., Elemento, O., Mason, C.E., and Jaffrey, S.R. (2012). Comprehensive analysis of mRNA methylation reveals enrichment in 3' UTRs and near stop codons. Cell *149*, 1635-1646.

Morris, D.P., and Greenleaf, A.L. (2000). The splicing factor, Prp40, binds the phosphorylated carboxyl-terminal domain of RNA polymerase II. J. Biol. Chem. *275*, 39935-39943.

Mougin, A., Gottschalk, A., Fabrizio, P., Luhrmann, R., and Branlant, C. (2002). Direct probing of RNA structure and RNA-protein interactions in purified HeLa cell's and yeast spliceosomal U4/U6.U5 tri-snRNP particles. J. Mol. Biol. *317*, 631-649.

Nayler, O., Hartmann, A.M., and Stamm, S. (2000). The ER repeat protein YT521-B localizes to a novel subnuclear compartment. The Journal of cell biology *150*, 949-962.

Neish, A.S., Anderson, S.F., Schlegel, B.P., Wei, W., and Parvin, J.D. (1998). Factors associated with the mammalian RNA polymerase II holoenzyme. Nucleic Acids Res. *26*, 847-853.

Nguyen, T.H., Galej, W.P., Fica, S.M., Lin, P.C., Newman, A.J., and Nagai, K. (2016). CryoEM structures of two spliceosomal complexes: starter and dessert at the spliceosome feast. Curr. Opin. Struct. Biol. *36*, 48-57.

Ninomiya, K., Kataoka, N., and Hagiwara, M. (2011). Stress-responsive maturation of Clk1/4 pre-mRNAs promotes phosphorylation of SR splicing factor. The Journal of cell biology *195*, 27-40.

Ohno, M., Segref, A., Bachi, A., Wilm, M., and Mattaj, I.W. (2000). PHAX, a mediator of U snRNA nuclear export whose activity is regulated by phosphorylation. Cell *101*, 187-198.

Orzalli, M.H., Broekema, N.M., Diner, B.A., Hancks, D.C., Elde, N.C., Cristea, I.M., and Knipe, D.M. (2015). cGAS-mediated stabilization of IFI16 promotes innate signaling during herpes simplex virus infection. Proc. Natl. Acad. Sci. U. S. A. *112*, E1773-1781.

Palmer, J.L., and Abeles, R.H. (1979). The mechanism of action of S-adenosylhomocysteinase. J. Biol. Chem. *254*, 1217-1226.

Pan, Q., Shai, O., Lee, L.J., Frey, B.J., and Blencowe, B.J. (2008). Deep surveying of alternative splicing complexity in the human transcriptome by high-throughput sequencing. Nat. Genet. *40*, 1413-1415.

Pan, X., Lei, B., Zhou, N., Feng, B., Yao, W., Zhao, X., Yu, Y., and Lu, H. (2012). Identification of novel genes involved in DNA damage response by screening a genome-wide Schizosaccharomyces pombe deletion library. BMC genomics *13*, 662.

Paneda, C., Gorospe, I., Herrera, B., Nakamura, T., Fabregat, I., and Varela-Nieto, I. (2002). Liver cell proliferation requires methionine adenosyltransferase 2A mRNA up-regulation. Hepatology (Baltimore, Md.) *35*, 1381-1391.

Parker, B.J., Moltke, I., Roth, A., Washietl, S., Wen, J., Kellis, M., Breaker, R., and Pedersen, J.S. (2011). New families of human regulatory RNA structures identified by comparative analysis of vertebrate genomes. Genome Res. *21*, 1929-1943.

Patil, D.P., Chen, C.K., Pickering, B.F., Chow, A., Jackson, C., Guttman, M., and Jaffrey, S.R. (2016). m6A RNA methylation promotes XIST-mediated transcriptional repression. Nature *537*, 369-373.

Pendleton, K.E., Chen, B., Liu, K., Hunter, O.V., Xie, Y., Tu, B.P., and Conrad, N.K. (2017). The U6 snRNA m6A Methyltransferase METTL16 Regulates SAM Synthetase Intron Retention. Cell *169*, 824-835.e814.

Pertea, M., Pertea, G.M., Antonescu, C.M., Chang, T.C., Mendell, J.T., and Salzberg, S.L. (2015). StringTie enables improved reconstruction of a transcriptome from RNA-seq reads. Nat. Biotechnol. *33*, 290-295.

Ping, X.L., Sun, B.F., Wang, L., Xiao, W., Yang, X., Wang, W.J., Adhikari, S., Shi, Y., Lv, Y., Chen, Y.S., *et al.* (2014). Mammalian WTAP is a regulatory subunit of the RNA N6-methyladenosine methyltransferase. Cell Res. *24*, 177-189.

Quinlan, A.R., and Hall, I.M. (2010). BEDTools: a flexible suite of utilities for comparing genomic features. Bioinformatics (Oxford, England) *26*, 841-842.

Raghunathan, P.L., and Guthrie, C. (1998). RNA unwinding in U4/U6 snRNPs requires ATP hydrolysis and the DEIH-box splicing factor Brr2. Current biology : CB *8*, 847-855.

Ran, F.A., Hsu, P.D., Wright, J., Agarwala, V., Scott, D.A., and Zhang, F. (2013). Genome engineering using the CRISPR-Cas9 system. Nat. Protoc. *8*, 2281-2308.

Rosonina, E., Ip, J.Y., Calarco, J.A., Bakowski, M.A., Emili, A., McCracken, S., Tucker, P., Ingles, C.J., and Blencowe, B.J. (2005). Role for PSF in mediating transcriptional activator-dependent stimulation of pre-mRNA processing in vivo. Mol. Cell. Biol. *25*, 6734-6746.

Sahin, B.B., Patel, D., and Conrad, N.K. (2010). Kaposi's sarcoma-associated herpesvirus ORF57 protein binds and protects a nuclear noncoding RNA from cellular RNA decay pathways. PLoS Path. *6*, e1000799.

Sakabe, N.J., and de Souza, S.J. (2007). Sequence features responsible for intron retention in human. BMC genomics *8*, 59.

Schmitt, M.E., Brown, T.A., and Trumpower, B.L. (1990). A rapid and simple method for preparation of RNA from Saccharomyces cerevisiae. Nucleic Acids Res. *18*, 3091-3092.

Schramm, L., and Hernandez, N. (2002). Recruitment of RNA polymerase III to its target promoters. Genes Dev. *16*, 2593-2620.

Schwartz, S., Agarwala, S.D., Mumbach, M.R., Jovanovic, M., Mertins, P., Shishkin, A., Tabach, Y., Mikkelsen, T.S., Satija, R., Ruvkun, G., *et al.* (2013). High-resolution mapping reveals a conserved, widespread, dynamic mRNA methylation program in yeast meiosis. Cell *155*, 1409-1421.

Schwartz, S., Mumbach, M.R., Jovanovic, M., Wang, T., Maciag, K., Bushkin, G.G., Mertins, P., Ter-Ovanesyan, D., Habib, N., Cacchiarelli, D., *et al.* (2014). Perturbation of m6A writers reveals two distinct classes of mRNA methylation at internal and 5' sites. Cell reports *8*, 284-296.

Sergiev, P.V., Serebryakova, M.V., Bogdanov, A.A., and Dontsova, O.A. (2008). The ybiN gene of Escherichia coli encodes adenine-N6 methyltransferase specific for modification of A1618 of 23 S ribosomal RNA, a methylated residue located close to the ribosomal exit tunnel. J. Mol. Biol. *375*, 291-300.

Shi, H., Wang, X., Lu, Z., Zhao, B.S., Ma, H., Hsu, P.J., Liu, C., and He, C. (2017). YTHDF3 facilitates translation and decay of N6-methyladenosine-modified RNA. Cell Res. *27*, 315-328.

Shimba, S., Bokar, J.A., Rottman, F., and Reddy, R. (1995). Accurate and efficient N-6-adenosine methylation in spliceosomal U6 small nuclear RNA by HeLa cell extract in vitro. Nucleic Acids Res. *23*, 2421-2426.

Shiraki, N., Shiraki, Y., Tsuyama, T., Obata, F., Miura, M., Nagae, G., Aburatani, H., Kume, K., Endo, F., and Kume, S. (2014). Methionine metabolism regulates maintenance and differentiation of human pluripotent stem cells. Cell Metab. *19*, 780-794.

Shyh-Chang, N., Locasale, J.W., Lyssiotis, C.A., Zheng, Y., Teo, R.Y., Ratanasirintrawoot, S., Zhang, J., Onder, T., Unternaehrer, J.J., Zhu, H., *et al.* (2013). Influence of threonine metabolism on S-adenosylmethionine and histone methylation. Science (New York, N.Y.) *339*, 222-226.

Sibley, C.R., Blazquez, L., and Ule, J. (2016). Lessons from non-canonical splicing. Nature reviews. Genetics *17*, 407-421.

Sims, R.J., 3rd, Millhouse, S., Chen, C.F., Lewis, B.A., Erdjument-Bromage, H., Tempst, P., Manley, J.L., and Reinberg, D. (2007). Recognition of trimethylated histone H3 lysine 4

facilitates the recruitment of transcription postinitiation factors and pre-mRNA splicing. Mol. Cell *28*, 665-676.

Singh, R.K., and Cooper, T.A. (2012). Pre-mRNA splicing in disease and therapeutics. Trends Mol. Med. *18*, 472-482.

Sledz, P., and Jinek, M. (2016). Structural insights into the molecular mechanism of the m(6)A writer complex. eLife *5*.

Slobodin, B., Han, R., Calderone, V., Vrielink, J.A., Loayza-Puch, F., Elkon, R., and Agami, R. (2017). Transcription Impacts the Efficiency of mRNA Translation via Co-transcriptional N6-adenosine Methylation. Cell *169*, 326-337.e312.

Spies, N., Nielsen, C.B., Padgett, R.A., and Burge, C.B. (2009). Biased chromatin signatures around polyadenylation sites and exons. Mol. Cell *36*, 245-254.

Staknis, D., and Reed, R. (1994). SR proteins promote the first specific recognition of Pre-mRNA and are present together with the U1 small nuclear ribonucleoprotein particle in a general splicing enhancer complex. Mol. Cell. Biol. *14*, 7670-7682.

Stanek, D., and Neugebauer, K.M. (2004). Detection of snRNP assembly intermediates in Cajal bodies by fluorescence resonance energy transfer. The Journal of cell biology *166*, 1015-1025.

Stanek, D., Rader, S.D., Klingauf, M., and Neugebauer, K.M. (2003). Targeting of U4/U6 small nuclear RNP assembly factor SART3/p110 to Cajal bodies. The Journal of cell biology *160*, 505-516.

Sterner, D.A., Carlo, T., and Berget, S.M. (1996). Architectural limits on split genes. Proc. Natl. Acad. Sci. U. S. A. *93*, 15081-15085.

Stubbs, S.H., and Conrad, N.K. (2015). Depletion of REF/Aly alters gene expression and reduces RNA polymerase II occupancy. Nucleic Acids Res. *43*, 504-519.

Sutter, B.M., Wu, X., Laxman, S., and Tu, B.P. (2013). Methionine inhibits autophagy and promotes growth by inducing the SAM-responsive methylation of PP2A. Cell *154*, 403-415.

Tarn, W.Y., and Steitz, J.A. (1996). Highly diverged U4 and U6 small nuclear RNAs required for splicing rare AT-AC introns. Science (New York, N.Y.) *273*, 1824-1832.

Tillo, D., and Hughes, T.R. (2009). G+C content dominates intrinsic nucleosome occupancy. BMC Bioinformatics *10*, 442.

Tirumuru, N., Zhao, B.S., Lu, W., Lu, Z., He, C., and Wu, L. (2016). N(6)-methyladenosine of HIV-1 RNA regulates viral infection and HIV-1 Gag protein expression. eLife *5*.

Tu, B.P., Mohler, R.E., Liu, J.C., Dombek, K.M., Young, E.T., Synovec, R.E., and McKnight, S.L. (2007). Cyclic changes in metabolic state during the life of a yeast cell. Proc. Natl. Acad. Sci. U. S. A. *104*, 16886-16891.

Valadkhan, S. (2005). snRNAs as the catalysts of pre-mRNA splicing. Curr. Opin. Chem. Biol. *9*, 603-608.

Vazquez-Chantada, M., Fernandez-Ramos, D., Embade, N., Martinez-Lopez, N., Varela-Rey, M., Woodhoo, A., Luka, Z., Wagner, C., Anglim, P.P., Finnell, R.H., *et al.* (2010). HuR/methyl-HuR and AUF1 regulate the MAT expressed during liver proliferation, differentiation, and carcinogenesis. Gastroenterology *138*, 1943-1953.

Wang, E.T., Sandberg, R., Luo, S., Khrebtukova, I., Zhang, L., Mayr, C., Kingsmore, S.F., Schroth, G.P., and Burge, C.B. (2008). Alternative isoform regulation in human tissue transcriptomes. Nature *456*, 470-476.

Wang, J.X., and Breaker, R.R. (2008). Riboswitches that sense S-adenosylmethionine and S-adenosylhomocysteine. Biochemistry and cell biology = Biochimie et biologie cellulaire *86*, 157-168.

Wang, P., Doxtader, K.A., and Nam, Y. (2016a). Structural Basis for Cooperative Function of Mettl3 and Mettl14 Methyltransferases. Mol. Cell *63*, 306-317.

Wang, T., Birsoy, K., Hughes, N.W., Krupczak, K.M., Post, Y., Wei, J.J., Lander, E.S., and Sabatini, D.M. (2015a). Identification and characterization of essential genes in the human genome. Science (New York, N.Y.) *350*, 1096-1101.

Wang, X., Feng, J., Xue, Y., Guan, Z., Zhang, D., Liu, Z., Gong, Z., Wang, Q., Huang, J., Tang, C., *et al.* (2016b). Structural basis of N(6)-adenosine methylation by the METTL3-METTL14 complex. Nature *534*, 575-578.

Wang, X., Lu, Z., Gomez, A., Hon, G.C., Yue, Y., Han, D., Fu, Y., Parisien, M., Dai, Q., Jia, G., *et al.* (2014). N6-methyladenosine-dependent regulation of messenger RNA stability. Nature *505*, 117-120.

Wang, X., Zhao, B.S., Roundtree, I.A., Lu, Z., Han, D., Ma, H., Weng, X., Chen, K., Shi, H., and He, C. (2015b). N(6)-methyladenosine Modulates Messenger RNA Translation Efficiency. Cell *161*, 1388-1399.

Wang, Z., and Burge, C.B. (2008). Splicing regulation: from a parts list of regulatory elements to an integrated splicing code. RNA (New York, N.Y.) *14*, 802-813.

Wei, C.M., Gershowitz, A., and Moss, B. (1975). Methylated nucleotides block 5' terminus of HeLa cell messenger RNA. Cell *4*, 379-386.

Will, C.L., and Luhrmann, R. (2011). Spliceosome structure and function. Cold Spring Harb. Perspect. Biol. *3*.

Wong, J.J., Ritchie, W., Ebner, O.A., Selbach, M., Wong, J.W., Huang, Y., Gao, D., Pinello, N., Gonzalez, M., Baidya, K., *et al.* (2013). Orchestrated intron retention regulates normal granulocyte differentiation. Cell *154*, 583-595.

Xiao, W., Adhikari, S., Dahal, U., Chen, Y.S., Hao, Y.J., Sun, B.F., Sun, H.Y., Li, A., Ping, X.L., Lai, W.Y., *et al.* (2016). Nuclear m(6)A Reader YTHDC1 Regulates mRNA Splicing. Mol. Cell *61*, 507-519.

Xu, C., Wang, X., Liu, K., Roundtree, I.A., Tempel, W., Li, Y., Lu, Z., He, C., and Min, J. (2014). Structural basis for selective binding of m6A RNA by the YTHDC1 YTH domain. Nat. Chem. Biol. *10*, 927-929.

Yang, H.B., Xu, Y.Y., Zhao, X.N., Zou, S.W., Zhang, Y., Zhang, M., Li, J.T., Ren, F., Wang, L.Y., and Lei, Q.Y. (2015). Acetylation of MAT IIalpha represses tumour cell growth and is decreased in human hepatocellular cancer. Nature communications *6*, 6973.

Yap, K., Lim, Z.Q., Khandelia, P., Friedman, B., and Makeyev, E.V. (2012). Coordinated regulation of neuronal mRNA steady-state levels through developmentally controlled intron retention. Genes Dev. *26*, 1209-1223.

Ye, C., Sutter, B.M., Wang, Y., Kuang, Z., and Tu, B.P. (2017). A Metabolic Function for Phospholipid and Histone Methylation. Mol. Cell *66*, 180-193.e188.

Yue, Y., Liu, J., and He, C. (2015). RNA N6-methyladenosine methylation in post-transcriptional gene expression regulation. Genes Dev. *29*, 1343-1355.

Zeiner, G.M., Cleary, M.D., Fouts, A.E., Meiring, C.D., Mocarski, E.S., and Boothroyd, J.C. (2008). RNA analysis by biosynthetic tagging using 4-thiouracil and uracil phosphoribosyltransferase. Methods in molecular biology (Clifton, N.J.) *419*, 135-146.

Zhang, C., Samanta, D., Lu, H., Bullen, J.W., Zhang, H., Chen, I., He, X., and Semenza, G.L. (2016). Hypoxia induces the breast cancer stem cell phenotype by HIF-dependent and ALKBH5-mediated m(6)A-demethylation of NANOG mRNA. Proc. Natl. Acad. Sci. U. S. A. *113*, E2047-2056.

Zhang, S., Zhao, B.S., Zhou, A., Lin, K., Zheng, S., Lu, Z., Chen, Y., Sulman, E.P., Xie, K., Bogler, O., *et al.* (2017). m6A Demethylase ALKBH5 Maintains Tumorigenicity of Glioblastoma Stem-like Cells by Sustaining FOXM1 Expression and Cell Proliferation Program. Cancer Cell *31*, 591-606.e596.

Zhao, B.S., Wang, X., Beadell, A.V., Lu, Z., Shi, H., Kuuspalu, A., Ho, R.K., and He, C. (2017). m6A-dependent maternal mRNA clearance facilitates zebrafish maternal-to-zygotic transition. Nature *542*, 475-478.

Zheng, G., Dahl, J.A., Niu, Y., Fedorcsak, P., Huang, C.M., Li, C.J., Vagbo, C.B., Shi, Y., Wang, W.L., Song, S.H., *et al.* (2013). ALKBH5 is a mammalian RNA demethylase that impacts RNA metabolism and mouse fertility. Mol. Cell *49*, 18-29.

Zhou, J., Wan, J., Gao, X., Zhang, X., Jaffrey, S.R., and Qian, S.B. (2015). Dynamic m(6)A mRNA methylation directs translational control of heat shock response. Nature *526*, 591-594.

Zhou, Z., and Fu, X.D. (2013). Regulation of splicing by SR proteins and SR protein-specific kinases. Chromosoma *122*, 191-207.